Natural Resources Canada | Ressources naturelles Canada

GEOLOGICAL SURVEY OF CANADA
OPEN FILE 8907

Churchill – Kivalliq GIC study: regional resistivity model and synthetic magnetotelluric impedance responses, Manitoba and Nunavut

I.J. Ferguson, D. Saindon, J.A. Craven, and D.H. Boteler

2022

Canada

ISSN 2816-7155
ISBN 978-0-660-44574-8
Catalogue No. M183-2/8907E-PDF

GEOLOGICAL SURVEY OF CANADA
OPEN FILE 8907

Churchill – Kivalliq GIC study: regional resistivity model and synthetic magnetotelluric impedance responses, Manitoba and Nunavut

I.J. Ferguson[1], D. Saindon[1], J.A. Craven[2], and D.H. Boteler[3]

[1]Department of Earth Sciences, University of Manitoba, 125 Dysart Road, Winnipeg, Manitoba
[2]Geological Survey of Canada, 601 Booth Street, Ottawa, Ontario
[3]Natural Resources Canada, Canadian Hazards Information Service, 2617 Anderson Road, Ottawa, Ontario

2022

Permanent link: https://doi.org/10.4095/330339

This publication is available for free download through GEOSCAN (https://geoscan.nrcan.gc.ca/).

Recommended citation

Ferguson, I.J., Saindon, D., Craven, J.A., and Boteler, D.H., 2022. Churchill – Kivalliq GIC study: regional resistivity model and synthetic magnetotelluric impedance responses, Manitoba and Nunavut; Geological Survey of Canada, Open File 8907, 1 .zip file. https://doi.org/10.4095/330339

Publications in this series have not been edited; they are released as submitted by the author.

Executive summary

This report was completed as part of Natural Resources Canada's GEM-GeoNorth program and specifically as part of the Churchill-Kivalliq corridor sub-priority area. The primary objective of the work is to compute synthetic magnetotelluric (MT) impedance responses along the path of the planned Kivalliq Hydro-Fibre link from Gillam, Manitoba, to Kivalliq, Nunavut, to enable modelling of the levels of geomagnetically induced currents (GIC) on the hydro link.

This work included a review of legacy MT and geomagnetic depth soundings conducted near the Gillam-Kivalliq corridor as well as relevant soundings completed in the same geological terranes crossed by the corridor. The planned hydro-fibre link crosses the North American Central Plains (NACP) conductor to the north of Gillam so other MT soundings of the NACP were also reviewed. More than 15 individual studies were considered in this review. The main features revealed by these studies are very high crustal resistivity in the southern Rae craton near the north end of the hydro-fibre link and in the Superior craton south of south end of the hydro-fibre link. The Chesterfield Block exhibits decreasing resistivity at crustal levels with distance to the south. MT studies in the Trans Hudson Orogen and Hearne craton margin rocks of the Wollaston domain exhibit more conductive and more heterogeneous crust and mantle. The top of the NACP in many studies is at a depth of 10–20 km but in some cases, e.g., on LITHOPROBE Line L, there are conductive zones extending to near the surface. Depending on the modelled thickness of the conductive feature, its resistivity is between 25 and <1 Ω·m. A number of crossings of the NACP also indicate that it is associated with a conductive region in the mantle.

For the purposes of GIC modelling it is desirable to consider MT impedance responses for the period range of 1 s to 1 day (~10^5 s) and at 50 km spatial scale. A 1300 km long north-south profile was established for 2-D inversion and modelling of the legacy data set based on the observation of pervasively east-west strikes for the large-scale geological features. Projection of the legacy MT data onto this profile (from distances of up to 200 km away from the profile) leaves two large gaps in the data coverage, with the south gap located mainly above the Wathaman-Chipewyan Batholith and the north gap crossing the Great Island and Nejanilini (Hearne margin) terranes and well as the southern and central parts of the Hearne craton. To overcome the problems of the gaps in the profile, the MT responses from 12 sites in corresponding geological terranes crossed by LITHOPROBE Line L to the southwest were imported to form a padded MT data set. In order to provide the required period range, inversions models were examined in which the resistivity of layers at depths of 260–800 km was constrained by a very deep penetrating MT and geomagnetic depth sounding study from Carty Lake in the southern Superior craton.

Four 2-D MT inversion models were produced. Model A is based on the available MT data along the modelling profile. Model B is based on the available MT data but incorporates deep layers determined in the southern Superior craton study. In Model C gaps in the MT profile are padded with MT data from the corresponding geological terranes from LITHOPROBE Line L. The importation of data from elsewhere (Model C) is intended to provide responses with the same statistical character as those in the terranes crossed, but not to necessarily provide the true structure. Model D is based on the padded data and the deeper layers from the Carty Lake study. The two models incorporating deep layer resistivity constraints (Models B and D) are considered to provide the more reliable MT impedance responses at periods exceeding 10^4 s.

The four inversion models are quite similar, but display some differences at large depth and in the data gaps. The models fit the edited observed data reasonably well with normalized RMS misfit values of ~3.0 for error floors of 5% for the phase and 20% for apparent resistivity for the 2-D transverse electric (TE) and transverse magnetic (TM) modes. The 2-D inversion models reproduce the large-scale

resistivity structures observed in earlier studies of the legacy data including very resistive crust and upper mantle in the Rae and Superior cratons underlain at 75 to 150 km depth by more conductive rocks. More conductive crust and mantle is present in the Chesterfield Block, Hearne craton, and Trans Hudson Orogen. In the inversion models, the most conductive part of the NACP is at ~10 km depth but this geometry is not tightly constrained by the modelling. The models include relatively conductive crust at shallow depths adjacent to the NACP.

MT apparent resistivity and phase responses for both the TE and TM modes were exported from the four MT models at 10 km spacing using a series of synthetic sites created in the WinGLink software. This process means that the high spatial-density data are produced directly as part of the 2-D modelling rather than requiring any additional spatial interpolation. The least-squares fitting process and regularization used in the MT inversion also create some smoothing and reduction of aliasing of smaller scale resistivity heterogeneity inherent in the observed data set.

The transverse electric and transverse magnetic (TE and TM) apparent resistivity and phase responses were converted into equivalent impedance values. Results define significantly higher impedance magnitude in the Rae and Superior cratons at periods less than 10^3 s. There are low impedance magnitudes and high spatial gradients in the southern 300 km of the profile, including in the region around Gillam. The largest relative differences between the available MT data models (A and B) and the padded models (C and D) occur at moderate to low impedance magnitudes and represent smaller absolute differences. The TM impedance magnitude exhibits stronger spatial gradients than the TM impedance phase or the TE responses. These effects extend to the longest periods and can be attributed to static effects associated with the TM mode electromagnetic induction process.

Finally, TE and TM impedance responses were spatially averaged into 50 km segments using arithmetic averaging of complex impedance responses over segments of these lengths. Examination of the results in terms of the corresponding impedance magnitude and phase show that the 50 km averaged values capture most of the spatial variability observed in the 10 km responses but they do not accurately represent some smaller wavelength features.

Table of contents

List of figures

List of tables

1. Introduction

This report, along with its associated electronic appendix, constitutes the deliverables for the contract "*Churchill–Kivalliq GIC Study: Development of Regional Resistivity Model and Synthetic Magnetotelluric Impedance Responses*". It is prepared by I. Ferguson and D. Saindon (University of Manitoba) with oversight from J. Craven (Geological Survey of Canada). The work forms part of the NRCan GEM-GeoNorth project.

One of the priority areas of GEM GeoNorth is Western Hudson Bay and the Churchill-Kivalliq corridor is a sub-priority (Figure 1). This corridor encompasses the path of the planned Kivalliq Hydro-Fibre link from Gillam, Manitoba to Kivalliq, Nunavut, (Figure 2) which will promote clean energy solutions and improved communications for development of Canada's North (Herath et al., 2019; Kivalliq Hydro-Fibre Link, 2021).

Strong geomagnetic disturbances can lead to widespread power system problems along major power lines due to geomagnetically induced electrical currents (GICs) (e.g., Molinski, 2002; Beggan, 2015; Torta et al., 2015; Love et al., 2016, 2018; Boteler, 2001, 2019). The problem is especially severe for high latitude power lines in the Arctic (Beggan 2015; Pulkkinen et al., 2015) and exacerbated by regional electrical conductivity structures in the crust (Beggan, 2015; Bedrosian and Love, 2015; Kelbert et al., 2019). Previous studies have indicated the presence of a large east-oriented conductive feature beneath the planned Kivalliq Hydro-Fibre link. This feature is interpreted as a continuation of the largest conductor in North America, the North American Central Plains (NACP) conductor (Gupta et al., 1989; Jones et al., 1993, 2005; Jones and Craven, 1990). The potential contribution of this conductor to a GIC effect along the power transmission corridor is unknown. However, the feature has been noted to have a significant effect on DC power transmission in terms of its effect on ground potential rise associated with grounding electrodes (Adetunji and Ferguson, 2012).

Previous modelling of GIC's in the northern Manitoba region has been based on simplified 1-D layered models for the regional resistivity structure (Boteler et al., 1998; Trichtchenko et al., 2019a, 2019b). In this report we describe a synthetic modelling study based on legacy magnetotelluric (MT) data and the known geological and geophysical information to build a synthetic 2-D earth conductivity model for the Gillam-Kivalliq region (including the NACP). Future work will use the model to make calculations about possible GIC strengths in the planned corridor during a major geomagnetic disturbance.

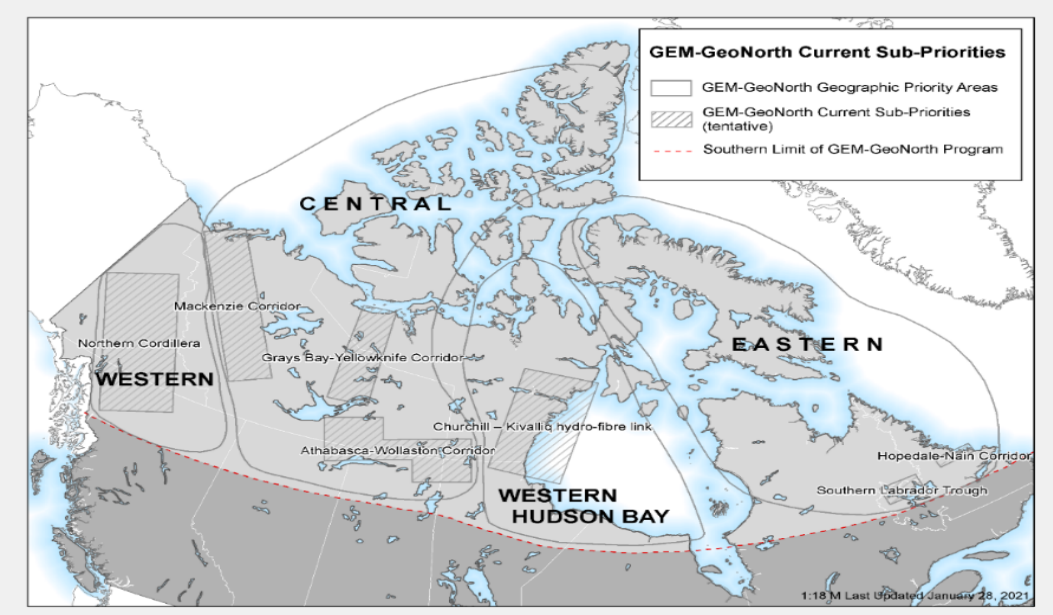

Figure 1. GEM GeoNorth draft priority regions (GEM GeoNorth, 2021).

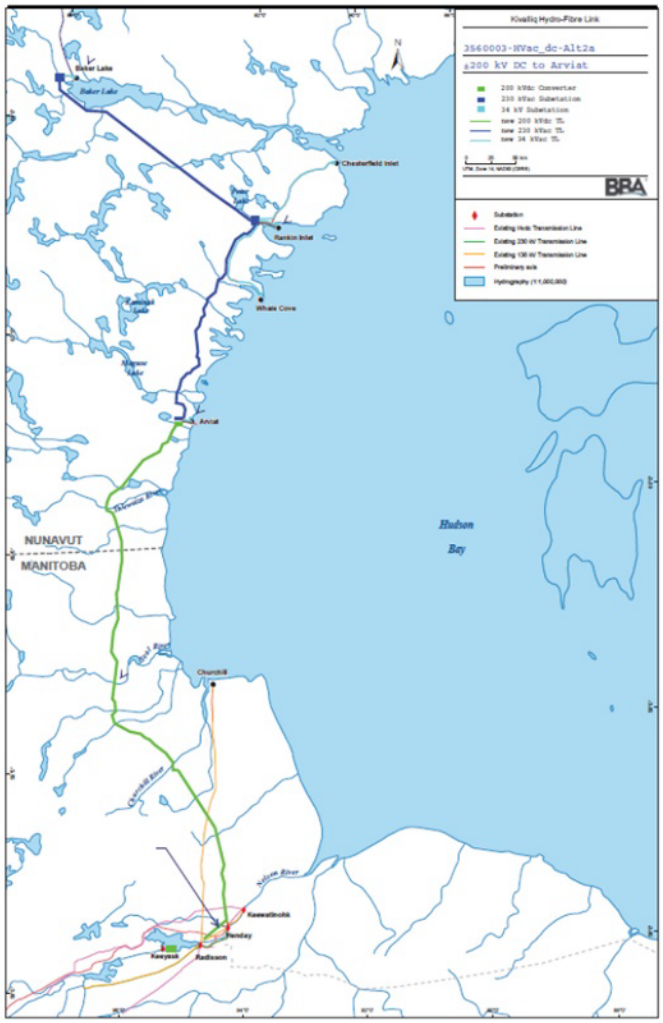

Figure 2. Map of possible path of Kivalliq Hydro-Fibre link (Kivalliq Inuit Association and ANBARIC Development Partners, 2020).

The MT method provides relatively large-scale imaging of the electrical resistivity structure of the Earth's crust and lithospheric mantle. In most geophysical studies, the primary MT responses, the impedance and the tipper, are used to resolve the large-scale sub-surface resistivity structure from which the distribution of different rock types and tectonic structures can be interpreted (Vozoff, 1991; Simpson and Bahr, 2005; Chave and Jones, 2012). However, the measured MT impedances, or synthetic MT impedances derived from resistivity models, also form critical information for estimating the GICs induced on power lines and other infrastructure (e.g., Love et al., 2016, 2018; Boteler, 2001, 2019). Electrical resistivity of sedimentary rocks depends dominantly on their porosity, the salinity of the pore fluids, and the shale content. Electrical resistivity of crystalline Precambrian crust is generally very high but is can be strongly reduced locally by increased abundance and interconnection of graphite, oxides, and sulphides and at upper crustal depths by increased porosity and fluid content of shear zones.

2. Geologic setting

The geology of the Gillam-Kivalliq area includes crystalline Precambrian basement terranes from Archean to Proterozoic in age, Paleozoic to Mesozoic sedimentary rocks of the Hudson Bay Basin, and Quaternary to Holocene surficial sediments of the Hudson Bay Lowlands and Hudson Bay (Figure 3).

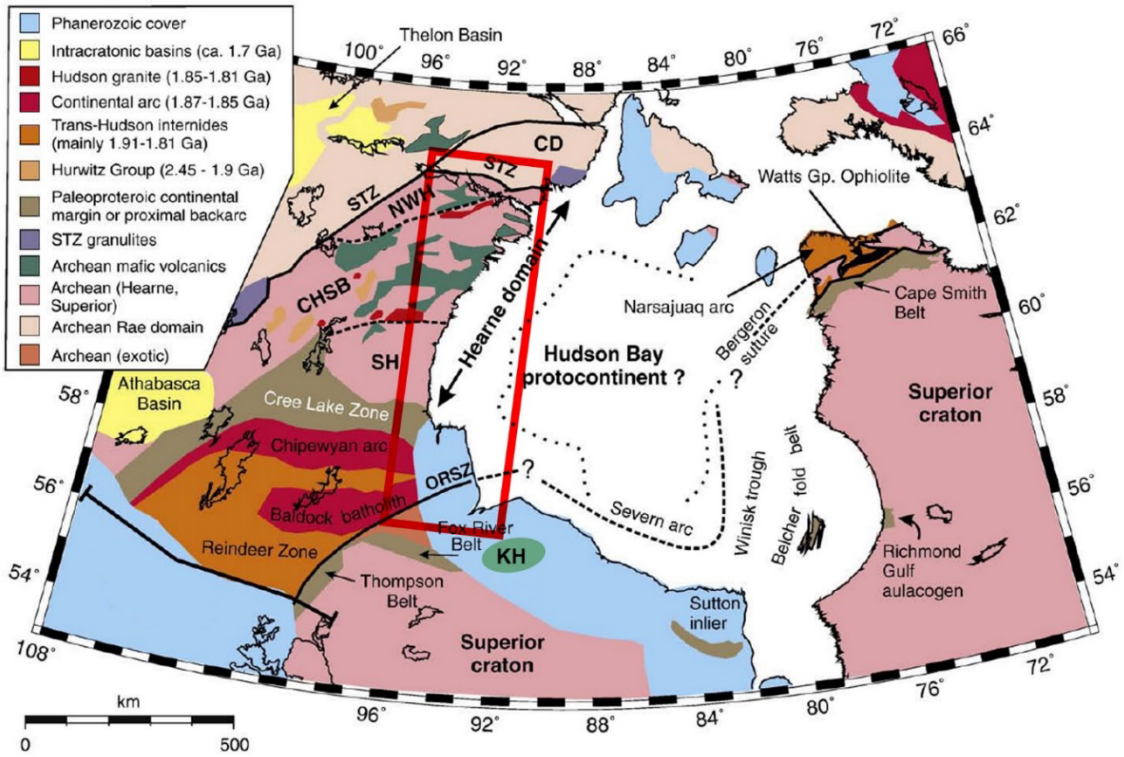

Figure 3. Geological framework of Gillam-Kivalliq area (modified from Eaton and Darbyshire, 2010). Red rectangle shows extent of the Gillam-Kivalliq Fibre-Hydro area. KH indicates the area of the Kaskattama Highlands. ORSZ, Owl River shear zone; SH, southern Hearne domain; CHSB, central Hearne supracrustal belt; NWH, northwest Hearne domain, CD, Chesterfield domain; STZ, Snowbird Tectonic Zone.

2.1 Precambrian basement rocks

Precambrian rocks exposed to the west and north of Hudson Bay form part of the western Churchill Province. The two main components of this province are the Rae and Hearne cratons (or domains) (Figure 3). These two Archean units are separated by the Snowbird Tectonic Zone (STZ). The Chesterfield Block (or Domain) is a distinct crustal block on the southern side of the STZ (Figure 3). To the south of the Gillam-Kivalliq study area, Archean rocks also occur in the Superior craton which is separated from the Hearne craton by Proterozoic rocks of the Trans Hudson Orogen.

2.1.1 Rae, Hearne, and Chesterfield continental blocks

The central Rae craton is located immediately to the north of the study area. The Rae craton contains Meso- to Neoarchean, amphibolite to granulite grade gneisses and thin greenstone belts (Berman et al., 2013b; Pehrsson et al., 2013). It contains a number of distinct Meso- to Neoarchean blocks, with the Committee Bay Block and Repulse Bay blocks are located north and northeast of the current study area respectively (Spratt et al., 2014). These blocks are underlain by Meso- to Neoarchean granodioritic to tonalitic orthogneisses and volcano-sedimentary rocks (Pehrsson et al., 2013). The Rae craton was intruded by 2.72–2.64 Ga tonalite and voluminous 2.62–2.58 Ga monzogranite (Peterson et al., 2015). It was deformed at 2.56–2.50 Ga during the

MacQuoid orogeny (Davis et al., 2006; Berman et al., 2013b) and during the early Paleoproterozoic (2.5–2.3 Ga) Arrowsmith orogeny (Berman et al., 2013b). It was subsequently reworked in the Paleoproterozoic during the 2.0–1.91 Talston and Thelon orogenies in which the Slave craton and Buffalo Head terrane collided with the northwest of the Rae craton and during the 1.9–1.8 Ga Hudsonian orogeny in which the Superior craton and smaller microcontinents collided with the southeast of the western Churchill craton, preserving juvenile Trans Hudson rocks in some locations (Berman et al., 2013b). Four distinct Paleoproterozoic cover sequences were ultimately deposited during these events between ca. 2.2 and 1.9 Ga (Rainbird et al., 2010).

The Chesterfield Block is now considered a distinct crustal block and contains Neoarchean rocks and 2.74–2.67 Ga supracrustal rocks (Berman et al., 2007). The Chesterfield Block and Rae craton were amalgamated prior to 2.61–2.58 Ga (Spratt et al., 2014).

The Hearne craton has a distinct geological history from the Rae craton, for example, it contains a different dyke swarm and some different intrusive events (Pehrsson et al., 2013; Berman et al., 2007, 2013b). It has a central core of dominantly Neoarchean, low–metamorphic grade supracrustal, and plutonic rocks overlain by 2.35–1.75 Ga volcanosedimentary cover and intruded by 1.83 and 1.78 Ga plutons (Spratt et al., 2014). There are two significant Paleoproterozoic cover sequences in the Hearne craton, the Hurwitz Group that occurs in the Central Hearne (Figure 3) and the extensive Wollaston Supergroup (part of the Cree Lake Zone in Figure 3) that is best exposed along the southeast margin of the Hearne domain (Rainbird et al., 2010; Corrigan et al., 2017). The Wollaston domain consists of tightly folded Paleoproterozoic metasedimentary rocks overlying late Archean granitic gneiss

The STZ is a major tectonic feature (Figure 3) that is interpreted to have juxtaposed the Rae and Hearne cratons at 1.9 Ga (Berman et al., 2007). Different interpretations have been proposed for the STZ, but there is evidence supporting that it was a 1.9–1.87 Ga collisional phase of the Trans Hudson orogeny that resulted in accretion of microcontinents including the Hearne domain to the southeast margin of the amalgamated Rae-Chesterfield Block (Berman et al., 2007, 2013a).

2.1.2 Superior craton and Trans Hudson Orogen continental blocks Precambrian rocks to the south and southwest of Hudson Bay form parts of the Archean Superior craton and Paleoproterozoic Trans Hudson orogen. The western Superior Province, which has been stable since 2.6 Ga, consists of linear, sub-parallel subprovinces including greenstone-granite terranes and is hypothesized to have formed through successive formation and accretion of island arcs and accretionary prisms (Percival et al., 2006). Boundaries between subprovinces are defined by faults and shear-zones, intrusive contacts, unconformities, and discontinuities in metamorphic grade (Williams et al., 1992). The earlier history of the Superior Province involved a number of composite superterranes. In the northwestern Superior Province, rocks of the Northern Superior superterrane, Oxford Lake–Stull Lake terrane, and Munro Lake terrane have distinctive geological histories (Skulski et al., 2000). The ca. 3.0 Ga North Caribou (NC) terrane formed a separate superterrane.

Juvenile Paleoproterozoic and altered Archean rocks of the Trans Hudson Orogen formed during collision of the Archean Superior and Hearne (Ansdell, 2005; Corrigan et al., 2007). Geological units formed on and near the boundary of the Superior Province during the Trans Hudson Orogen are collectively referred to as the Superior Boundary Zone (SBZ) (Minifie et al., 2013). This zone includes Archean rocks of the Superior Province and overlying Paleoproterozoic supracrustal rocks. Both the basement and cover sequences were deformed and metamorphosed during the ca. 1.83–1.78 Ga collision between the Superior Craton and internal rocks of the Trans-Hudson Orogen (Corrigan et al., 2017). Just to the south of the current study area, the Fox River belt is a low-grade, north-dipping sequence located at the northwest margin of the Superior Province and the Trans Hudson Orogen. It has a width of 20 to 25 km and extends for 152 km (Barager and Scoates, 1981; Scoates, 1990). The belt includes the Fox River sill, an ultramafic-mafic complex. In most recent interpretations the Fox River Belt is interpreted to have formed away from the edge of the Superior craton, with

the younger Proterozoic rocks subsequently thrust over the top of the edge of the Superior craton (Weber, 1990).

During the collision between the Superior craton and western Churchill craton, smaller fragments of Archean crust (such as the Sask craton) were trapped between the Superior and western Churchill cratons and, along with the shape of the two main cratons, are thought to have prevented the complete convergence of the two Archean cratons. In studies closer to the Thompson area in Manitoba, an older block of Archean crust has been recognized in rocks previously interpreted to be part of the Trans Hudson Orogen (Böhm et al., 2000). This Archean block does not appear to be associated with the Superior craton. There is some uncertainty as to the exact position of the northwestern margin of the Trans Hudson Orogen but Böhm et al. (2000) interpreted the Owl River Shear Zone, a dextral strike-slip fault that extends northeast from the Manitoba promontory to form the margin of the Trans Hudson Orogen (Figure 3).

The internal part of Trans Hudson Orogen, the Reindeer Zone, includes a series of arc rocks formed in, and at margins of, the Manikewan Ocean, which formed between the Hearne, Sask, and Superior cratons at ca. 2.07–1.92 Ga (Corrigan et al., 2017). The Reindeer Zone, comprises ca. 1.9–1.8 Ga magmatic arc and sedimentary basin rocks accreted to the margins during successive arc–continent collisions prior to a terminal collision at ca. 1.8 Ga. The NACP is hosted in the rocks of the equivalent La Ronge Domain (Saskatchewan) and Lynn Lake/Leaf Rapids Domain (Manitoba), which form a curvilinear belt approximately 50 km wide by 750 km long that is exposed from Lac La Ronge in northcentral Saskatchewan to north-central Manitoba. Father along strike, to the east of the Gillam-Kivalliq corridor, near the Manitoba-Ontario border, the rocks north of the Fox River Belt have a subdued magnetic response very similar to that of the Burntwood Suite of the Kisseynew Gneiss Belt. The ca. 1.862 to 1.848 Ga Wathaman-Chipewyan batholith (Chipewyan arc in Figure 3), is an Andean-type continental magmatic arc emplaced along the northwestern Reindeer zone during the accretion of Sask and Superior cratons to previously accreted arc terranes on the southern flank of the Hearne craton (Corrigan et al., 2017; Berman et al., 2013a).

2.2 Hudson Bay Basin

The thickness of sedimentary rocks in the Paleozoic-Mesozoic Hudson Bay Basin ranges up to around 2500 m in the middle of Hudson Bay (Figure 4). Seismic surveys in marine parts of the basin have imaged an offset of older units by basement penetrating faults (Figures 4, 5).

Figure 6 shows the stratigraphic section for the Hudson Bay Basin and Figure 7 shows the large-scale geology. In northeastern Manitoba, the onshore Hudson Bay Basin rocks are Upper Ordovician to Middle Devonian in age, and along the Gillam to Churchill leg of the Gillam-Kivalliq corridor the rocks consist mainly of the Ordovician Bad Cache Rapids, Churchill River, and Red Head Rapids units (Figure 8). Subcrop near Churchill, Manitoba, includes a thin section of the Silurian Severn River Formation.

The Bad Cache Rapids Group lies unconformably on the Precambrian basement and consists dominantly of carbonate and shale (Norris, 1993b; Nicolas, 2011). The thickness of the complete unit ranges from 62 m to 94 m in northeastern Manitoba (Nicolas and Lavoie, 2012). The group is subdivided into the Portage Chute and the Surprise Creek Formations. The Portage Chute is made up of sandstone at the base, dolostone in the middle, and limestone on the top, whereas the Surprise Creek consists mainly of dolomitic limestone (Norris, 1993b; Nicolas, 2011). It also contains minor evaporitic cycles (Lavoie et al., 2013).

Rocks of the Churchill River Group occur as a narrow outcrop belt that unconformably overlies those of the Bad Cache Rapids Group. This group consists of mainly dolomitic mudstone to wackestone (Lavoie et al. 2013). The unit has been divided into the Caution Creek Formation (wackestone) and the Chasm Creek (mudstone) Formation. The thickness of the Churchill River group ranges from 59 m to 92 m across northeastern Manitoba (Nicolas and Lavoie, 2012).

The Red Head Rapids Formation conformably overlies the Churchill River Group. It is composed dominantly of dolostone and calcareous dolomite but also includes beds of evaporite (Norris 1993b). It is massive to laminated and has occasional porous beds (Nicolas and Lavoie, 2012). The thickness of the Red Head Rapids Formation in northeastern Manitoba ranges from 32 m to 49 m (Nicolas and Lavoie, 2012).

There is a general thickening of the Paleozoic sequence from Gillam towards Churchill although there are some local variations (Figure 8). Stratigraphic drilling results and MT survey results from near Churchill show a variation in the depth to the Precambrian rocks from 100 m near the coastline to 200 m around 10 km farther south (Roberts and Craven, 2012).

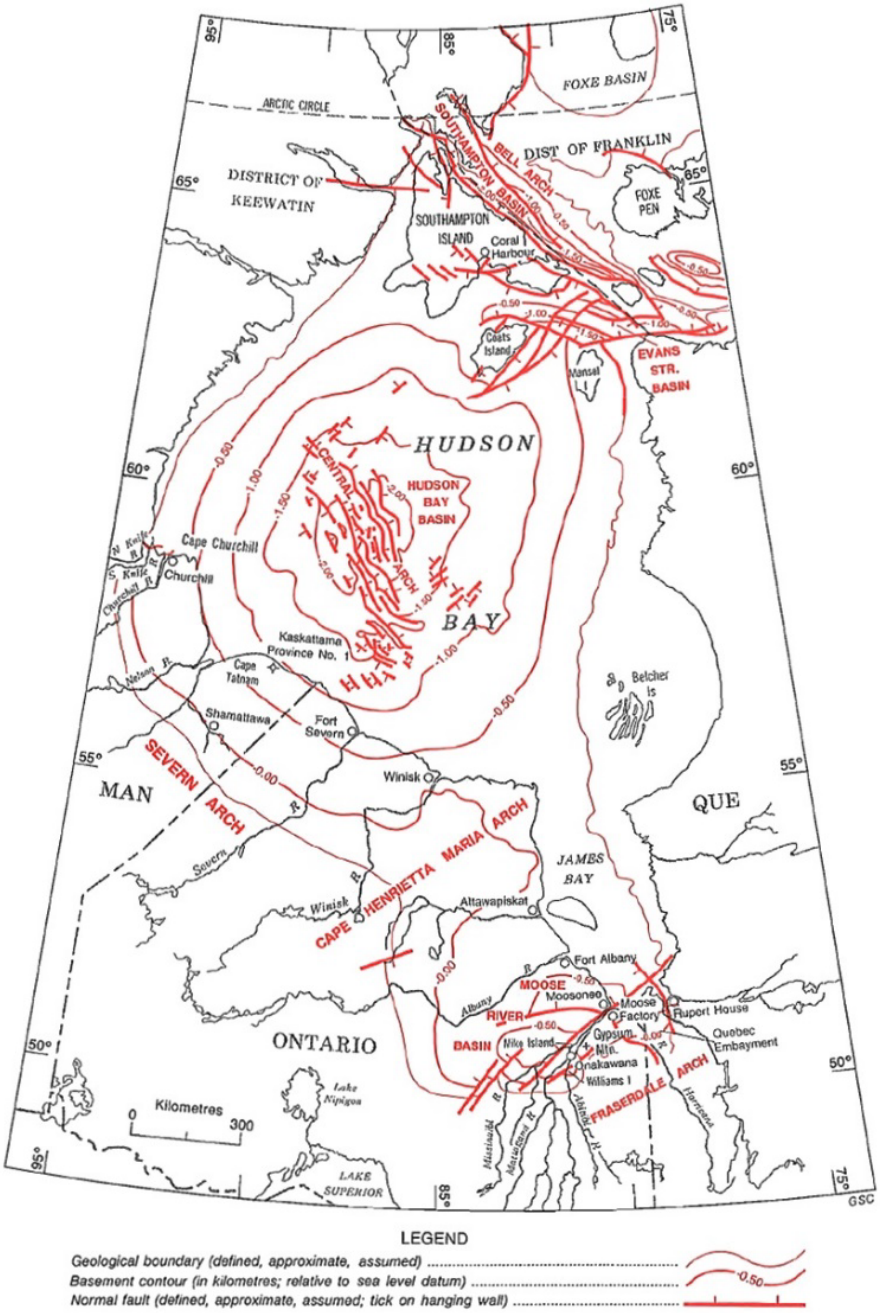

Figure 4. Basement structure map for Hudson Bay Basin and adjacent basins showing thickness of Phanerozoic sequence (Norris, 1993b).

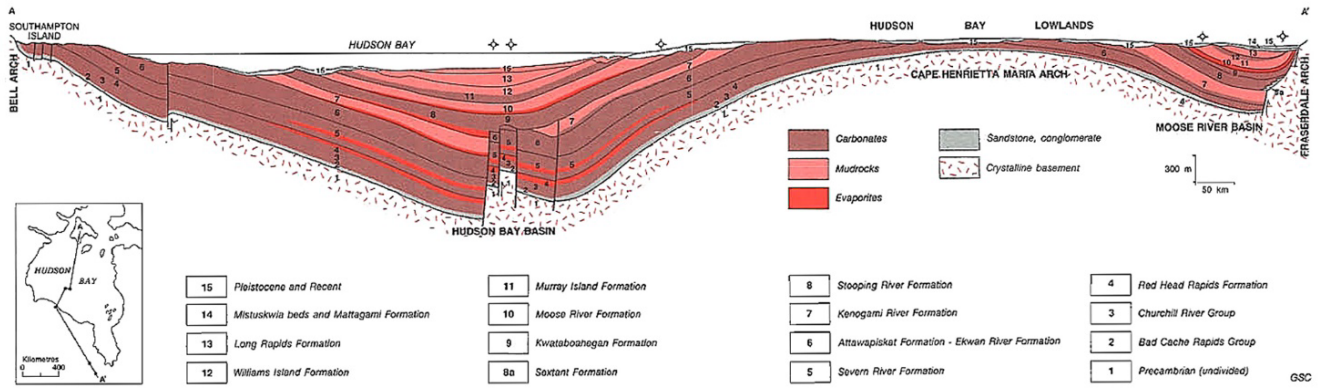

Figure 5. Schematic north-south section of Hudson Bay platform (Norris, 1993a).

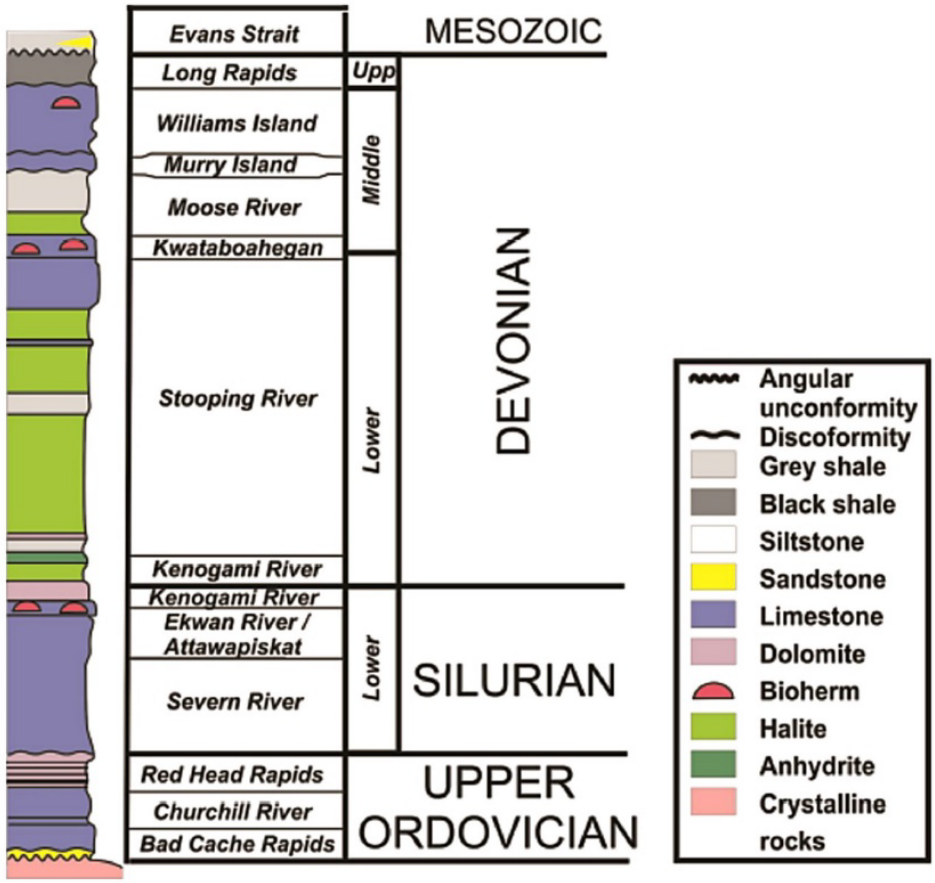

Figure 6. Schematic lithostratigraphic column for the Hudson Bay and Moose River basins (Lavoie et al., 2013).

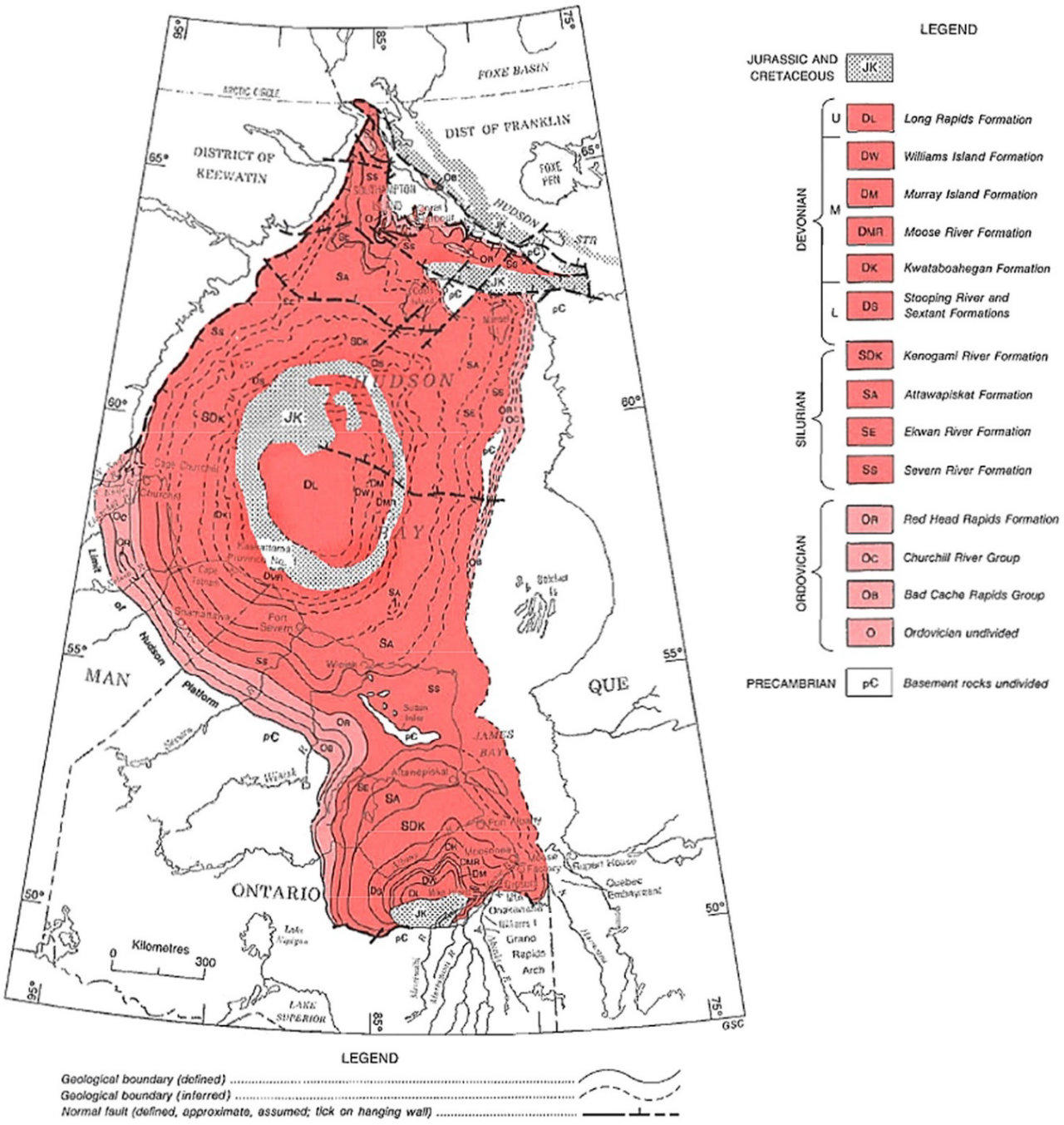

Figure 7. Geological map of Hudson Bay Basin and adjacent basins (Norris, 1993a).

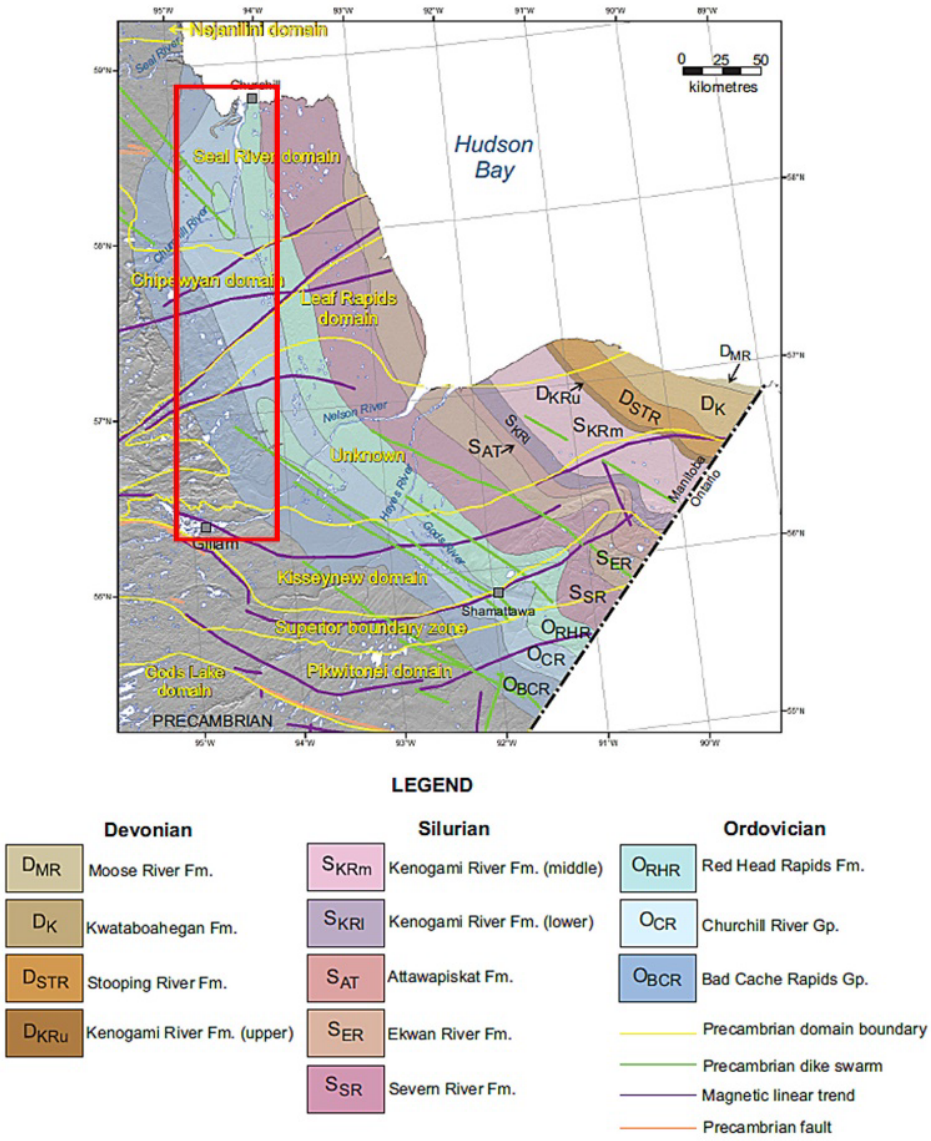

Figure 8. Hudson Bay Basin geology in Gillam-Churchill area (Nicolas and Clayton, 2015). The Paleozoic geology is superimposed on a 90 m pixel-spacing digital elevation and overlain with the Precambrian domain boundaries of the Trans Hudson Orogen, magnetic linear trends, faults and dike swarms. Red rectangle shows study area.

2.3 Surficial and marine geology

The surface geology of the Hudson Bay Lowland is dominated by offshore glaciomarine silt and clay with minor deposits of marginal glaciomarine clay, silt, and sand (Matile and Keller, 2007). The lowlands include Pleistocene aged deposits from the Illinoisan (or older) and Wisconsinian glaciations and deposits form the interglacial Sangamonian interval (Shilts, 1986; Cowan, 1993). Holocene deposits include marine sediments of the Tyrrell Sea and fluvial sand and gravel deposits.

Water depth across western Hudson Bay is relatively shallow, with the depth for much of this area in the range 80 to 160 m (Figure 9; Pelletier, 1986; Josenhans et al., 1988). The average water temperature is about 0°C and the average salinity is about 32.5 (psu) (Prinsenberg, 1986) corresponding to an electrical conductivity of 2.7 $S.m^{-1}$. The sedimentary sequence is relatively thin, with the total thickness of Quaternary sediments in western Hudson Bay being 0–10 m (Figure 10). Postglaical muds are generally <5 m thick and typically thickest near river mouths (Pelletier, 1986; Josenhans et al., 1988).

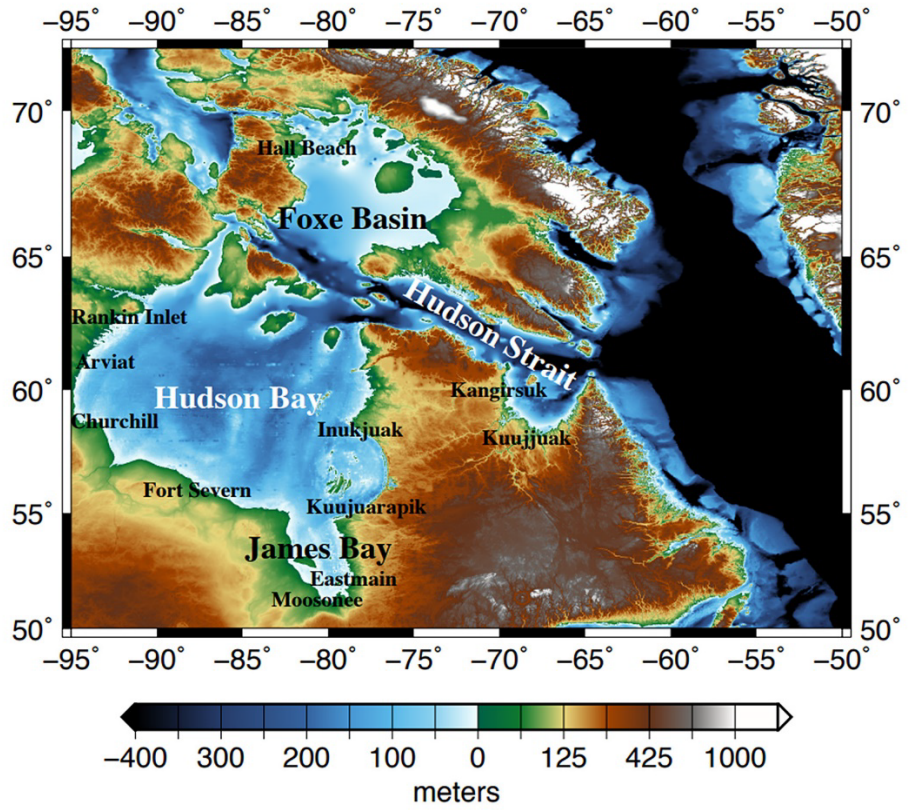

Figure 9. Bathymetry of Hudson Bay and surrounding topography (Hayden, 2020).

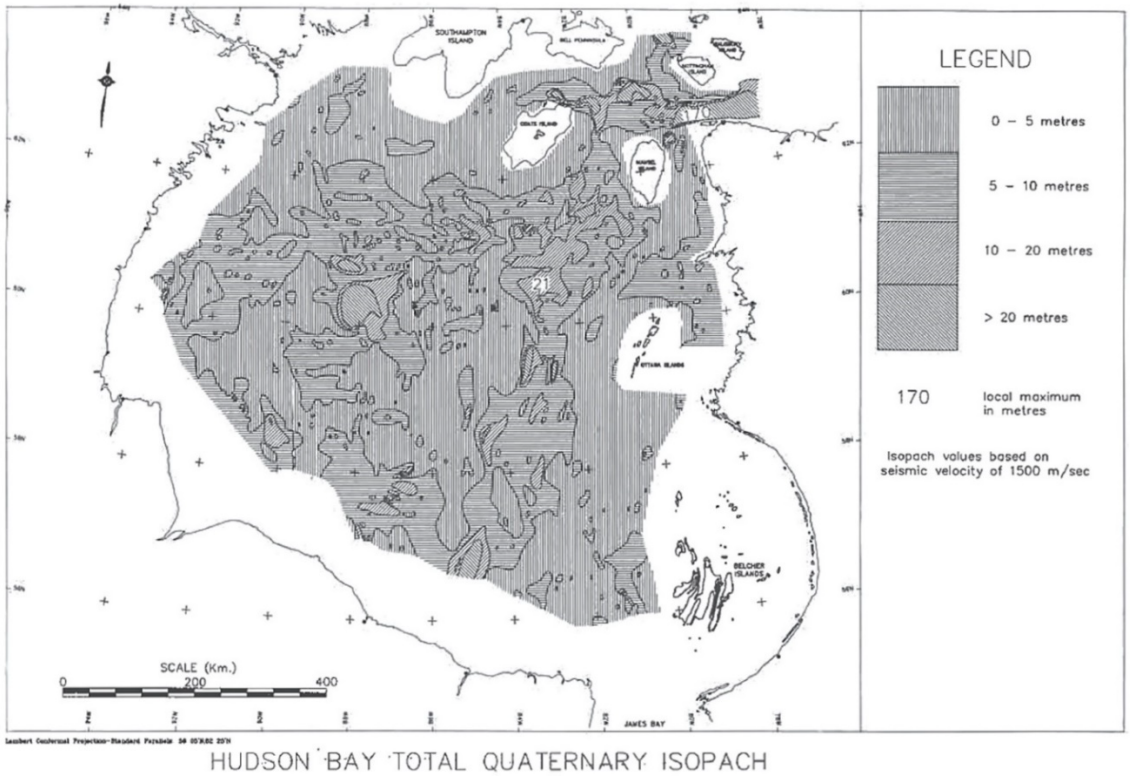

Figure 10. Isopach map of Quaternary sediments in Hudson Bay (Josenhans et al., 1988).

3. MT surveys and resistivity information

Information on the resistivity structure in the Gillam-Kivalliq Hydro-Fibre link area is available from a number of deep-penetrating MT surveys. Additional constraints on the resistivity structure come from tipper and geomagnetic depth sounding (GDS).

3.1 Deep penetrating MT and tipper studies

Information on the scientific basis and procedures of the MT method can be found in standard references such as Vozoff (1991), Simpson and Bahr (2005) and Chave and Jones (2012). In MT, the period-dependent impedance response has four tensor components relating time-variations of the horizontal electric field components at the Earth's surface to time-variations of the horizontal magnetic field. The impedance response is sensitive to the resistivity structure at depths from several hundred metres at the shortest periods (~10^{-4} s) to several hundred kilometres at the longest periods (>10^{4} s). The period-dependent tipper response has two components relating time-variations in the vertical magnetic field to those of the of the horizontal magnetic field. Induction arrows provide a graphical representation of this response.

The MT method is often divided into broad period ranges: audio-frequency MT (AMT) surveys use periods of 10^{-4} s to 10^{-1} s and provide information on resistivity structures extending from near the surface to a few kilometres depth; broad-band MT (BBMT) surveys use periods of 10^{-3} or 10^{-2} s to >10^{3} s and provide information on resistivity structures in the upper crust to upper sub-continental lithospheric mantle; and long-period MT (LMT) surveys use periods from 1 s to >10^{4} s and provide information from the upper to middle crust to several hundred kilometres depth, typically to the lithosphere-asthenosphere boundary.

In GIC studies, it is necessary to consider MT impedance responses for the period range of 1 s to 1 day (~10^{5} s). Much of the relevant resistivity information comes from impedance and tipper responses from BBMT and LMT surveys. Additional constraints come from long-period GDS studies (Simpson and Bahr, 2005; Chave and Jones, 2012). Most MT impedance and shorter-period (<10^{4} s) tipper responses are derived using a representation of the geomagnetic source as being laterally uniform. In contrast, in long-period GDS studies, a more realistic representation of the geomagnetic source geometry is considered, providing an electromagnetic response related to depths up to and exceeding 600 km in the mantle. This information allows computation of theoretical MT responses for the period range 10^{4} s–10^{5} s.

Individual period-dependent MT impedance and tipper responses are represented as a complex-valued quantities and have both a magnitude and a phase or an in-phase (real) and quadrature-phase (imaginary) component. The MT impedance magnitude can be used to estimate an apparent resistivity, a volumetrically-averaged resistivity over the penetration depth of the signals. The impedance phase also provides information on the resistivity structure, and depends on the change of apparent resistivity with period. In a horizontally-layered structure, at periods for which apparent resistivity is increasing with period (resistivity increasing with depth) the phase is between 0° and 45°, and at periods for which apparent resistivity is decreasing with period (resistivity decreasing with depth) the phase is between 45° and 90°.

The MT response tensor provides information on the dimensionality of the underlying resistivity structure and can be used to discern between 1-D, 2-D, and 3-D structures. Different modelling and inversion algorithms are applied for structures of different dimensionality. In 1-D structures, such as in an undeformed sedimentary rock sequence, the resistivity is horizontally-layered. In 2-D structures, such as at a straight geological boundary, the resistivity is invariant in the direction of the geological strike. Associated MT impedance responses are termed the transverse electric (TE) response for the electric field parallel to the boundary and the transverse magnetic (TM) response for the electric field perpendicular to the boundary. In 2-D structures, the induction arrow response is perpendicular to strike and, when plotted according to the Parkinson (1962) convention, the real (in-phase) arrow will typically point towards internal current concentrations in more conductive regions (Jones, 1986). In 3-D structures, the resistivity structure will have

a more complex form. MT responses can also be distorted by small-scale heterogeneities. In the simplest situation, called static shift, the galvanic distortion will cause a period-independent upward or downward shift of apparent resistivity. In this case, and for more complex galvanic distortion, the MT phase response will provide a more robust indication of the regional MT response (e.g., Jones, 2012).

Information on the resistivity structure in the Gillam-Kivalliq Hydro-Fibre link area is available from a number of deep-penetrating MT surveys. Additional constraints on the resistivity structure come from tipper studies based on data collected from a north-south line of magnetometer sites. These sites were established in 1976 as part of the International Magnetospheric Study (IMS) (Gupta et al., 1985) and were subsequently used for the CANOPUS (Canadian Auroral Network for the OPEN Program Unified Study) and CARISMA Canadian Array for Realtime Investigations of Magnetic Activity) array (e.g., Mann et al. 2008). Resistivity information is also available from smaller-scale electromagnetic surveys (e.g., Adetunji and Ferguson, 2012) in the region, and from geophysical well-logs from both onshore and offshore exploratory oil and gas wells.

Table 1 summarizes the main MT surveys done in and close to the current study area. Figure 11 shows the location of the MT surveys closest to the Gillam-Kivalliq hydro-fibre link area. The surveys and results for studies close to the current study area are reviewed below. Results for Trans Hudson Orogen studies located farther south are reviewed in the Section 5 with a focus on the NACP responses.

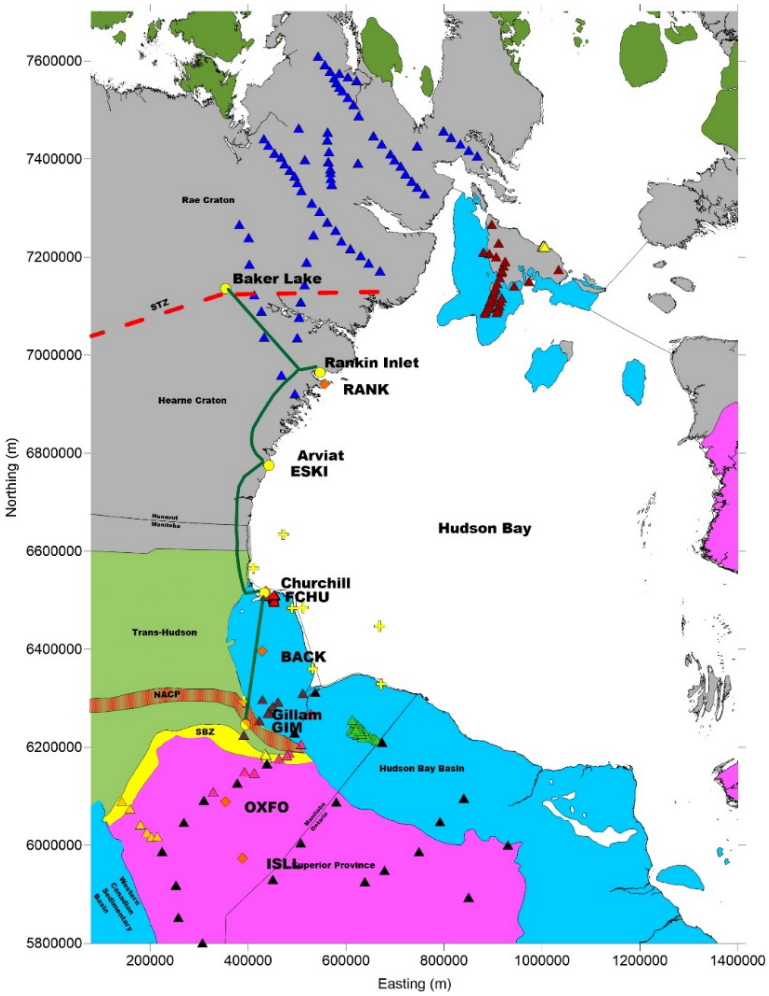

Figure 11. Location of MT soundings along Gillam-Kivalliq link in relation to major geological divisions. Coordinates are UTM15 in metres. Triangles show MT sites, diamonds show location of nearby offshore oil and gas wells with deep-penetrating resistivity or induction logs, and three or four letter codes show the location of IMS/CANOPUS/CARISMA sites.

Table 1. Deep-penetrating MT surveys in study area.

Survey name/year	Location	Data type	Sites	Main reference(s)
IMS (1976–1980)	Superior craton to Rae craton in area of current study	LMT (tipper only)	10	Gupta et al. (1985)
PanCanadian and GSC THO (1984–1987)	Trans Hudson Orogen southwest of current study area in Williston Basin	BBMT	71	Jones and Craven (1990) Jones et al. (2005)
LITHOPROBE THO Transects (Line L, X) (1992–1994)	Trans Hudson Orogen south and west of current study area	AMT, BBMT, LMT	140	Jones et al. (2005)
University Washington - GSC NOD survey (1992)	Trans Hudson Orogen in North Dakota (Williston Basin)	LMT	64	Wu et al. (1993) Wu (1994) Jones et al. (2005)
LITHOPROBE Western Superior Transect MT (1996–2001)	Western Superior craton and THO with several sites in current study area and many sites to the southeast	LMT and BBMT	230	Craven et al. (2001) Ferguson et al. (2005a) Orellana (2006)
Snowbird Tectonic Zone (1998)	Rae craton and Hearne craton, Snowbird tectonic Zone	LMT	8	Jones et al. (2002)
LITHOPROBE Fox River Sill (2002)	Fox River Sill south of current study area	AMT BBMT	10 AMT 3 BBMT	Orellana (2006) Epp (2014) Ferguson et al. (2015)
POLARIS Superior Boundary Zone (2004)	THO and western Superior craton beneath Williston Basin in southern Manitoba	BBMT	21	Gowan et al. (2009)
GSC Knee Lake (KNL) MT survey (2005)	Superior craton and Trans Hudson orogen southeast of current study area	BBMT	13	McLeod (2013)
Southampton Island Integrated Geoscience Project (2007)	Rae craton and Hudson Bay Basin east of current study area	BBMT and LMT	29BBMT 6 LMT	Spratt et al. (2012)
GEM Central Rae craton (diamonds) (2010–2012)	Rae craton (immediately north of current study area)	BBMT and LMT	64	Spratt et al. (2014)
Manitoba Hydro BIPOLE III survey (2011)	Hudson Bay Basin overlying Trans Hudson orogen in current survey area	AMT and BBMT	8	Adetunji and Ferguson (2012)
GEM Churchill Project (2011)	Hudson Bay Basin overlying Trans Hudson orogen in current survey area	AMT and BBMT	46 AMT 3 BBMT	Roberts and Craven (2012) Bancroft et al. (2014) Hayward (2014)
GEM Kaskattama Highlands Project (2017)	Hudson Bay Basin overlying trans Hudson Orogen east of current survey area	AMT and BBMT	21	Craven et al. (2017)
GEM Cape Donovan, Southampton Island (ulu) Project (2018)	Hudson Bay Basin overlying Rae craton east of current survey area	Mainly AMT Some BBMT	24	Craven et al. (2018)

3.1.1 IMS survey (1976–1980) Magnetic recordings were made as part of the IMS in 1976 to 1980 along a north-south profile of sites (most of which were used in the subsequent CANOPUS and CARISMA arrays (Figure 12; Gupta et al., 1985). The profile extends from the Superior craton in the south to the Rae craton in the north. The recorded magnetic field data were used to produce the induction arrow (tipper) response for a period range from 150 s (2.5 minutes) to 9720 s (162 minutes) (Figure 13; Gupta et al., 1985).

The calculated induction arrows have a mainly north-south azimuth (Gupta et al., 1985) as would be expected for east-west striking resistivity structures. At periods of 150 s to 2400 s (40 minutes), the real induction arrow at three sites FSV, PEB, and IGL are relatively large (0.2–>0.5) and point offshore suggesting a geomagnetic coast-effect influence associated with the adjacent conductive ocean water. The real induction arrow response at periods of 150 s to 600 s (10 minutes) at RIT and EXP is also towards the centre of Hudson Bay suggesting a geomagnetic coast effect at these sites.

The induction arrow at sites from RIT to ISL defines a reversal in the induction arrow response consistent with the presence of an east-west striking conductive zone located between GIM and BKC (Gupta et al. 1985). This reversal is evident for the period range from 150 s to >1500 s (25 minutes) (Figure 14). The response was modelled using a simple resistivity model consisting of a 2-D conductive body located north of GIM. The body extends through most of the crust and its upper surface dips to the north. The body has a resistivity of 25 Ω·m and is much more conductive than the background crust (5000 Ω·m). The induction arrow response and broad station spacing means the true width of the body is poorly resolved, so it could also be much more narrow with a lower resistivity. Based on the location of the body relative to the regional geology of the Trans Hudson Orogen it was interpreted to correspond to the NACP.

Figure 12. Site locations in the IMS study (Gupta et al., 1985). The Gillam-Kivalliq Hydro-Fibre link extends from near GLM in the south to RIT in the north.

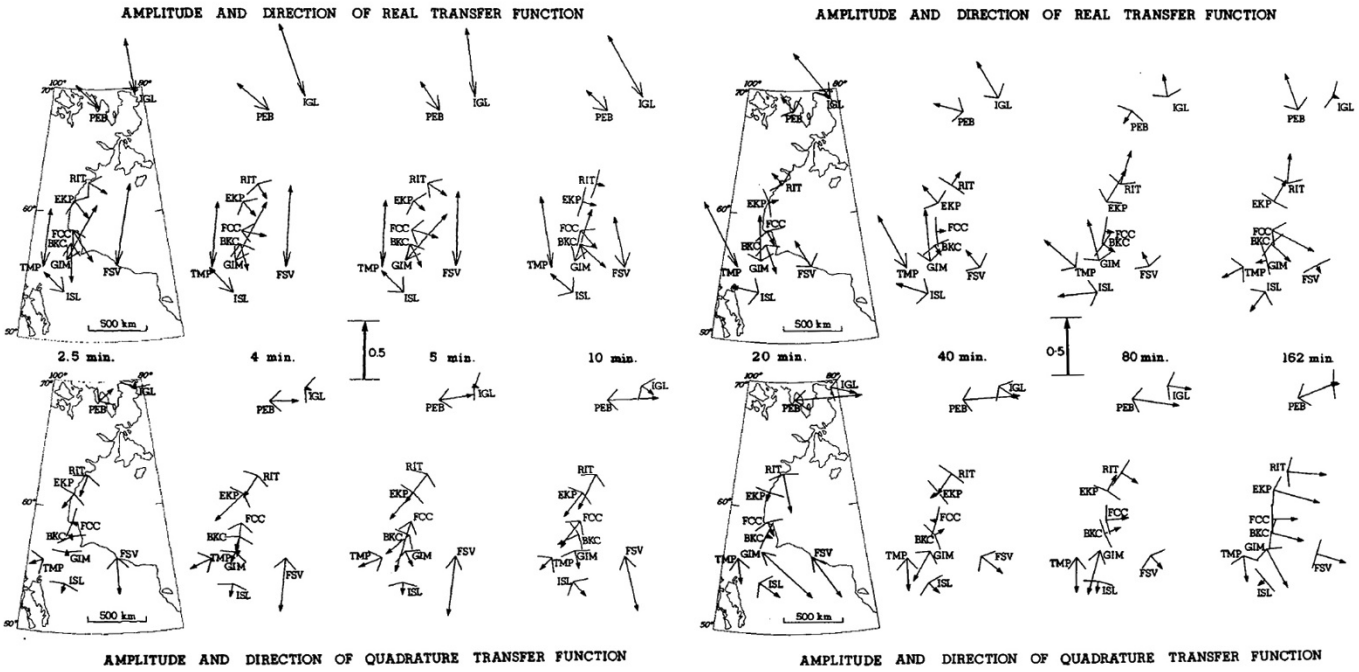

Figure 13. Induction arrow responses from the IMS study for periods from 150 s (2.5 minutes) to 9720 s (162 minutes) (modified from Gupta et al., 1985). Upper maps are for the real induction arrow response and lower maps for the quadrature induction arrow response.

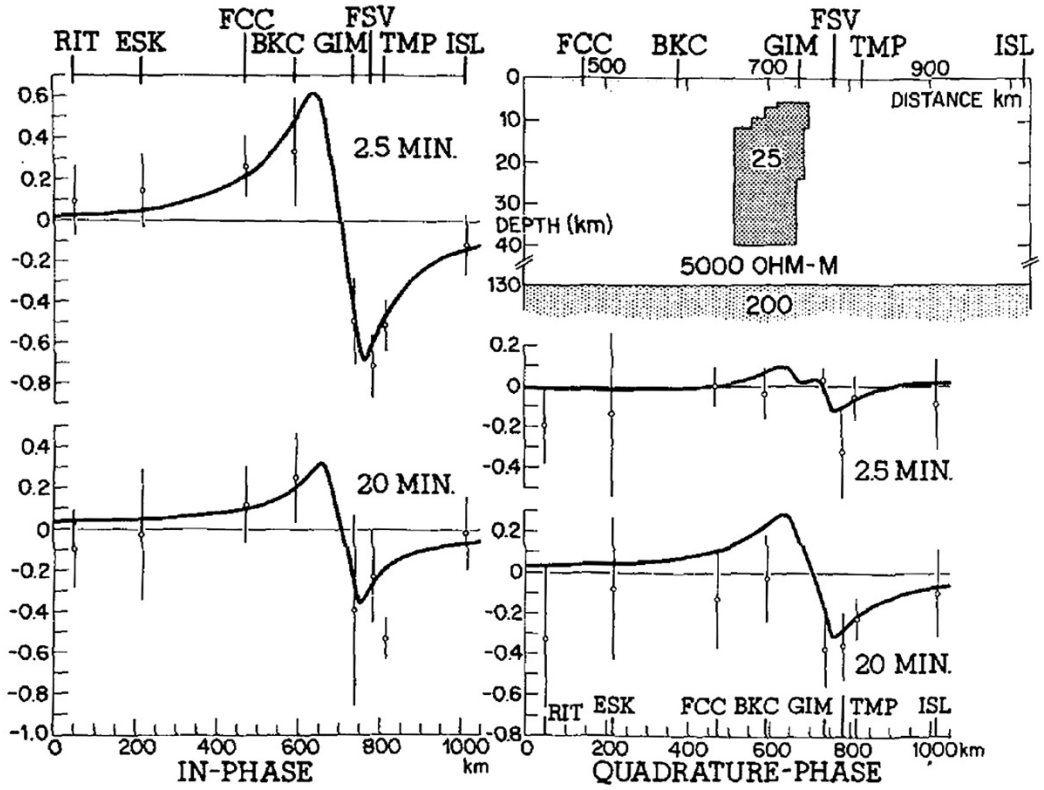

Figure 14. Induction arrow response showing the reversal and simple resistivity model (Gupta et al., 1985). Points with error bars show the observed responses and the line shows the response of the model in the top right panel.

3.1.2 Trans Hudson Orogen surveys (1984–2004) There have been a number of MT surveys conducted in the Trans Hudson Orogen, with a particular focus on the NACP (Figure 15). Most studies have included both BBMT and LMT sites. Earlier studies are described in Jones and Craven (1990) and Jones et al. (2005, 2014) provide reviews of the studies and their large-scale results. Bedrosian and Finn (2021) describe a more recent study of the southern part of the Trans Hudson Orogen and NACP. Geoelectric strike analyses show that throughout much of the Trans Hudson Orogen the resistivity structure has a locally approximately 2-D form with strike directions controlled by the large-scale tectonic structure (Figure 16). These results suggest that the strike direction in the Trans Hudson Orogen along the Gillam-Kivalliq corridor will be approximately east-west and at a high angle to the corridor.

Large-scale 2-D inversions of the data from LITHOPROBE Line L reveal the strongest large-scale resistivity features along the line (Figure 17). Resistive Features C and F correspond to the Archean Sask craton and Archean Superior craton respectively, and include resistivity values at crustal depths exceeding 10,000 Ω·m. More detailed analyses of smaller parts of the LITHOPROBE MT data set confirm these results (White et al., 1999; Ferguson et al., 2005b; Garcia and Jones, 2005). The high grade metamorphic rocks in the Pikwitonei Domain near the northwest margin of the Superior craton are particularly resistive. Detailed studies suggest some of the supracrustal rocks in the Thompson Belt of the Superior Boundary Zone include relatively small conductive zones (White et al., 1999; White et al., 2000).

There are a number of conductive zones in the interior of the Trans Hudson Orogen. The Kisseynew Gneiss Belt (KGB and feature E in Figure 17) contains parts with resistivity of <100 Ω·m (White et al., 1999; Jones et al., 2005). Volcanic arc rocks including those in the Flin Flon Belt and La Ronge Domain also contain relatively conductive components (Ferguson et al., 1999; Ferguson et al., 2005b; Jones et al. 2005; Garcia and Jones, 2005). These conductive zones tend have complex internal resistivity distributions.

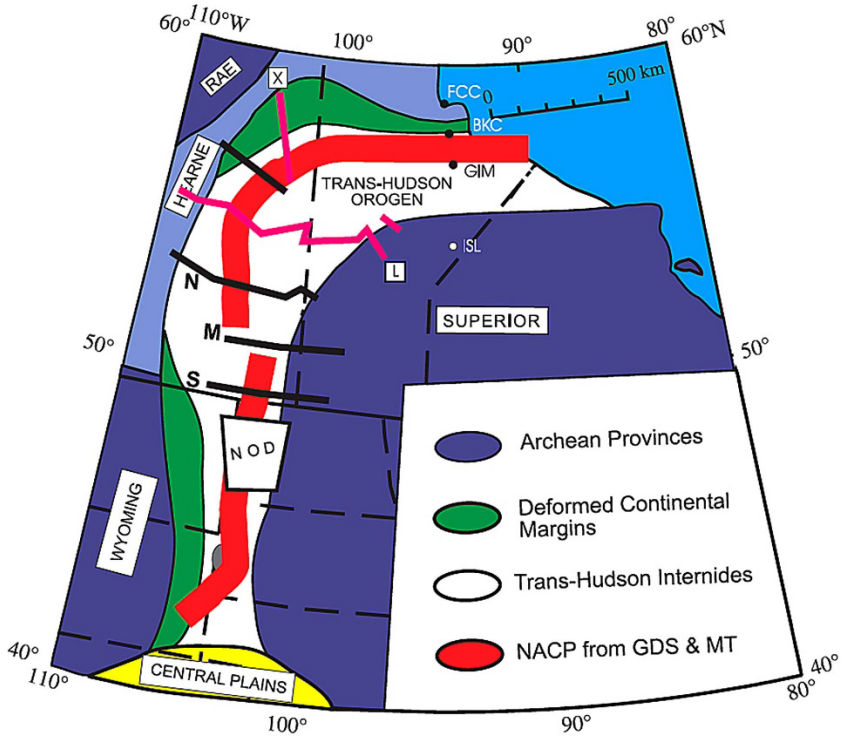

Figure 15. Location of main MT surveys (NOD, S, M, N, L, and X), in the Trans Hudson Orogen prior to 2004 (Jones et al., 2005). Also shown are the locations of the NACP and the stations used by Gupta et al. (1985): BKC, Back; GIM, Gillam; FCC, Fort Churchill; ISL, Island Lake.

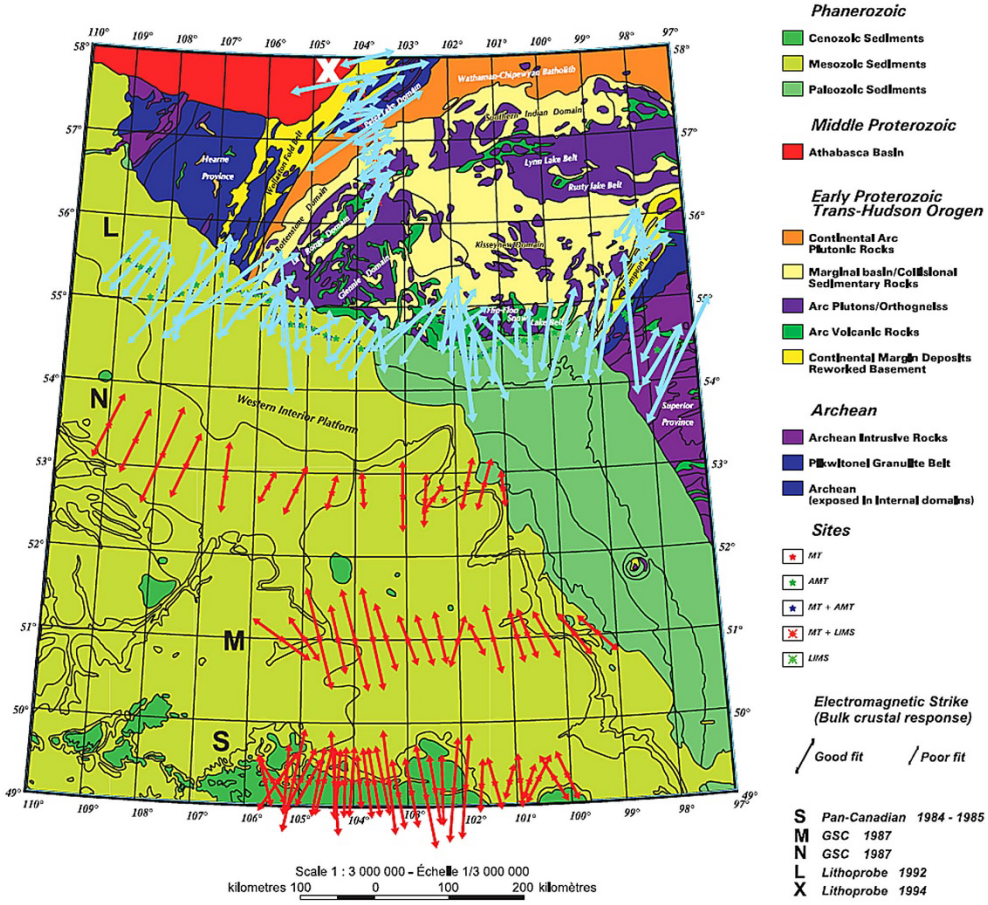

Figure 16. Geoelectric strike directions throughout the Trans Hudson Orogen (Jones et al., 2005). Strike directions are shown for the period range 10–1000 s.

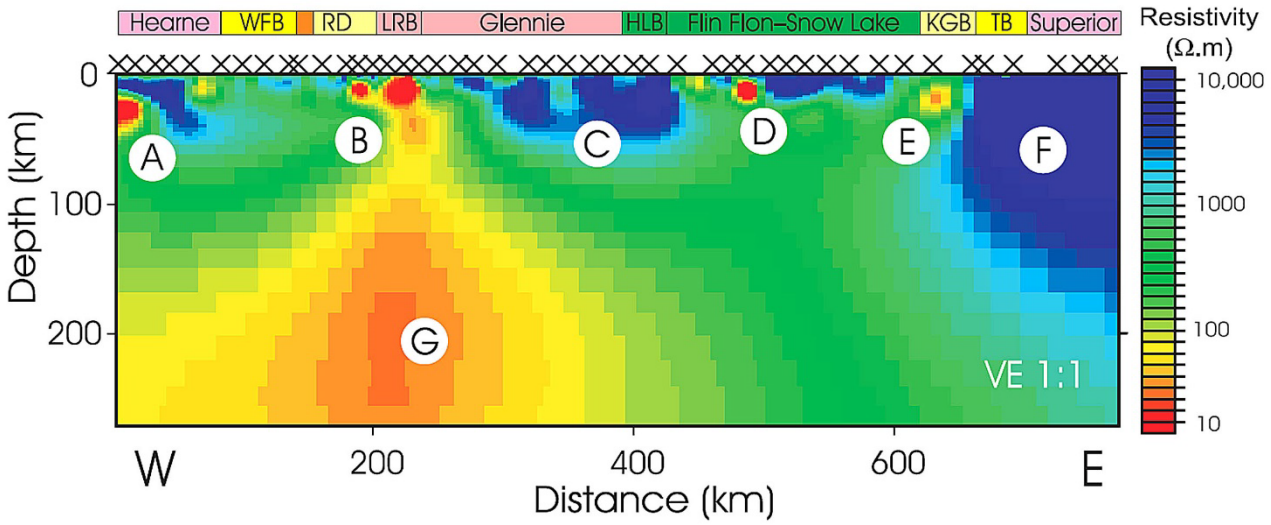

Figure 17. 2-D inversion model for Line L (Jones et al., 2005). The seven labelled features are primary features of the crustal and lithospheric mantle resistivity structure. WFB, Wollaston fold belt; RD, Rottenstone domain; LRB, La Ronge belt; HLB, Hanson Lake block; KGB, Kisseynew gneiss belt; TB, Thompson belt.

The Flin Flon Belt hosts a more conductive feature (D in Figure 17) named the Athapapuskow Lake conductor (Ferguson et al., 1999). This feature lies on the eastern margin of the Sask craton in a similar tectonic

position to an anomaly observed in central and southern Manitoba that was originally named the Thompson Belt (TOBE) conductor (Jones and Craven, 1990 and references therein; Gowan et al., 2009). There is no indication of a strong conductor in the Thompson Belt at the latitude of the LITHOPROBE profiles (White et al., 1999; Jones et al., 2005) so it is possible that both the Athapapuskow and TOBE anomalies are flanking the margin of the Sask craton in the interior of the Trans Hudson Orogen rather than the exterior margin.

The NACP lies in the La Ronge domain (feature B in Figure 17) and is a large conductor containing resistivity values of 10 Ω·m or less. The feature is also observed in the NOD survey (Wu et al., 1993; Wu 1994), Lines S, M, N (Jones and Craven, 1990), and Line X (Garcia and Jones, 2005). Figure 18 shows the resistivity model along LITHOPROBE Line X.

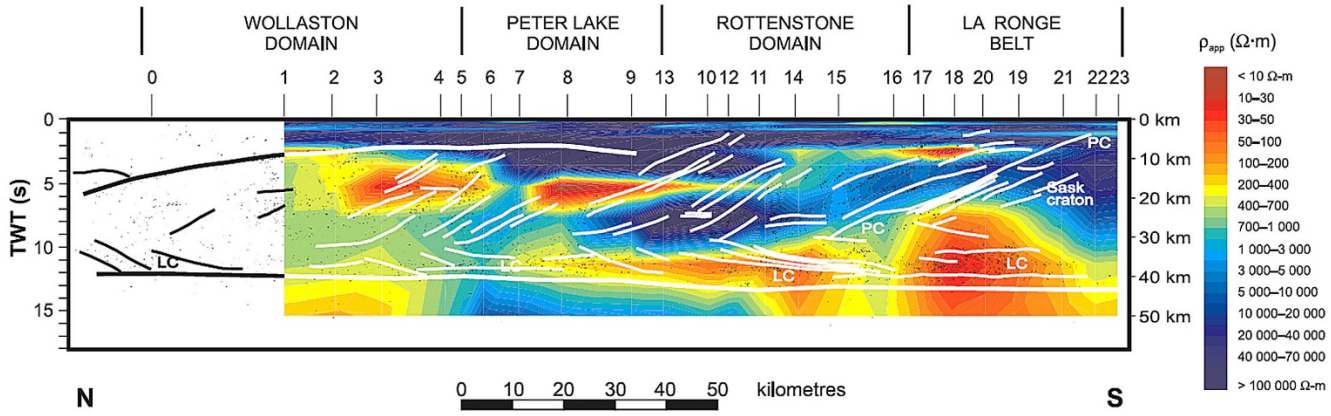

Figure 18. 2-D inversion model for Line X (Garcia and Jones, 2005). The conductor in the La Ronge Belt in the NACP conductor.

The MT results show significant zones of enhanced conductivity in the rocks on the margin of the Hearne craton (Feature A in Figure 17). The Wollaston Domain includes contains conductive crust, with resistivity values <30 Ω·m, on both LITHOPROBE line L (Figure 17) and line X (Figure 18). These results suggest a comparable conductor may occur where the Gillam-Kivalliq corridor crosses the domain.

3.1.3 LITHOPROBE Western Superior Transect The LITHOPROBE Western Superior Transect, which was completed between 1996 and 2001, included MT soundings at a number of sites in the HBB and adjacent area (Figure 19; Ferguson et al., 2005a). These sites have BBMT recordings. Analyses of the Western Superior MT data from the current study area, and just to the south, are described in Ferguson et al. (2005a), Orellana (2006) and Roots and Craven (2017). The remaining parts of the West Superior Transect data set were collected to the south and southeast of Gillam.

In general, real reversed induction arrows in the northwestern Superior craton point outwards towards the Trans Hudson Orogen suggesting that at a large-scale, the Trans Hudson rocks are more conductive. One of the northern sites from the near the current study area (wst30 at ~56 ° N, 93° W) points south towards the Fox River Sill and SBZ. The other two northern sites (wst25 at 56° N, 90° W and wst29 at 57° N, 92.5° W) have arrows pointing north towards Hudson Bay (Figure 19). Geoelectric strike azimuths in the northwest of the study area tend to be sub-parallel to the major geological boundaries (Figure 20). Apparent resistivity and phase responses (Figure 21) confirm that the western Superior craton is characterized by a resistive core centred on the North Caribou terrane with more conductive zones around the margin of the craton. The high phase results seen across much of the northwest craton suggest there is a transition to more conductive rocks in the lithospheric mantle and modelling suggests this occurs at ~150 km depth (Orellana, 2016).

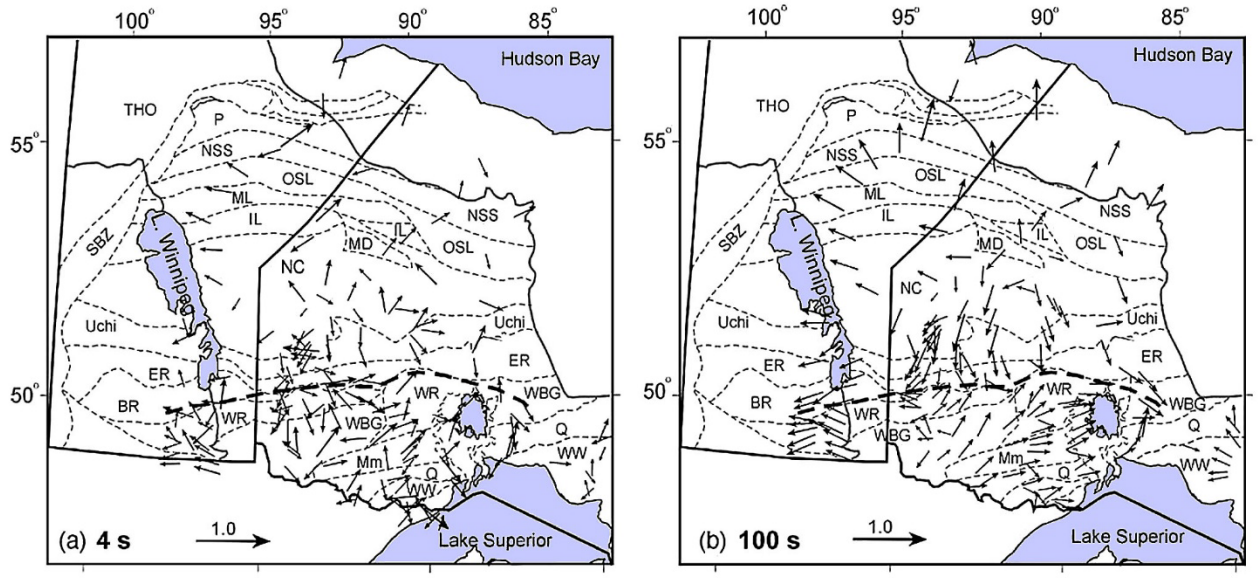

Figure 19. Sites and long-period real-reversed induction arrows from the LITHOPROBE Western Superior Transect (Ferguson et al., 2005a). THO: Trans Hudson Orogen; SBZ: Superior Boundary Zone; NSS: northern Superior superterrane, OSL: Oxford-Stull Lake terrane, ML: Munro Lake subprovince, IL: Island Lake subprovince, MD: Muskrat Dam subprovince, NC: North Caribou terrane, ER: English River subprovince, BR: Bird River-Separation Lake subprovince, WR: Winnipeg River subprovince, P: Pikwitonei, WBG: Wabigoon subprovince, MM: Marmion subprovince, Q: Quetico subprovince, WW: Wawa subprovince.

2-D modelling of MT data from sites in the northwest Superior craton and adjacent Trans Hudson Orogen was completed by Orellana (2006) (Figure 22). The resolution was limited by the approximately 100 km site spacing. The results show the crust of the Trans Hudson Orogen is indeed more conductive than for the Superior craton. There is particularly conductive crust beneath wst30. The northwest and central profiles show conductive material extending from depths of ~50 km in the Trans Hudson Orogen to depths of 100–150 km beneath the Superior craton (Orellana, 2006). This feature may be responsible for the southward pointing induction arrow at wst30. The same structures may exist for the southeast profile but is not as clearly resolved.

3-D inversion of data from the western Superior craton confirms the generally resistive nature of the crust and uppermost mantle in the northwest part of the craton (Figure 23; Roots and Craven, 2017) with more conductive materials to the south. It also shows the increase in conductivity beneath the northwest of the craton at depths exceeding 110 km.

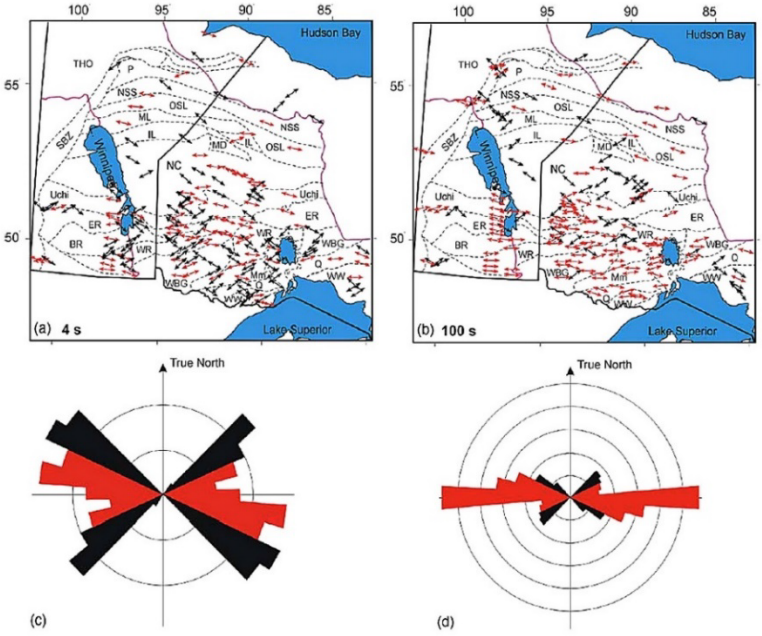

Figure 20. Groom–Bailey regional strike directions at (a) 4 s period and (b) 100 s period (modified from Ferguson et al., 2005a). There is a 90º ambiguity in the determination of the geoelectric strike: results have been plotted in the quadrant containing the dominant surface geological strike, i.e. they are constrained to lie between azimuths of 45º and 135º. Symbols are colour coded to discriminate between strike populations. Angles close to east–west (60–120º) are shown in red and angles close to northeast–southwest or northwest–southeast (0–60º and 120–180º) are shown in black. Rose diagrams of the (c) 4 s and (d) 100 s GB strike directions are shown using the same colour coding.

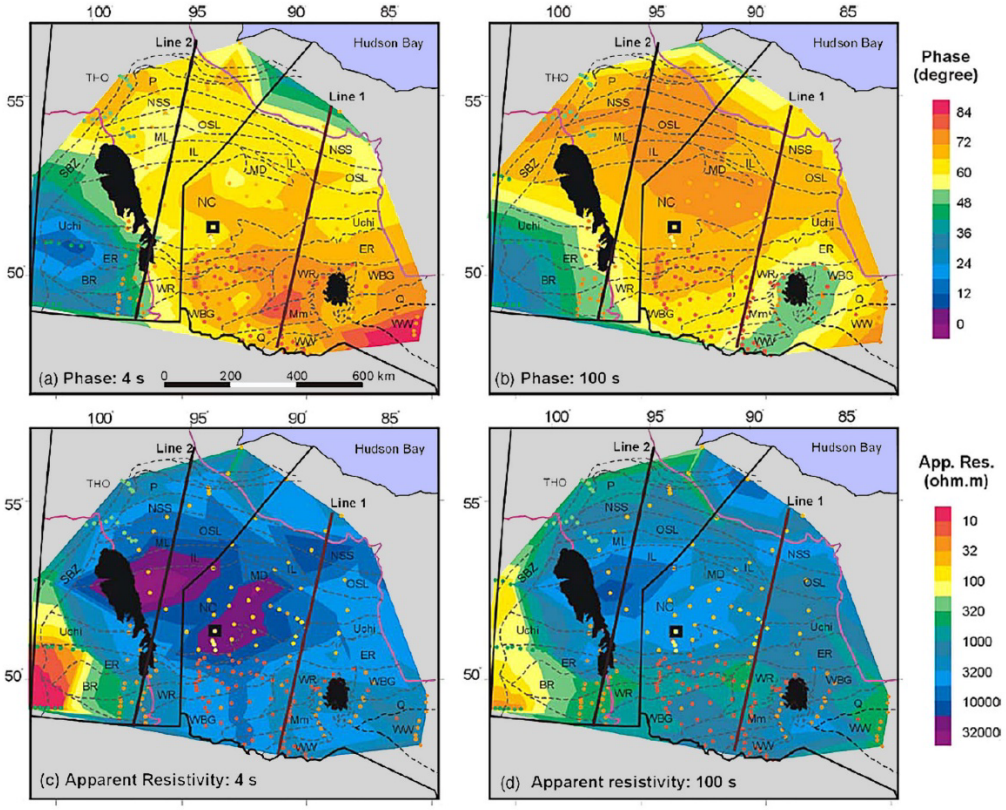

Figure 21. Contour maps of the determinant apparent resistivity response and phase response: (a) phase at 4 s; (b) phase at 100 s; (c) apparent resistivity at 4 s; (d) apparent resistivity at 100 s (modified from Ferguson et al., 2005a).

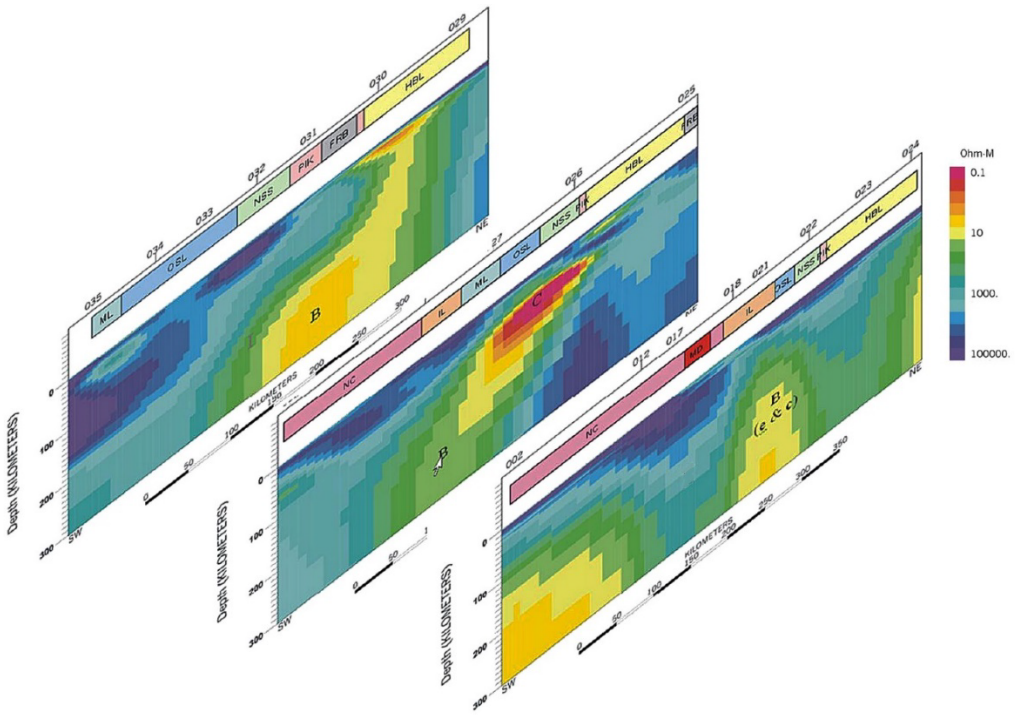

Figure 22. 2-D models of MT data from sites in northwest Superior craton and adjacent Trans Hudson Orogen (Orellana, 2016). Profiles are shown in approximately their true southwest to northeast orientation.

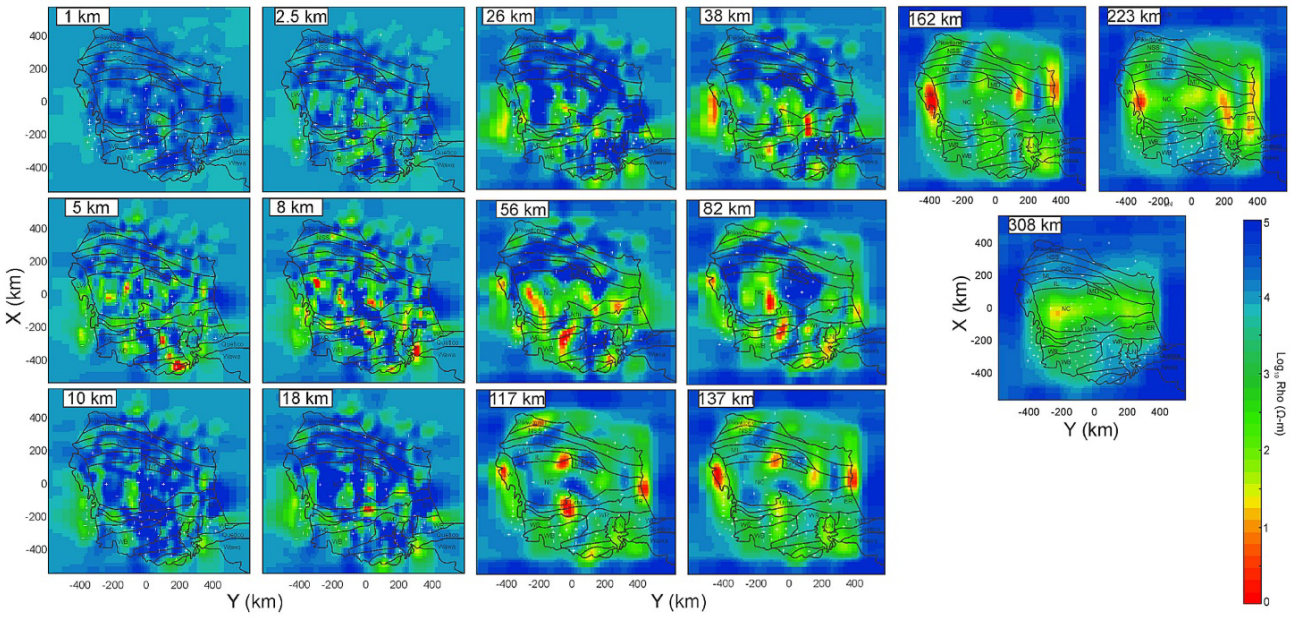

Figure 23. Depth slices through the 3-D inversion model (Roots and Craven, 2017). Crosses indicate site locations. Solid black lines indicate subprovince boundaries. NSS: northern Superior superterrane, OSL: Oxford-Stuff Lake terrane, ML: Munro Lake subprovince, IL: Island Lake subprovince, MK: Muskrat Dam subprovince, NC: North Caribou terrane, ER: English River subprovince, WR: Winnipeg River subprovince, WB: Wabigoon subprovince, LW: Lake Winnipeg, LN: Lake Nipigon.

3.1.4 Snowbird Tectonic Zone (1998) LMT recordings were made at 8 sites crossing the STZ from the Rae to the Hearne province in 1998 (Figure 24; Jones et al., 2002). These sites overlap with the Rankin Inlet to Baker Lake part of the Gillam-Kivalliq Hydro-Fibre link. Teleseismic recordings were made at the same sites.

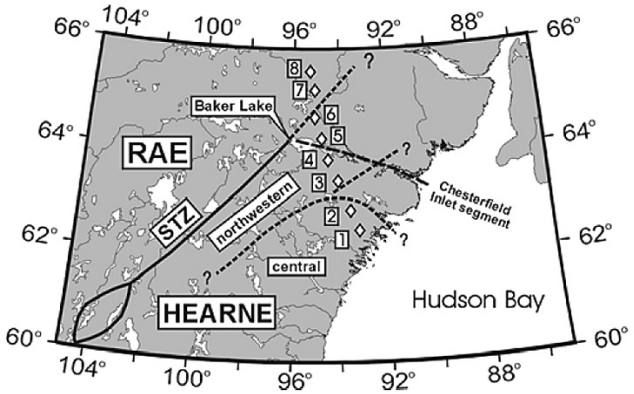

Figure 24. LMT site locations in the 1998 STZ survey (Jones et al., 2002).

After correction for galvanic distortion, MT data indicated a N110º E strike direction. The azimuth of induction arrows is rather variable but indicates E-W to SW-NE trending conductive features (Figure 25). South of Baker Lake, the fast direction indicated by SKS analysis of teleseismic data is roughly perpendicular to the conductors whereas to the north it is parallel (Jones et al., 2002). 2-D inversion models reveal a consistently resistive crust at the two most northern sites (Figure 26). Farther south, there is a major change in crustal structure near Baker Lake. To the north, sites 5 and 6 exhibit a conductive upper crust and resistive lower crust whereas to the south, the upper crust is resistive and the lower crust is conductive (Jones et al., 2002). The sub-continental lithospheric mantle (SCLM) is less resistive to the south, and this is interpreted as a change from Rae mantle to Hearne mantle (Jones et al., 2002).

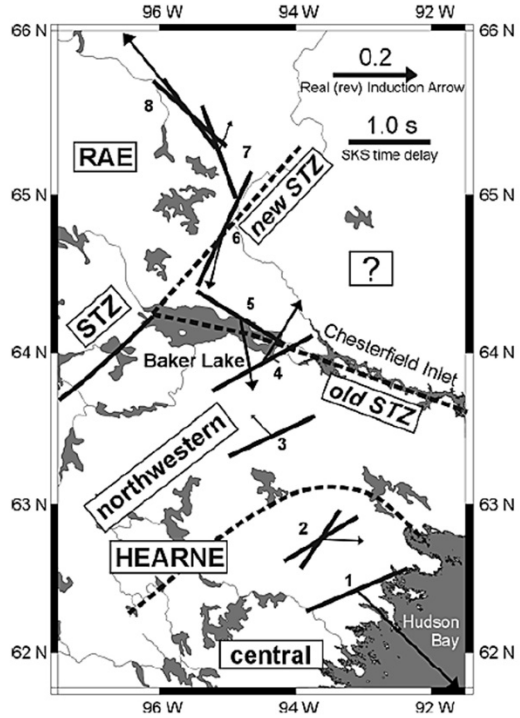

Figure 25. MT and SKS responses from STZ survey (Jones et al., 2002). Headed arrows: Real (reversed) induction arrows at 320 s scaled to the 0.2 s arrow shown in the legend. Unheaded arrows: single-event SKS splitting analyses scaled to the 1.0 s arrow shown in the legend.

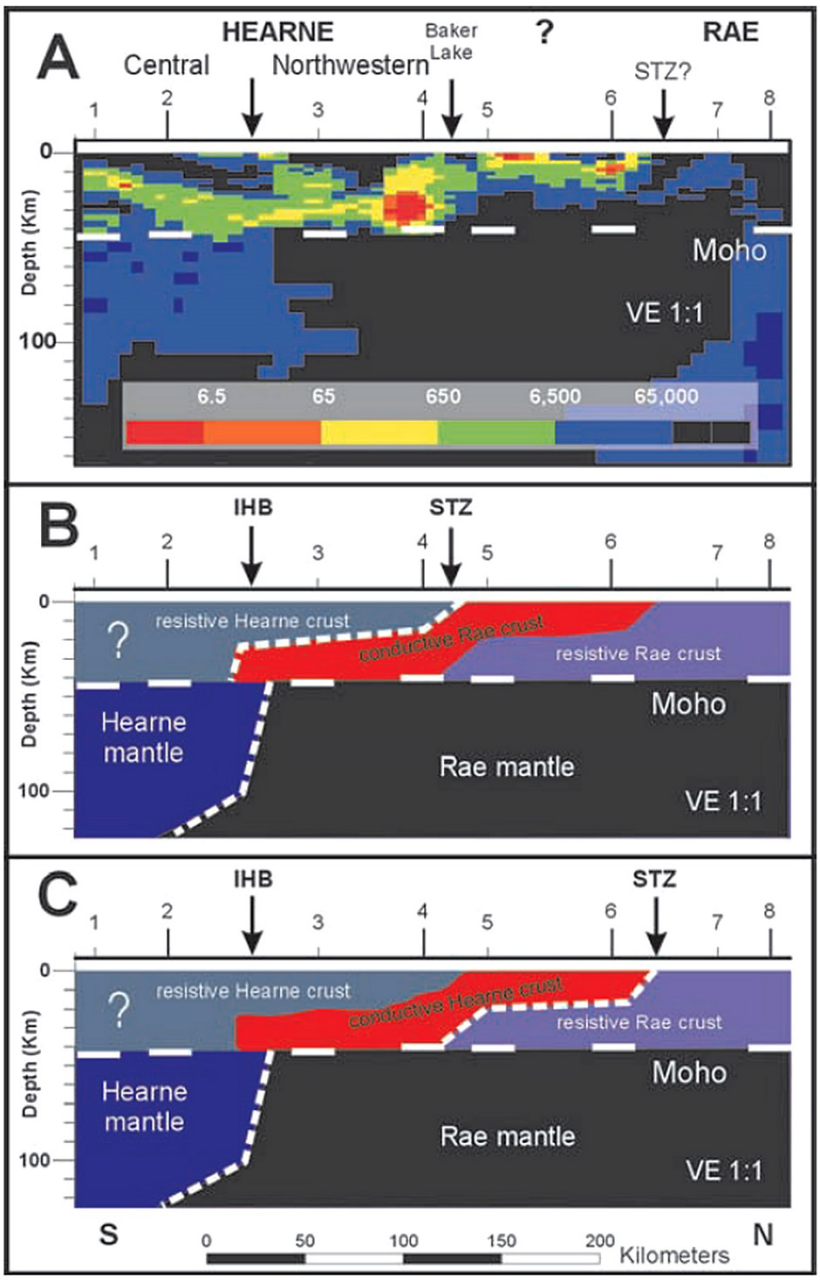

Figure 26. 2-D resistivity model and alternative interpretation (Jones et al., 2002).

3.1.5 Fox River Sill and Knee Lake MT profiles (2002–2004) In 2005 the Geological Survey of Canada conducted a MT survey in a roughly southwest-northeast profile that extended from the northern end of Lake Winnipeg to Hudson Bay (Figure 27). The Knee Lake survey sites are located over the Hudson Bay Basin (HBB) and the geological domains of the North Superior superterrane (NSS), Oxford-Stull Lake (OSL), Fox River Belt (FRB) and Pikwitonei Green Belt (PGB) in the Superior Province. Site spacing used for the Knee Lake profile varied greatly, from 8 to 60 km. Fox River Belt (FRB) data were acquired as part of the LITHOPROBE Western Superior Transect in 2000 (Figure 27) and comprised 10 AMT and 3 BBMT sites. The total length of the profile that crossed the sill was 1.4 km with variable site spacing ranging from 65 to 200 m controlled by site accessibility. A study conducted by McLeod (2014) used the Knee Lake and Fox River profiles and additional MT data from the LITHOPROBE Western Superior Transect.

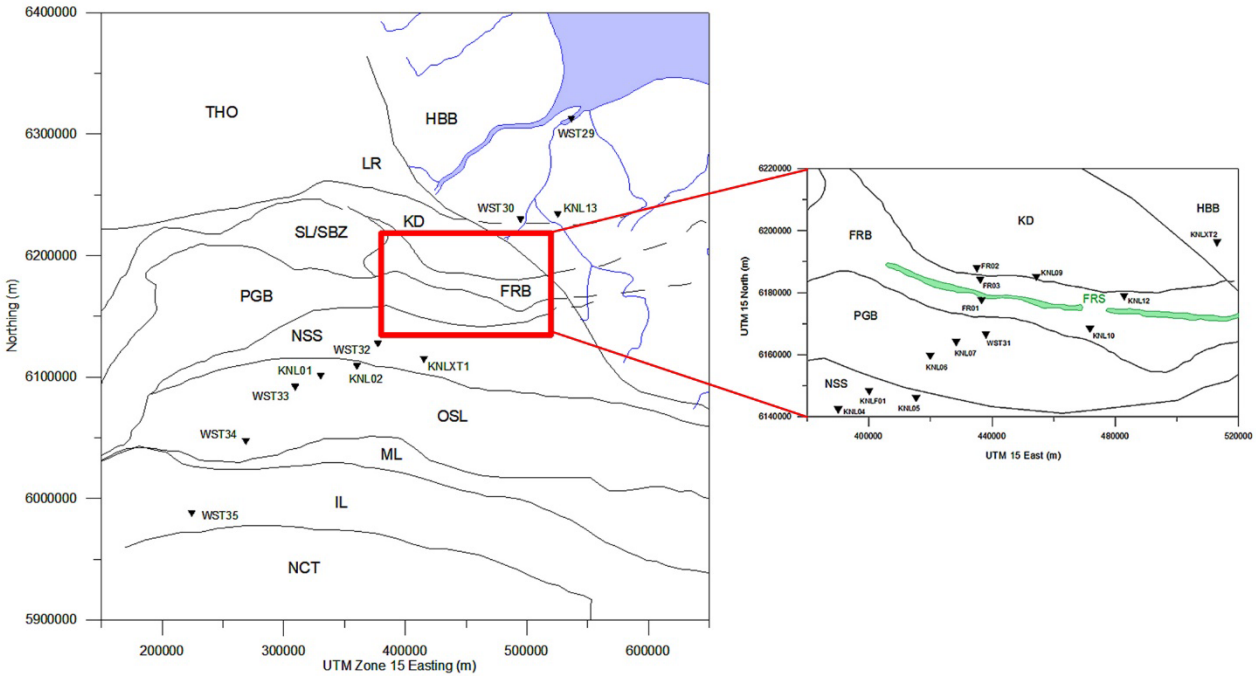

Figure 27. Map showing the Knee Lake (KNL) and Fox River Belt (red rectangle) survey sites in relation to the geological domains (modified from McLeod, 2014). NCT = North Caribou terrane; IL = Island Lake terrane; ML = Munro Lake terrane; OSL = Oxford-Stull Lake terrane; NSS = North Superior superterrane; PGB = Pikwitonei Gneiss domain; FRB = Fox River belt; FRS = Fox River Sill; SL/SBZ = Split Lake block/Superior Boundary Zone; KD=Kisseynew domain, LR=La Ronge domain; THO = Trans Hudson Orogen; HBB = Hudson Bay basin.

Various strike analysis methods were used such as the Swift strike, Groom-Bailey strike and a more advanced Groom-Bailey strike analysis (Groom and Bailey, 1989; Jones 2012). The latter provided the most acceptable results and was calculated using four period ranges; 0.0001 to 0.01 s, 0.01 to 1 s, 1 to 100 s and 100 to 10000 s. The data were then processed through the STRIKE program that utilizes the Niblett-Bostick depth transformation displaying geoelectric strike at various depths ranges (McNeice and Jones, 2001). The results are shown in Figure 28 where the 4 to 40 km depth range illustrates a crustal depth and 40 to 200 km represents the mantle (McLeod, 2014). Strike trends appear to be bimodal, sub-parallel with geological boundaries and north-south direction with some strikes falling between 112.5º and 135º (McLeod, 2014).

Regional dimensionality analysis was conducted on each survey site using the WALDIM program (Martí et al., 2004; Figure 29). The majority of the data exhibited 2-D behavior however, the response at periods larger than 0.1 s through the NSS and PGB profile displayed 3-D behavior between KNL-XT1 and WST 31 (McLeod, 2014). At periods of less than 0.01 s, sites KNL13 and WST29 through to WST30 display 1-D behavior beneath, which is expected for the locations on the Phanerozoic HBB strata.

The geoelectric strike chosen for modeling and inversions was Az127º, which correlated well with the linear and sub-parallel geological boundaries in the study area. Transverse electromagnetic (TE) and magnetic (TM) pseudo-sections were generated. All MT survey sites were used for a 2-D inversion. The inversion model provided a good fit to the main features in the pseudosections (Figure 30) and has an RMS value of 3.316 (for phase error floors of 6% for TE and 3% for TM and apparent resistivity error of 48% for TE and 24% for TM). Larger RMS values occurred in parts of the profile with denser site spacing, specifically in the PGD to FRD area (McLeod, 2014).

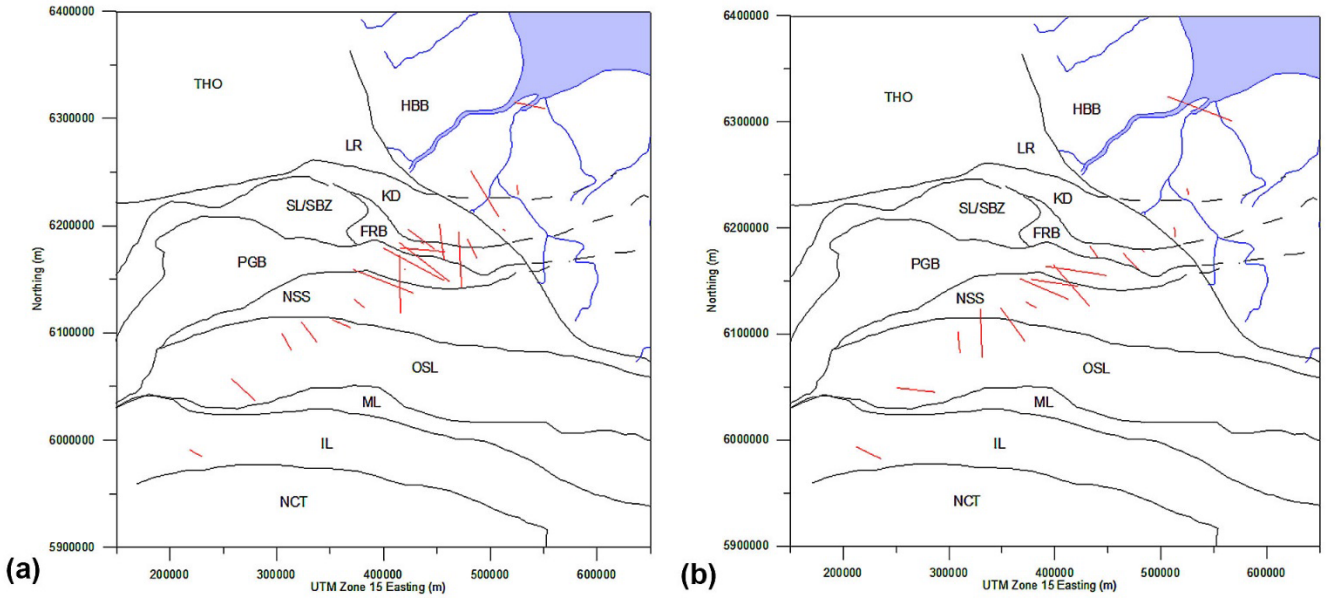

Figure 28. Geoelectric strikes (red lines) at a depth range of (a) 4 to 40 km representing crustal depth and (b) 40 to 200 km representing mantle depth (modified from McLeod, 2014).

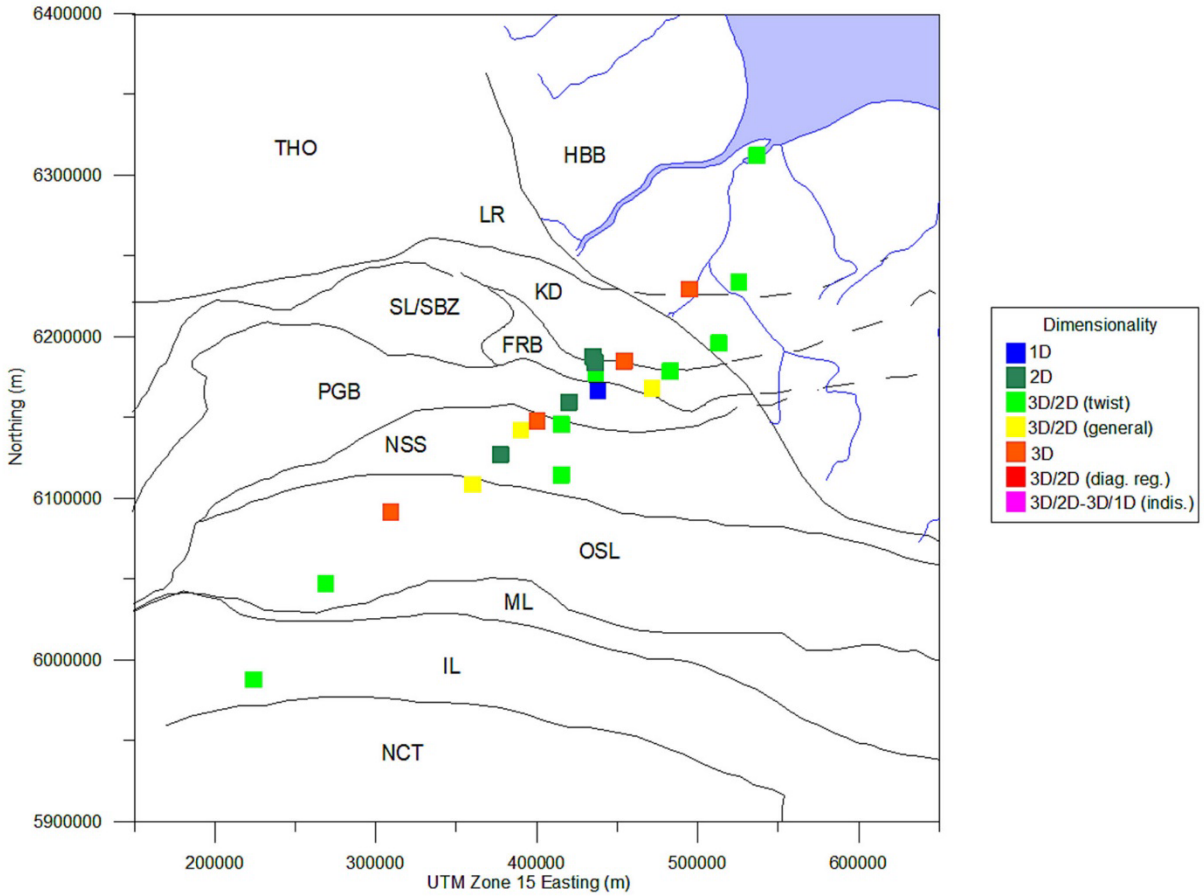

Figure 29. Dimensionality analysis of each MT survey site for the 1 to 100 s period band. Colored squares represent the dimensionality (modified from McLeod, 2014).

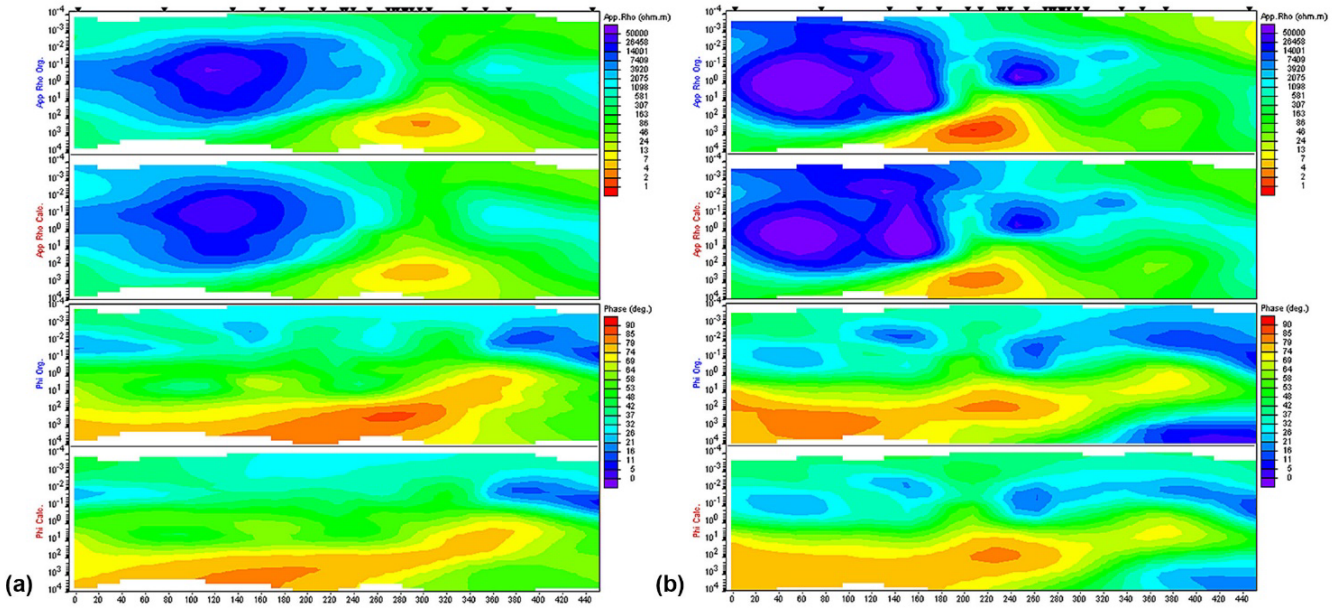

Figure 30. Observed and model pseudosection responses (modified from McLeod, 2014). (a) TE responses. First and third panels the observed pseudosections panels two and four are the inverted model pseudosection. (b) TM responses with the four panels showing the same information as for the TE results.

The final 2-D resistivity model by McLeod (2014) has three resolved conductive features to be noted; Figure 31 illustrates them as conductors A, B and C however, for the purposes of the current study, only conductor B and C will be discussed. The crustal part of the model displays characteristic high resistivity as noted in the earlier Western Superior and Trans-Hudson Orogen studies. For sites in the NSS at 40 to 90 km depth, there is an anomaly (conductor B) has conductivity values ranging from 1 to 3 Ω·m. Conductor C, occurs on the northern margin of the FRB. McLeod (2014) also suggested the conductor may represent an extension of the NACP. McLeod (2014) also suggested that the conductor may represent a continuation of the Thompson Belt Conductor (TOBE). To the southwest, this feature lies in the Trans Hudson Orogen on the eastern margin of the Sask craton and to the west of the Superior Boundary Zone (SBZ) (e.g., Figure 17).

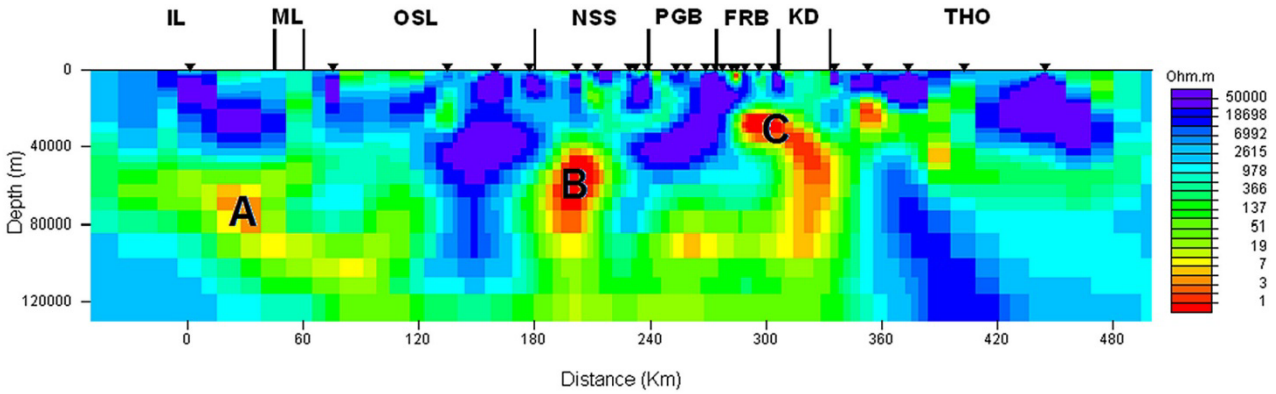

Figure 31. Final inversion along the profile of sites shown in Figure 29 (McLeod, 2014).

The Fox River Belt transect included a profile of three BBMT sites and ten (AMT sites crossing the Fox River Belt and Fox River sill. Analyses of the data area are described in Orellana (2006), Epp (2014), and Ferguson (2015). The resulting models include a moderate conductor at shallow depth that correlates with a magnetic unit in the Fox River Sill and has been interpreted as sheared magnetite-rich serpentinite.

3.1.6 Southampton Island Integrated Geoscience and Cape Donovan MT surveys (2007–2008, 2018) As part of the Southampton Island Integrated Geoscience Program, BBMT data were collected at 29 sites and LMT data at 6 sites on Southampton Island in 2007–2008 (Figure 32; Spratt et al., 2012). The sites span the transition from the eastern half of the island that exposes Precambrian rocks, and its southwest part which is overlain by Paleozoic cover, areas possessing very different geophysical trends.

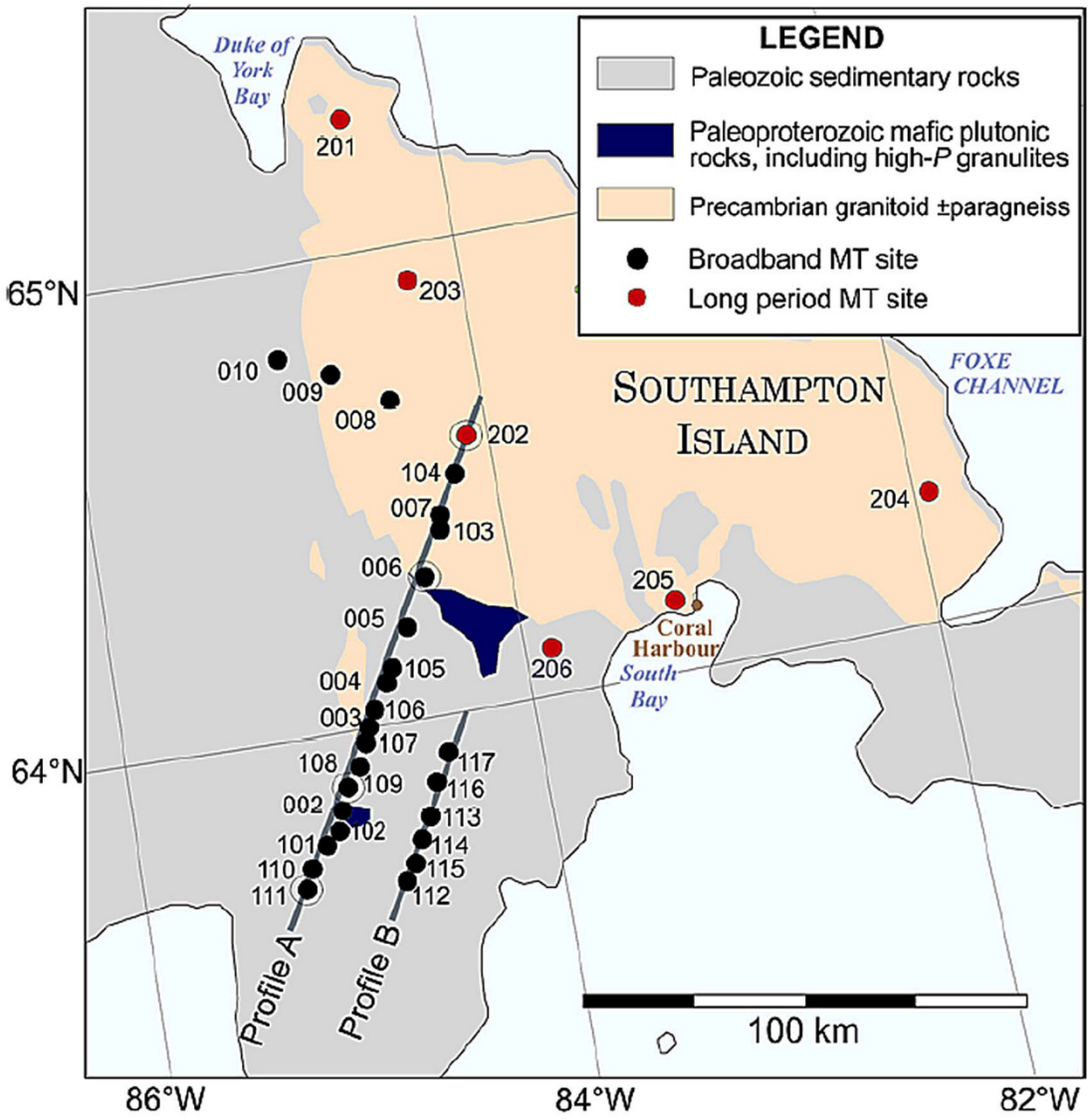

Figure 32. Simplified geological map of Southampton Island showing the location of MT sites (Spratt et al., 2012). The grey lines show the position of the profiles used for 2D modelling.

The geoelectric strike directions for the whole survey is pervasively in a NW-SE azimuth (Figure 33). The strength of the two-dimensionality does not show large-scale trends in location or period. Simplified 3-D modelling suggests the main effect of the oceans on the MT response at the survey sites occurs at periods exceeding 10 s (Figure 34).

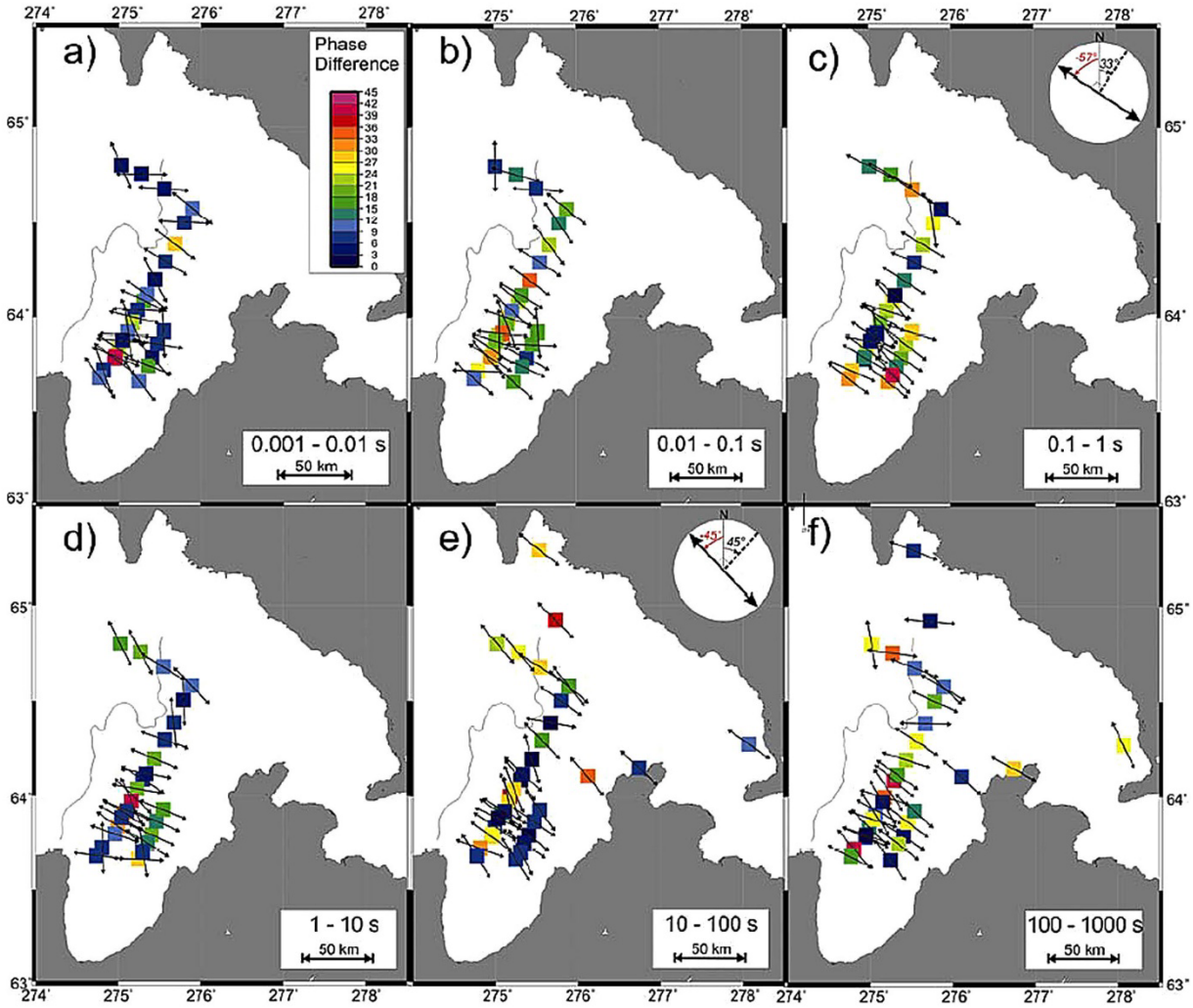

Figure 33. Maps showing the preferred geoelectric strike direction with a 90º ambiguity at each site for single decade period bands (Spratt et al., 2012). The color scale illustrates the maximum difference between the TM- and TE-mode phases (phase difference).

A 2-D model for Profile A is shown in Figure 35. A laterally uniform, resistive (>30,000 Ω·m) crust underlies the eastern half of the island and extends to a depth of 30 km. However, the rocks beneath the Paleozoic cover to the southwest include a conductive zone (<30 Ω·m in the upper crust). The deep structure along profile A includes a moderately conductive upper mantle (200–300 Ω·m) but it is unclear to what extent this feature is affected by large-scale 3-D structures such as the surrounding oceans.

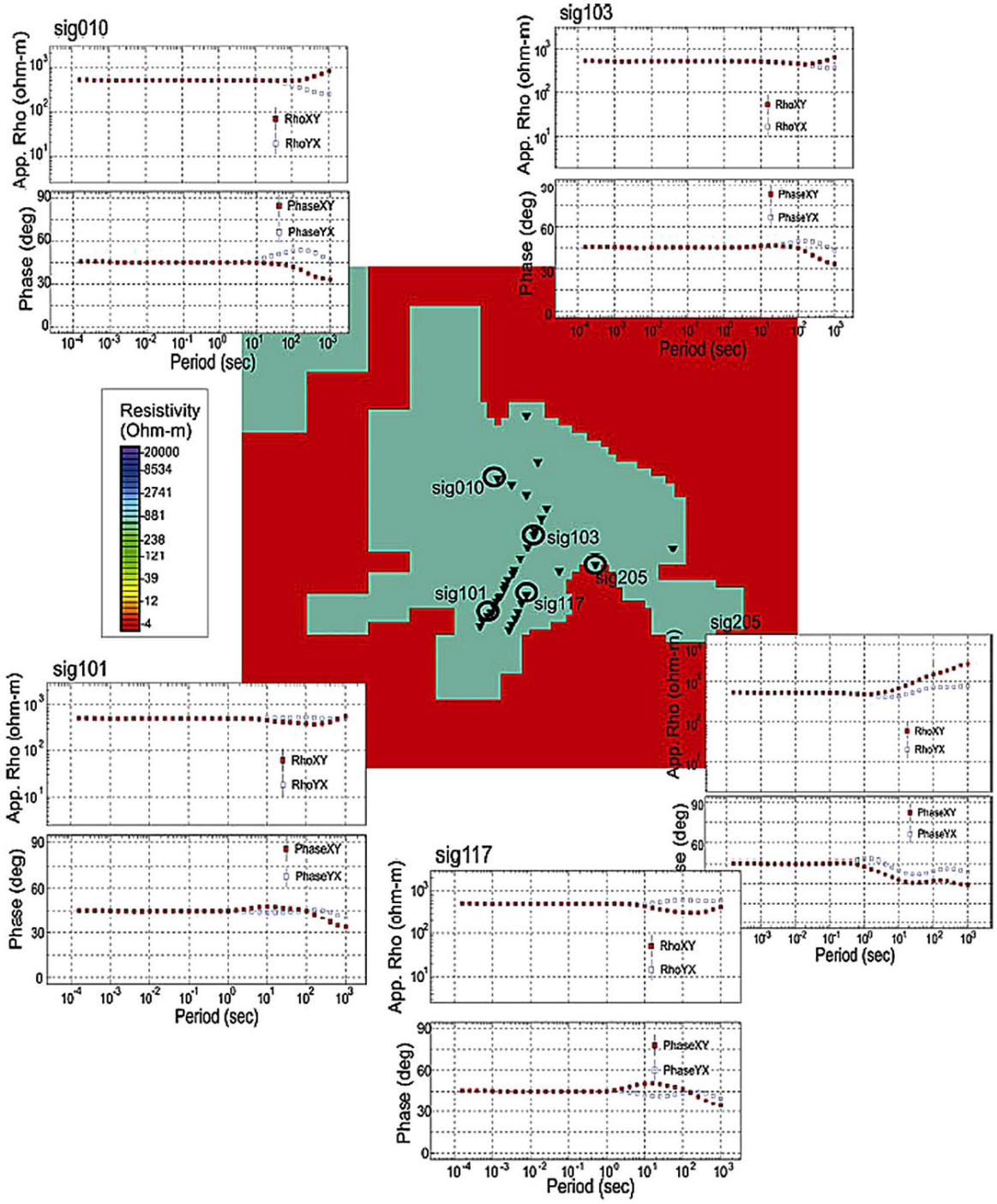

Figure 34. A 3-D mesh of the MT survey area showing simplified land versus ocean conductivity Contrast (Spratt et al., 2012). Examples of the forward calculated response curves are shown for profile A (SIG101, SIG103), profile B (SIG117), remote broadband (SIG010) and remote long period (SIG204) sites.

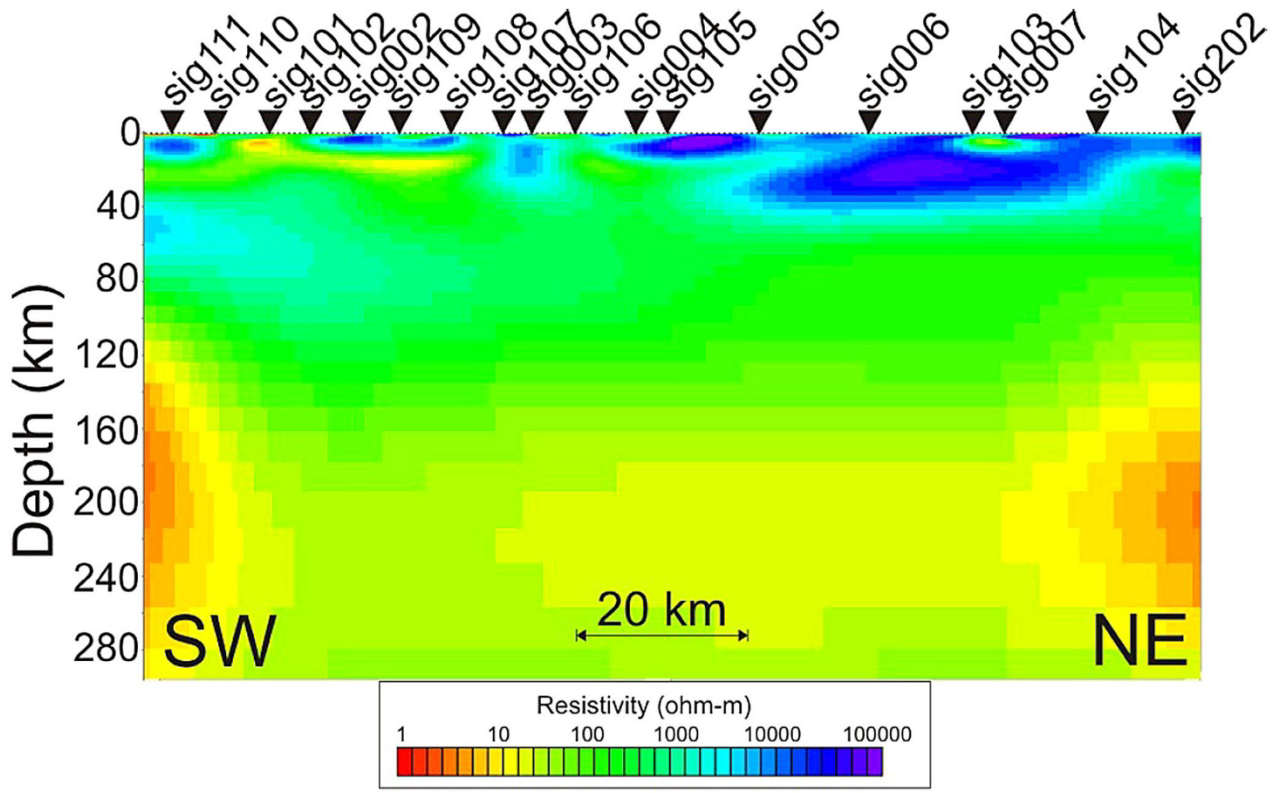

Figure 35. Preliminary 2-D model of the MT data along profile A, at a strike angle of -57°, shown to 300 km depth (Spratt et al., 2012).

A smaller-scale MT survey was completed at Cape Donovan on the northwest coast of Southampton Island in 2018 (Craven et al., 2018). The objective of the survey was to delineate a known occurrence of hydrothermal dolomite, and to define the subsurface geology and structural features on the cape (Marks, 2019). The survey included both BBMT and AMT recordings. Depth-dependent Groom-Bailey tensor decomposition defined a geoelectric strike of N55º W similar to that observed in the larger-scale MT survey on the island. The Ordovician sequence on Cape Donovan was determined to be ~300 m thick with a resistivity >1000 Ω·m. The relatively high resistivity values suggest the absence of conductive pore fluids. A fault system is the most likely interpretation for sub-vertical and sub-horizontal conductive features observed in the model, and this interpretation is supported by aeromagnetic data and visual observations. The faults may be related to post-Silurian uplift of the Boothia-Bell Arch and/or Upper Cretaceous-early Paleocene normal faulting (Marks, 2019).

3.17 Central Rae craton MT survey (2010–2012) MT surveys, including both BBMT and LMT recordings, were done in the central Rae craton in 2010–2012 along four profiles (Spratt et al., 2014). Parts of the survey to the north supplement information from the Melville Peninsular (Spratt et al., 2013), from Southampton Island (Spratt et al. 2012), and from Baffin Island (Evans et al., 2005) (Figure 36). Data from a number of these surveys was considered in a large-scale 3-D study of both MT and teleseismic data by Snyder et al. (2015).

The southern end of Profile 2 includes a second crossing of the southern part of the Rae craton and Chesterfield Block supplementing the information on these geological units in Jones et al. (2002) (see Section 3.1.5) (Figure 37). Sites dmn204–dmn204 in this area exhibit geoelectric strike azimuths, that allowing for the 90º ambiguity, are consistent with E-W to ENE-WSW strike directions (Figure 38). The two-dimensionality of the responses is moderate to strong.

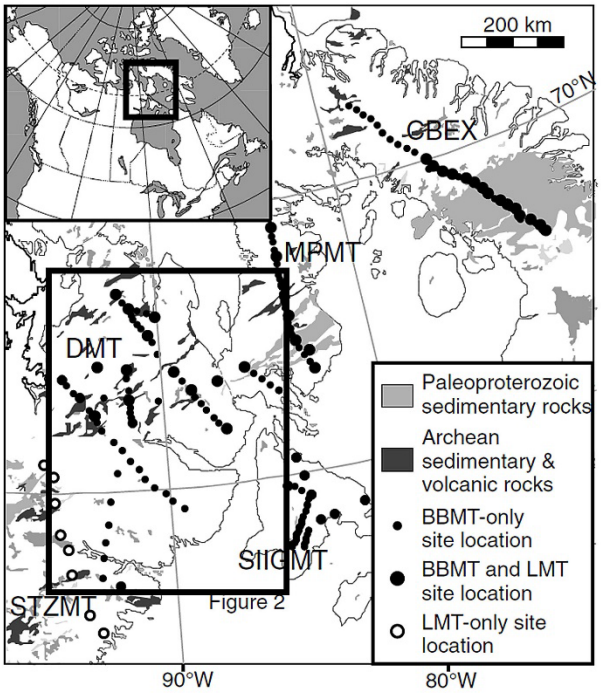

Figure 36. Recordings in the Central Rae craton (Spratt et al., 2014). CBEX = the Central Baffin Magnetotelluric Experiment, MPMT =Melville Peninsula Magnetotelluric survey, DMT = Diamonds Magnetotelluric survey, STZMT = Snowbird Tectonic Zone Magnetotelluric survey, and SIIGMT = Southampton Island Integrated Geoscience Magnetotelluric survey.

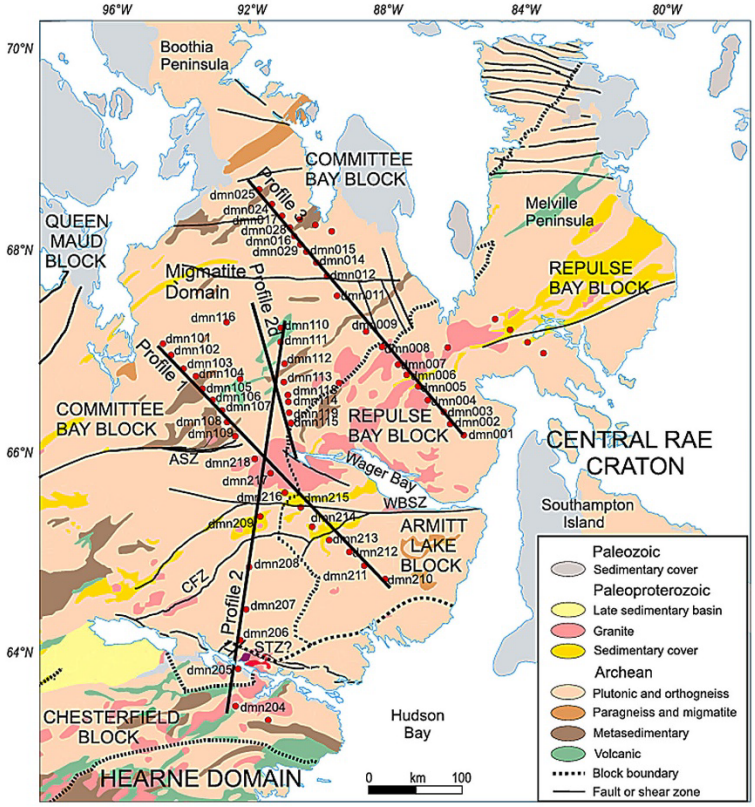

Figure 37. Location of MT sites and modelling profiles relative to geological features in the Central Rae craton (Spratt et al. 2014).

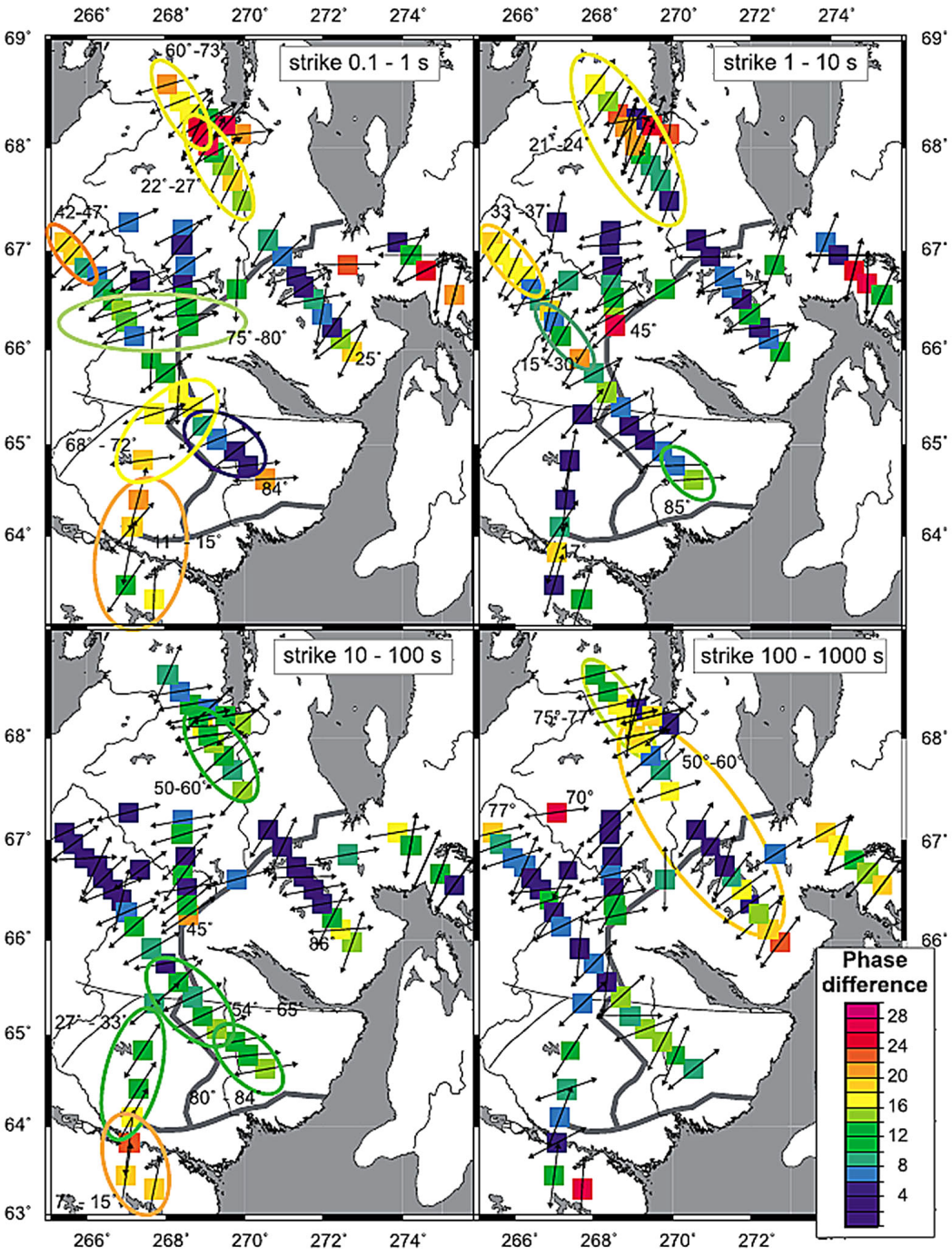

Figure 38. Maps showing the preferred geoelectric strike direction at each site along the profiles (Spratt et al., 2014) The color scale shows the maximum difference between the TM- and TE-mode phases. Ellipses highlight areas with a consistent strike among several sites.

For the whole survey area, 2-D inversion results reveal extremely resistive upper crust and more conductive lower crust but with conductors projecting to the surface near major structures (Spratt et al., 2014; Snyder et al., 2015). The uppermost mantle of the Rae craton increases in resistivity from the northeast to the south with resistivity values that range from ~3000 Ω m in the northeast (beneath Baffin Island and the Melville Peninsula) to ~10,000 Ω m beneath the central Rae craton, to >50,000 Ω m in the south near the Hearne Domain

(Spratt et al., 2014). It includes near-vertical zones of reduced resistivity that were tentatively interpreted to be related to areas affected by mantle melt or metasomatism associated with emplacement of Hudsonian granites. The models exhibited a regional decrease in resistivity to values of ~500 Ω·m at depths of 180–220 km, increasing to 300 km near the southern margin of the Rae craton, interpreted as the lithosphere-asthenosphere boundary. In contrast, 3-D inversions suggested a more resistive lower crust and that the mantle at 70–120 km is almost everywhere conductive (<500 Ω·m).

Figure 39 shows the 2-D model for Profile 2. The results are quite consistent with those of Jones et al., (2002) with the conductive part of the crust dipping southwards from the upper crust to the lower crust through the Chesterfield Block and with the mantle becoming more conductive to the south.

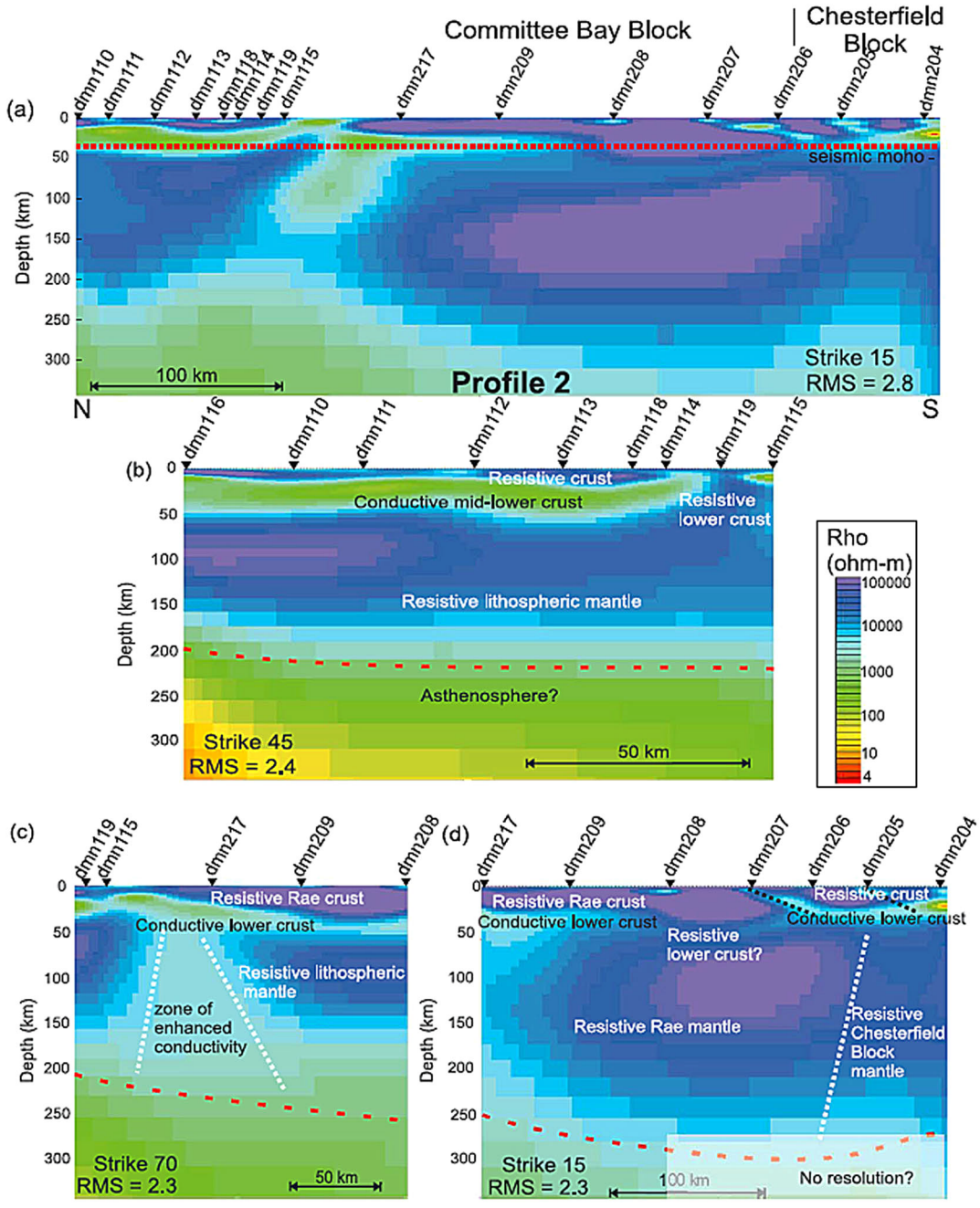

Figure 39. 2-D resistivity models along profile 2 (Spratt et al., 20014). Results are shown for different strike angles.

Results from Melville Peninsula and Baffin Island confirm the presence of extremely resistive upper crust in the Rae craton (Evans et al., 2005; Spratt et al., 2013). These surveys also revealed the very conductive response of Paleoproterozoic metamorphosed sedimentary rocks. In the Baffin Island survey, the Piling Group included rocks of <10 Ω·m with this response interpreted to be due to the <2 km thick graphitic Astarte River Formation. In the Melville Peninsula survey, the supracrustal pelitic gneiss of the Penrhyn Group included rocks of <10 Ω·m.

3.1.8 Manitoba Hydro Bipole III (2011) Electromagnetic measurements were done at Manitoba Hydro Bipole III candidate electrodes sites in 2010 using time domain electromagnetic (TEM) and frequency domain electromagnetic (FEM) surveys, MT, and borehole datasets. The survey was based on the eight potential location of electrode sites over a 10 x 10 km^2 area located near Nelson River, northeast of Gillam (Figure 40). The purpose of the study was twofold: to provide subsurface resistivity information in order to rank the Bipole III candidate electrode sites in northern Manitoba and to develop an electrode design. The study involved calculation of ground potential rise (GPR) which utilizes large scale regional deep resistivity information (Adetunji and Ferguson, 2012). The survey area overlies the rocks of the Hudson Bay Basin (Figure 40). Surficial sediments that range in depth from 25 to 75 m, thinnest at the margin of the Hudson Bay Basin and thickening towards the northeast. The Hudson Bay Basin, in turn overlies the Precambrian Trans Hudson Orogen basement.

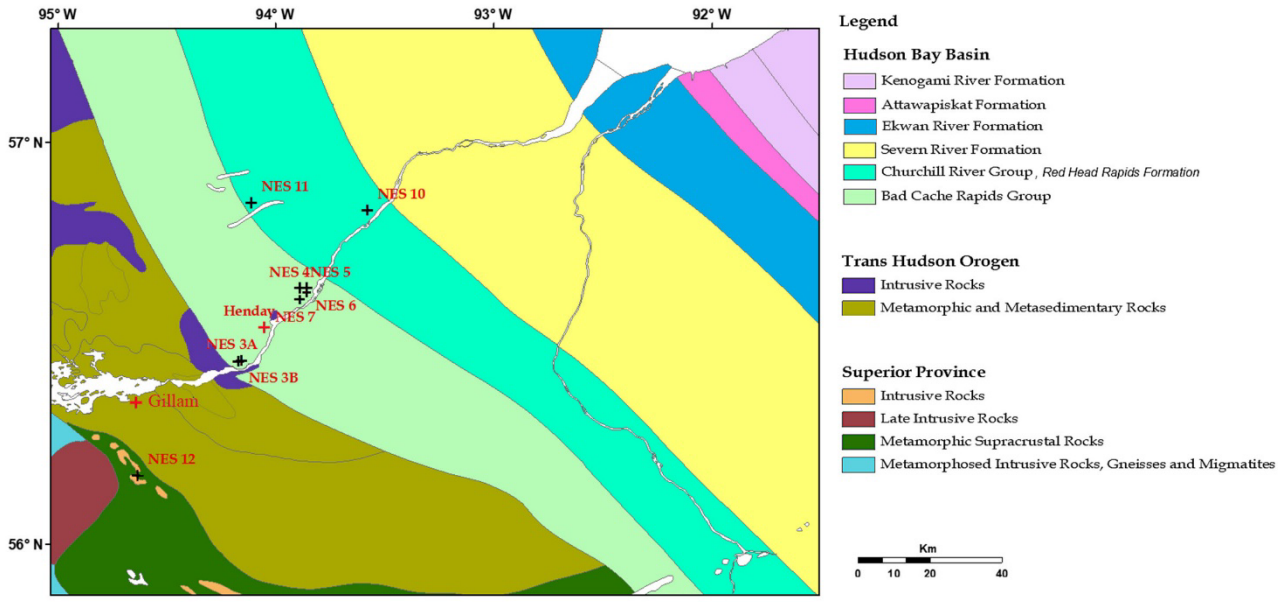

Figure 40. Simplified geology map of the survey area with MT sites, denoted as NES (Adetunji and Ferguson, 2012)

BBMT and AMT soundings were completed at the candidate electrodes sites by Quantec in 2010 (Tournerie and Coulson, 2010 referenced in Adetunji and Ferguson, 2012). The sites are denoted by the prefix *NES* in Figure 40. Higher frequency data were collected at a high frequency remote-reference site (denoted *Rmn_HF*) and lower frequency data at a low frequency remote reference site (denoted *Rmn-LF*). The MT survey used five channel, tensor and referenced remote recordings with frequencies ranging from 0.00002 to 400 Hz for MT and 1 Hz to 25 kHz for AMT. Lower frequency recordings had recording time between 14 to 48 hours. Tournerie and Coulson (2010) describe basic analyses of these data and Adetunji and Ferguson (2012) describe more detailed analysis including 2-D modelling.

Spectral analysis demonstrated that frequencies between 2 and 4 Hz suffer from severe electromagnetic interference due to nearby power lines, dams and railways. This noise was not able to be removed from the dataset and therefore the response at sites NES 3,4, 5, 6, 7 and 12 was muted over the frequency band 0.1 and 10 Hz. Data points were also excluded at periods near 10^{-3} s, in the AMT deadband. Short period data display matching *xy*- and *yx*-mode apparent resistivity curves suggesting 1-D behavior whereas at longer periods, the curves begin to separate indicating departure from 1-D to 3-D geoelectric structure (Figure 41).

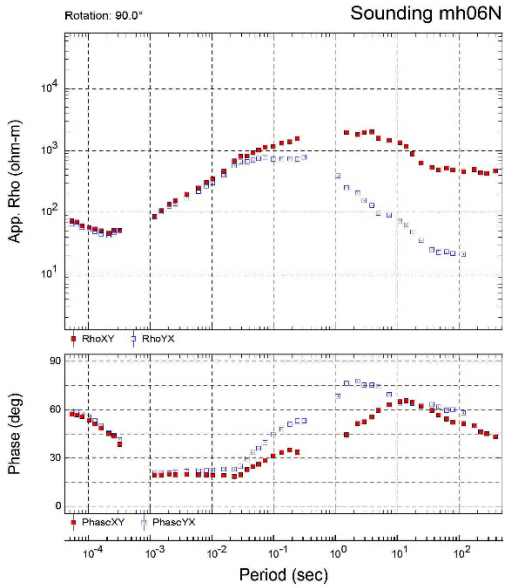

Figure 41. Apparent resistivity and phase curves from NES 6. At shorter periods the apparent resistivity curves are similar, but there is clear departure at larger periods (Adetunji and Ferguson, 2012)

MT induction arrows display a southwest trend for all sites with a reversal at NES 12 suggesting the presence of a conductor with a geoelectric strike in the southwest-northeast orientation between NES12 and the other sites (Adetunji and Ferguson, 2012; Figure 42). Comparison of the location of the conductor with the results of the IMS survey and with those from the Knee Lake profile suggest that it is likely the same feature and therefore that all three profiles are imaging the NACP.

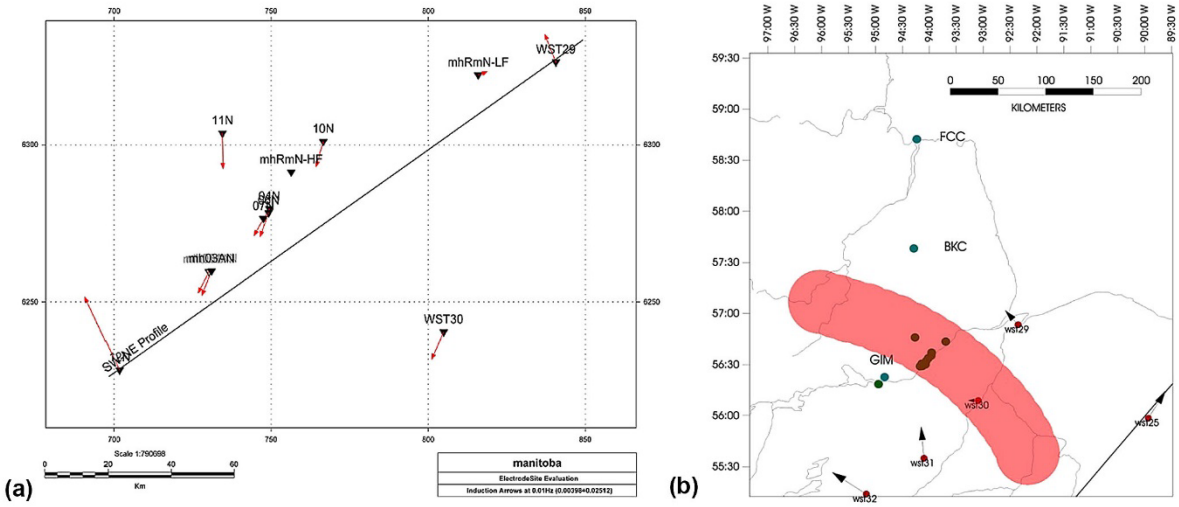

Figure 42. (a) Induction arrows (reversed real component) in the Bipole III study area for period of 100 s (Adetunji and Ferguson, 2012) (b) General location of conductive features identified in the IMS profile, the Bipole III study and the Knee Lake profile suggesting the imaging of the NACP (modified from Adetunji and Ferguson, 2012).

Distortion and strike analysis was conducted using the Groom-Bailey method and implemented with the STRIKE program. All MT survey sites have relatively low distortion with the exception of NES 7. At both crustal and mantle depths, the geoelectric strike and distortion values are similar suggesting a 2-D structure. Unconstrained and constrained 2-D modelling was done, with constrained inversions being used to determine if there was a resistive or conductive layer present at the top of the Precambrian basement. All models used a southwest-northeast profile (Az045º), inversion of 10 sites (including one site from the LITHOPROBE Western Superior transect study) and data corrected for tensor distortion.

All generated models are similar and share features which are assumed to be requirements of the MT data (Adetunji and Ferguson, 2012). Figure 43 shows the unconstrained model. The relatively conductive rocks of the Hudson Bay Basin are visible at the surface. The upper Precambrian crust is relatively resistive with a poorly-resolved shallow conductive features below site NES 12 and 3 at 0.5 to 1 km depth (Figure 43). Directly below sites NES4, 6 and 7 there is a near vertical conductor with its top at 500 m and resistivity values of 200 Ω·m (Adetunji and Ferguson, 2012). The conductor responsible for the induction arrow reversal is at ~20 km depth just north of NES12. It appears to connect with a conductive region of the mantle to the northeast, a geometry similar to the conductor seen in the Knee Lake profile.

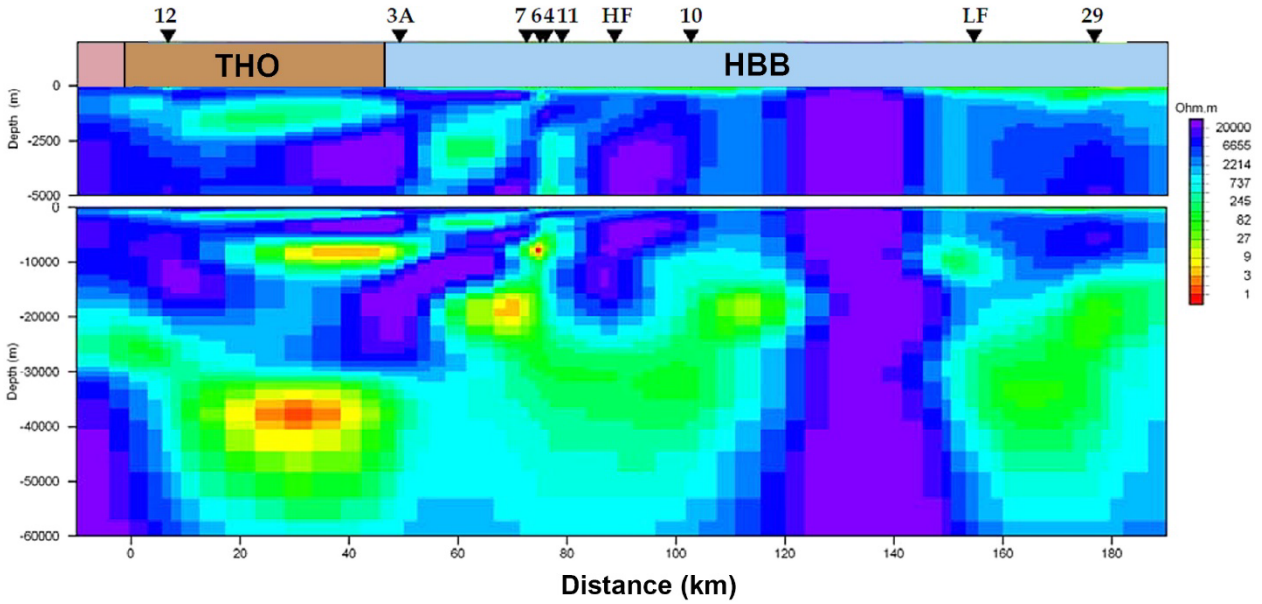

Figure 43. 2-D MT unconstrained model (modified from Adetunji and Ferguson, 2012). The model was obtained for inversion from a 1,000 Ω·m half-space starting model. Upper panel (V.E = 4) shows upper 5 km of model and the lower panel (V.E = 1) shows the upper 60 km. HBB = Hudson Bay Basin; THO = Trans Hudson Orogen.

To examine limiting cases for Bipole III electrode design, a resistive layer and conductive layer in the upper section of the Precambrian were separately included as a constraint in six different inversion models in order to test whether such a feature could be present (Figure 44). The resistive layer was set at 10,000 Ω·m. Results showed that a 600 m thick resistive layer caused no increase in data misfit, a 1 km thick layer caused a 1.2% increase in misfit, a 2 km thick layer caused a 4.2% increase, and a 5 km thick layer caused a 12.5% increase. The results suggest that, if there is a continuous very resistive layer present at the top of the Precambrian rocks, its thickness is less than about 1 km. The resulting inversions models resemble that for the unconstrained inversion. In the case of the continuous moderately-conductive layer, a 50 m thick layer of 300 Ω·m caused a 1.4% increase in the misfit of the data and a 100 m thick layer of 300 Ω·m caused an increase in misfit of 3.4%. These results show that if there is a weathered or fractured layer present, it must be relatively thin (<30 m) or relatively resistive.

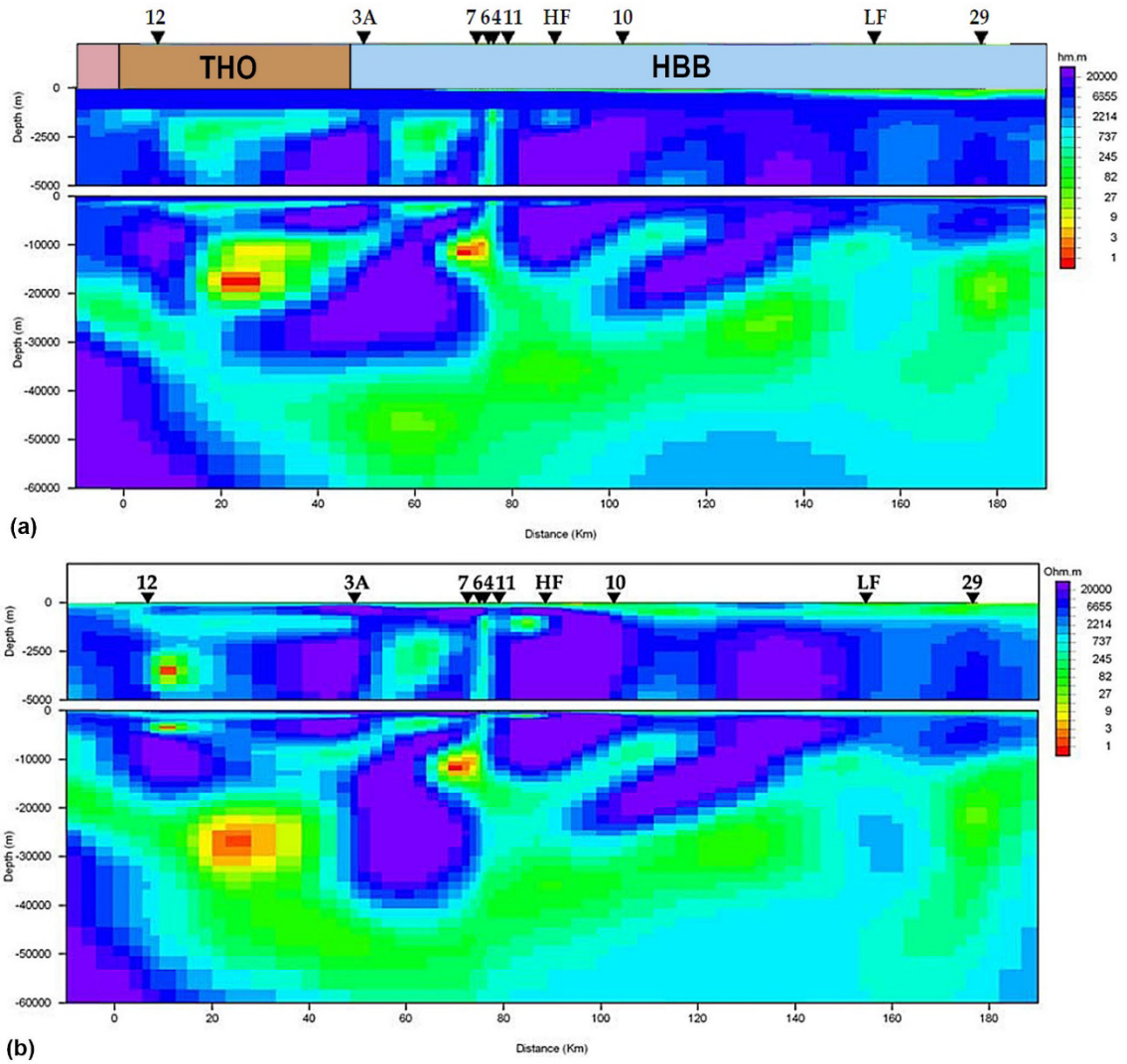

Figure 44. Results of constrained inversions (modified from Adetunji and Ferguson, 2012). Each inversion includes a fixed resistive (10,000 Ω·m) or conductive (300 Ω·m) layer at the top of the Precambrian basement to test whether the data can be fitted by such a model and to examine the impact on the remaining structures. (a) Model for a 1 km thick 10000 Ω·m layer in the upper section of the Precambrian basement. (b) Model for a 50 thick 300 Ω·m layer in the upper section of the Precambrian basement.

3.1.9. Churchill MT Project (2011) In 2011, as part of the GEM project, the Geological Survey of Canada used MT for hydrocarbon exploration studies in the Hudson Bay and Foxe basins. The main goal of Roberts and Craven (2012) was to identify potential Ordovician source rocks, focusing on the area of Churchill, Manitoba on the Hudson Bay coast. The location of the study area is near the Gillam-Kivalliq corridor. The Churchill study area is situated on the margins of the Hudson Bay and provides results on the rocks of the Hudson Bay Basin. These rocks are primarily late Ordovician and late Devonian marine sedimentary rocks that overlie the Precambrian basement of the Trans-Hudson Orogen (Bancroft et al., 2014).

A total of 46 AMT and BBMT sites were collected (Figure 45). Site spacing was between 400 to 400 m depending on the terrain and site conditions. Over the length of the study, there were three AMT stations and one BBMT station recording each night with the BBMT site left recording for multiple days at a time. A small drift in the GPS-sync clock occurred in the study, but this only affected AMT and not BBMT data (Roberts and Craven, 2012).

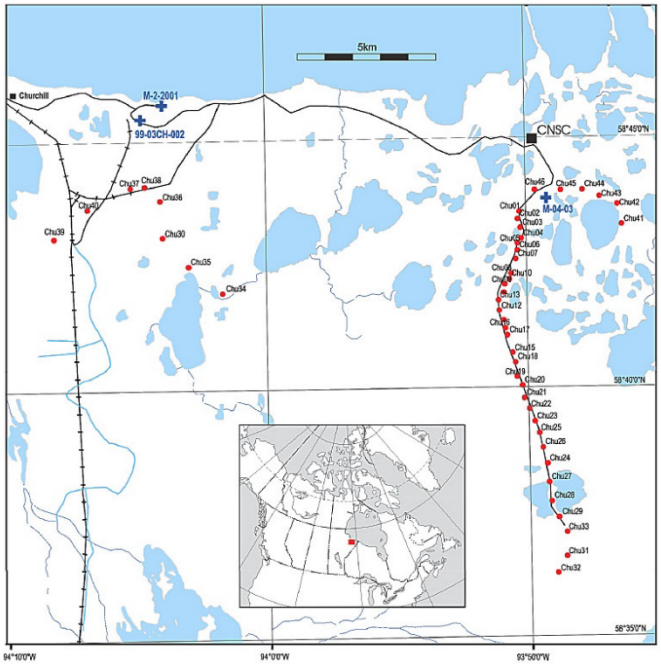

Figure 45. Churchill MT site locations (Roberts and Craven, 2012)

Data were edited and processed and inverted using 1-D and 3-D algorithms producing resistivity versus depth information as well as information on porosity. For periods of less than 0.1 s, the difference in phases were less than 10% suggesting a 1-D layered earth at shallow depths. The 1-D models were generated using Occam's inversion and the determinant average response with no constraints used. Figure 46 show results for concatenated 1-D models along a north-south profile. Highly resistive Precambrian rocks are observed at a depth of approximately 200 m on the south end of the profile and more shallow towards the north, where they occur at a depth of approximately 100 m. A large conductive region can be seen in the northern side of the profile at depths exceeding 4000 m and is interpreted to be associated with graphite or a sulphide mineral phase in the Precambrian basement rocks (Roberts and Craven, 2012). Hayward (2014) completed further 2-D modelling of this feature and confirmed that it was a required feature of the Precambrian basement and could not be explained by either the conductive water in Hudson Bay or anisotropy of the Hudson Bay Basin rocks. The depth to the interface between the Paleozoic and Precambrian rocks was confirmed by borehole M-04-03 at a depth of 99.6 meters, is in agreement with the MT data.

A three-dimensional model was generated by Roberts and Craven (2012) (Figure 47). A limited frequency bandwidth of 10^{-4} to 1 s periods was used and an RMS value of 2.0 was achieved. The data fit at most of the sites is good for periods of 10^{-4} and 0.1 seconds suggesting reliable shallow subsurface results. A cross-section from the 3-D model shows similar geometry to the 1-D model results (Figure 47).

Bancroft et al. (2014) conducted a study on eight MT sites near the town of Churchill that were not used in Roberts and Craven (2012) because of reduced data quality. The response from these sites had significant electromagnetic interference from cultural features in the town. After careful data editing, Bancroft et al. (2014) generated inversions of off-diagonal impedance responses and took the average of the two in order to create a single 1-D model. Their results are displayed in Figure 48 and are similar to those of Roberts and Craven (2012). The results of the two studies suggests the resistivity of most of the Ordovician to Silurian rock sequence is in the range of 10-300 Ω·m, but that there is a more conductive (<10 Ω·m layer of Ordovician rocks just above the Precambrian basement (Figures 45-47).

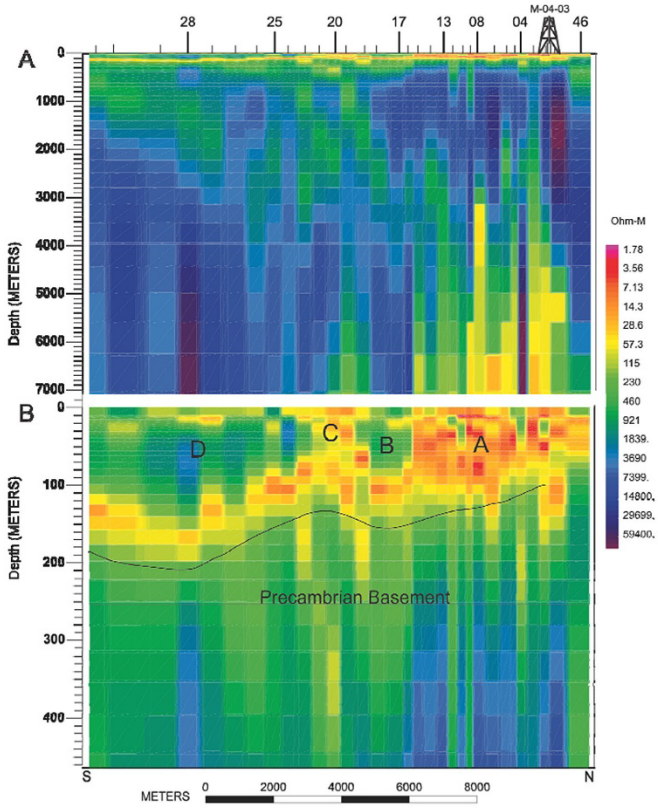

Figure 46. Concatenated 1-D model of MT data acquired in Churchill (Roberts and Craven, 2012). Lower panel shows results at a higher-resolution scale.

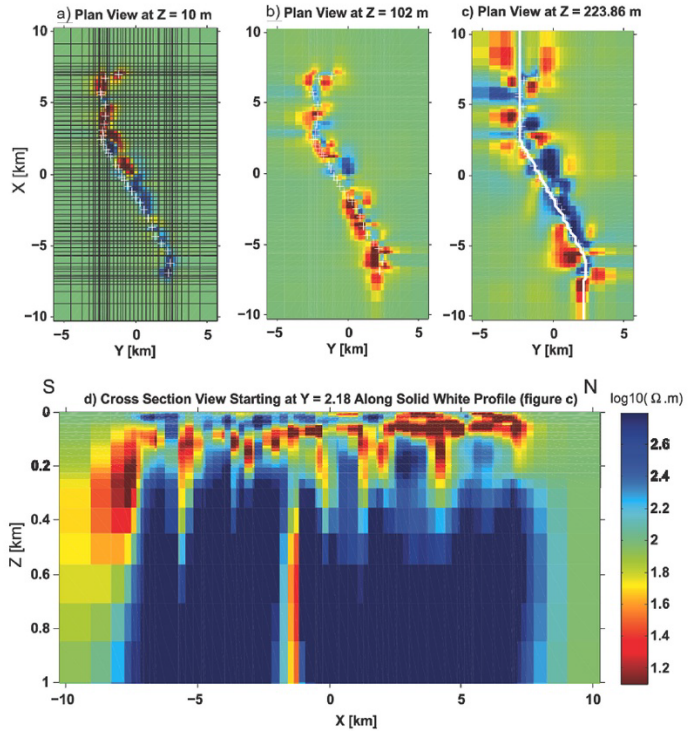

Figure 47. 3-D model inversion of the north-south Churchill MT profile. a), b) and c) illustrate apparent resistivity of the north-south profile in plan-view at various depths and d) illustrating a cross-section (Roberts and Craven, 2012).

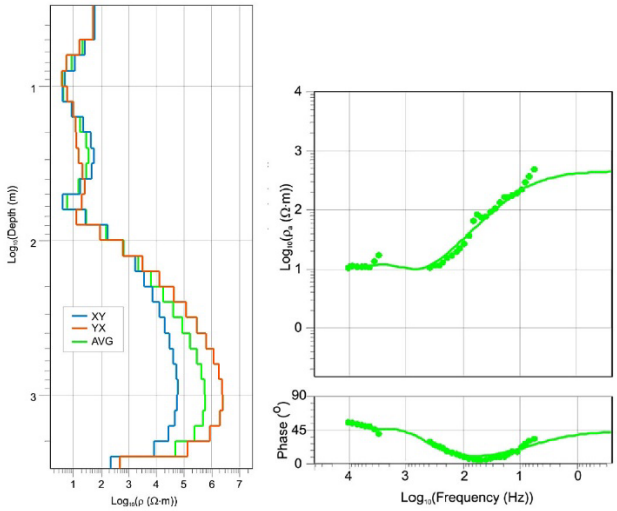

Figure 48. Left panel illustrates the *xy*-component (blue), *yx*-component (orange) inversion the average of the two (green). The right side panel illustrates the MT apparent resistivity and phase data with the corresponding model response for site Chu_36 (Bancroft et al., 2014).

Rock property analysis was conducted on core samples from borehole M-2-2001 (Roberts and Craven, 2012; Bancroft et al., 2014). Table 2 lists the physical properties for samples from Bancroft et al. (2014). The results show sedimentary rocks found in the HBB have large variation in resistivity. Borehole samples reveal a dolomitic facies at depths of 53 to 67 m, which correlates with the conductive anomaly found in the inversion models (Roberts and Craven, 2012). The response occurs in dolomitized limestone and wackestone found in Ordovician Bad Cache Rapids or Churchill River formation. Figure 49 compares the inversion model and sample resistivity measurements for one site. Overall, both datasets correlate well. However, physical property measurements yield higher resistivity values than the models derived from the MT data (Bancroft et al., 2014).

Table 2. Physical rock properties including as resistivity, chargeability, magnetic susceptibility, density and porosity (modified from Bancroft et al., 2014)

Depth	Lithology Notes	Sat Bulk Density [g/cc]	Porosity (Connected) [%]	Magnetic Susceptibility [SI]	Resistivity [Ohm.m]	Chargeability [ms]
102.7	Precambrian quarztite (fresh)	2.672	0.31	1.48E-04	4858	11.9
101.54	Precambrian quarztite (fresh)	2.686	0.32	2.50E-04	5579	5.0
99.75	Precambrian quarztite (weathered)	2.475	11.35	5.70E-05	1457	16.5
97.25	Bad Cache Rapids Gp, Portage Chute Fm, Member 1; argillaceous sandstone	2.235	22.31	4.62E-05	430	1.4
95.10	Bad Cache Rapids Gp, Portage Chute Fm, Member 1; argillaceous sandstone	2.213	25.89	3.17E-05	1681	1.5
88.75	Bad Cache Rapids Gp, Portage Chute Fm, Member 1; coarse sandstone	2.394	15.84	2.03E-05	42	0.7
85.90	Bad Cache Rapids Gp, Portage Chute Fm, Member 1; argillaceous sandstone	2.207	24.59	7.23E-06	4822	6.2
83.65	Bad Cache Rapids Gp, Portage Chute Fm, Member 1; quartzose sandstone	2.197	24.49	-3.59E-06	7431	4.2
81.20	Bad Cache Rapids Gp, Portage Chute Fm, Member 1; quartzose sandstone	2.208	7.68	3.05E-06	9821	0.8
76.80	Bad Cache Rapids Gp or Churchill River Gp(?); dolomitic wackestone	2.572	8.92	4.53E-05	330	8.0
57.40	Bad Cache Rapids Gp or Churchill River Gp(?); sandy, dolomitic limestone	2.553	10.17	1.56E-05	73	0.1
54.00	Bad Cache Rapids Gp or Churchill River Gp(?); dolomitic wackestone	2.528	11.96	1.03E-05	91	0.7
47.90	Bad Cache Rapids Gp or Churchill River Gp(?); dolomitic limestone	2.534	12.34	5.30E-06	65	0.1
41.25	Bad Cache Rapids Gp or Churchill River Gp(?); dolomitic wackestone	2.511	12.04	9.31E-06	79	1.3
31.20	Red Head Rapids Fm; argillaceous, dolomitic mudstone	2.736	3.29	5.17E-05	377	3.2
30.90	Red Head Rapids Fm; argillaceous, dolomitic wackestone	2.652	5.29	3.54E-05	195	10.7
26.95	Red Head Rapids Fm; argillaceous, dolomitic mudstone	2.760	1.36	3.01E-05	2478	1.1
24.00	Red Head Rapids Fm; dolomitic wackestone	2.683	6.26	4.41E-05	267	4.5
19.70	Red Head Rapids Fm; porous dolomitic wackestone	2.561	13.53	4.70E-05	106	0.9
13.25	Red Head Rapids Fm; argillaceous, dolomitic mudstone	2.674	7.39	4.27E-05	148	4.3
12.85	Red Head Rapids Fm; dolomitic wackestone	2.502	17.15	2.21E-05	31	0.4
6.75	Red Head Rapids Fm; dolomitic mudstone	2.406	22.9	3.69E-05	28	0.1
3.20	Red Head Rapids Fm; mottled, porous, dolomitic mudstone	2.677	7.69	2.21E-05	771	0.8
2.50	Red Head Rapids Fm; argillaceous, dolomitic mudstone	2.732	2.85	7.69E-06	7557	6.1
0.20	Severn River Fm; dolomitic mudstone	2.637	6.39	2.47E-05	239	1.1
outcrop	Precambrian granite	2.671	0.24	2.04E-04	7343	4.6

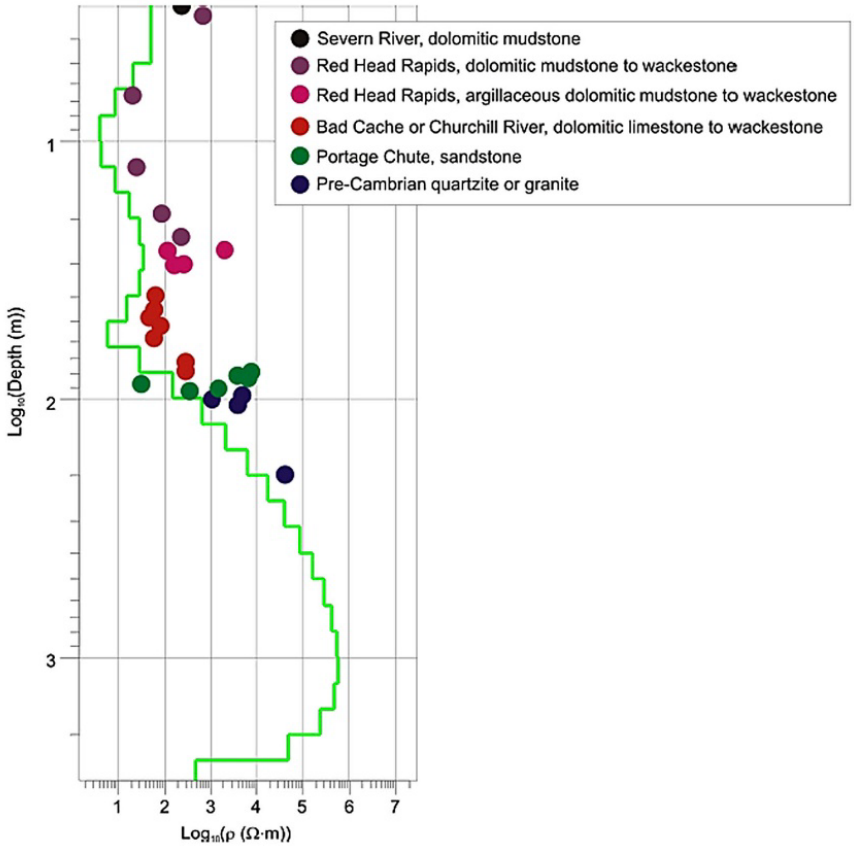

Figure 49. Comparison of 1-D inversion of the MT survey site Chu_36 (green line) with the resistivity measurements from the physical rock property dataset with their respective depth and resistivity values (Bancroft et al., 2014).

3.1.10. Kaskattama Highland MT Survey (2017) The Kaskattama MT survey was a 22 site helicopter-transported survey conducted in the Kaskattama Highlands of far northwestern Manitoba in 2017 (Figure 50) (Craven et al., 2017). The survey area is 240 km east of Gillam. It is located in an area in which a borehole had revealed anomalous Paleozoic-Mesozoic stratigraphy including a Cretaceous or Paleocene shale unit and the absence of some Silurian units. Underlying Precambrian basement rocks include the Fox River Belt of the Superior Boundary Zone, close to its truncation by the Winisk River Fault.

The survey results provide a determination of the resistivity of the Ordovician units subcropping along the Gillam-Kivalliq link. Figure 51 shows an inversion of the AMT-BBMT data set from site ksk01in which unit thicknesses are constrained from the KK1 and Comeault drill-holes (Figure 50). The resistivity of the assumed 178 m thick Ordovician sequence was determined to be 300 Ω·m. The overlying Silurian rocks of the Severn River Formation are significantly more conductive (~30 Ω·m). The results for the Ordovician units contrast with the results from near Churchill which suggested the occurrence of relatively conductive (<10 Ω·m) lower Ordovician units (Roberts and Craven, 2012). The Churchill results may be due to local hydrothermal dolomitic alteration or sea-water intrusion into the Ordovician units.

The Kaskattama MT survey results also provided some information on the resistivity of the Precambrian basement within the current study area. It indicated moderate conductivity (<50 Ω·m) in some parts of the Burntwood Gneiss unit of the Kisseynew Gneiss Belt. It also revealed enhanced conductivity (<50 Ω·m) within magnetic anomalies in the northern part of the Fox River Belt that likely correspond to iron formations.

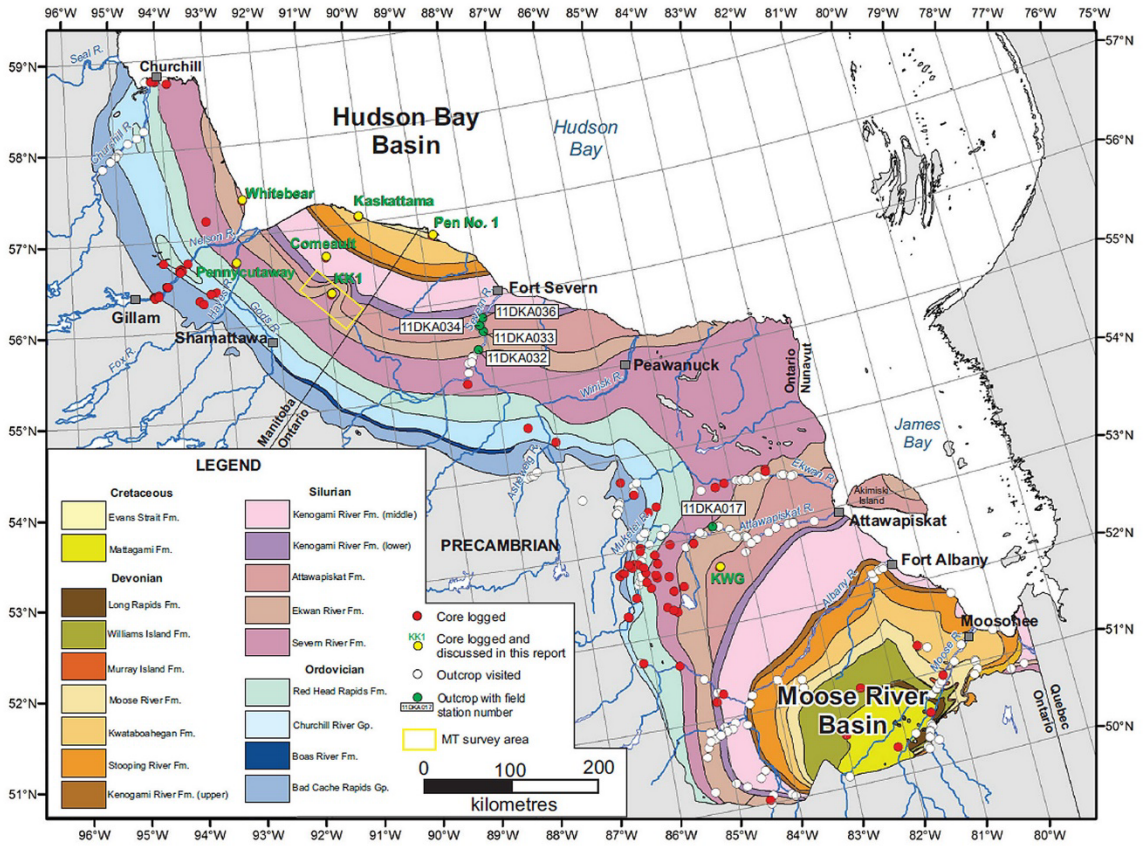

Figure 50. Location of the Kaskattama MT survey is shown by the yellow rectangle relative to the onshore Paleozoic-Mesozoic geology of the Hudson Bay and Moose River basins (Nicolas and Armstrong, 2017).

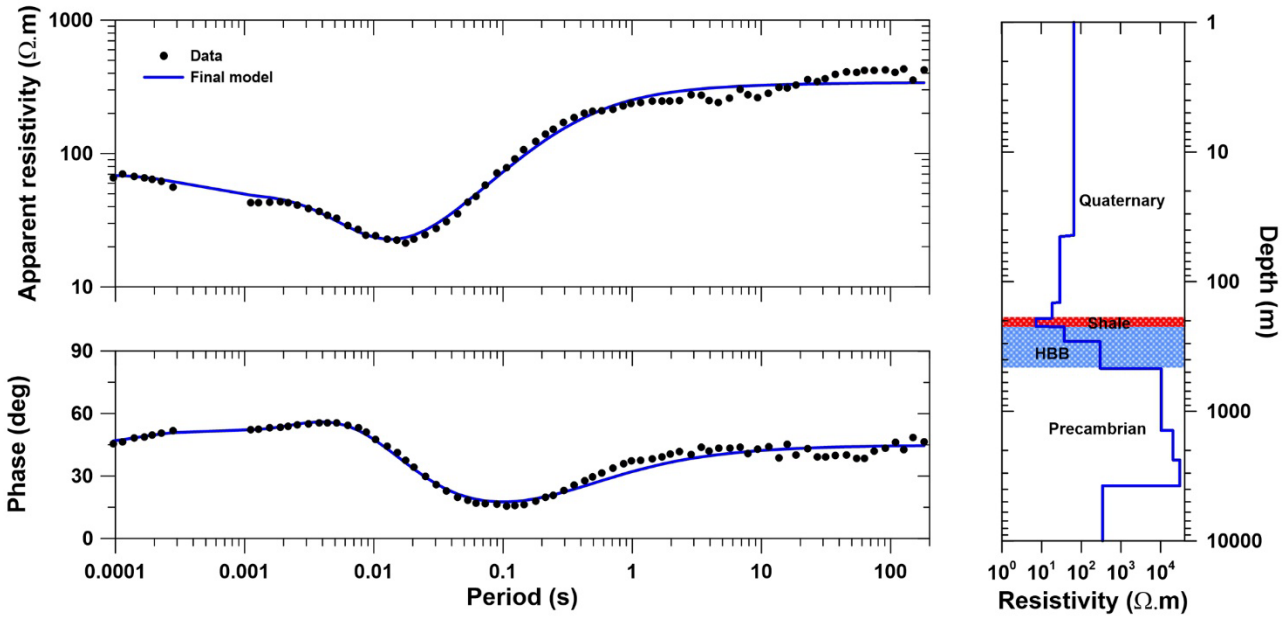

Figure 51. Constrained 1-D model fitted to MT data from the Kaskattama Highlands.

3.2 Small-scale electromagnetic measurements

Smaller-scale electromagnetic measurements have been made in Northern Manitoba include conductivity logs, frequency-domain (FEM) conductivity mapping measurements, and time-domain electromagnetic (TEM) soundings made as part of the Manitoba Hydro Bipole III electrode site determinations in the Nelson River area (Adetunji and Ferguson, 2012).

The conductivity log information is useful for parameterizing the conductivity of different types of surficial materials. Geotechnical logs from sites on surficial sediments classified as offshore glaciomarine deposits indicate that the upper 10 to 20 m of these deposits typically consists of a layer of peat, of zero to 3 m thickness, overlying a variable thickness of sandy-silt to silty-sand overlying clay till and silt till. At most locations there is a layer with higher clay content between 15 to 25 m depth. This unit overlies a clay till which contains some silt till in places. The electrical resistivity of the offshore glaciomarine deposits correlates inversely with the clay content (Adetunji and Ferguson, 2012). The upper 15 m at most locations has resistivity that decreases with depth from values of 50 to 100 Ω·m near the surface to 35 Ω·m. In the clay-rich layer between 15 and 25 m the resistivity decreases to values of less than 30 Ω·m. At many locations there is a 2 to 3 m thick layer in which the resistivity decreases to less than 25 Ω·m (Adetunji and Ferguson, 2012). The integrated conductivity of the conductive layer has values of 0.38 to 0.55 S in five logs in which the layer is well defined. Beneath the clay-rich layers the clay till has a resistivity of 30 to 40 Ω·m. Sites on alluvial deposits are expected to have a higher content of sand and silt and a smaller amount of clay than the offshore glaciomarine deposits (Adetunji and Ferguson, 2012). FEM results indicate that the deposits have a variable resistivity in the upper few metres, which likely reflects a variable clay and sand content. At greater depth the sites are characterized by a relatively uniform resistivity of 100–200 Ω·m.

Soundings were done in areas in which Ordovician rocks of the Bad Cache Rapids Group and the Churchill River Group subcrop. The TEM results indicated that these rocks were more resistive than the overlying sediments but provided limited resolution of the exact resistivity. The results provided weak constraints on the depth to bedrock, but suggested that at most of the sites on glaciomarine sediments sites it occurred between depths of 40 and 60 m and averaged about 45 m. The depth appeared to be larger, around 64 m, at a site on alluvial sediments near the Nelson River. Because of the relatively high conductivity of the surficial sediments the TEM data from most sites was unable to constrain the resistivity of the underlying sedimentary rocks. The results from only one site, in a location of more resistive surficial sediments, provided constraints. At this site, unconstrained inversion yielded a 190 m thick layer of 590 Ω·m below the surficial units. This result may be affected by equivalence. Well log data indicate that the thickness of the sedimentary rocks at the site is ~120 m rather than the 190 m in the TEM resistivity model. Using the thickness estimated from well logs and the conductivity-thickness product in the TEM model leads to a corrected resistivity of the Bad Cache Rapids Group and Churchill River Group rocks of 370 Ω·m. These results are consistent with those from the Kaskattama MT survey and contrast with the high conductivity of Ordovician units determined near Churchill (Roberts and Craven, 2012).

3.3 Geophysical well logs

Resistivity information for the rocks of the Hudson Bay Basin is available from geophysical well-logs from both onshore and offshore wells. The location of onshore wells is shown in Figure 50 and Figure 52 shows the location of offshore wells.

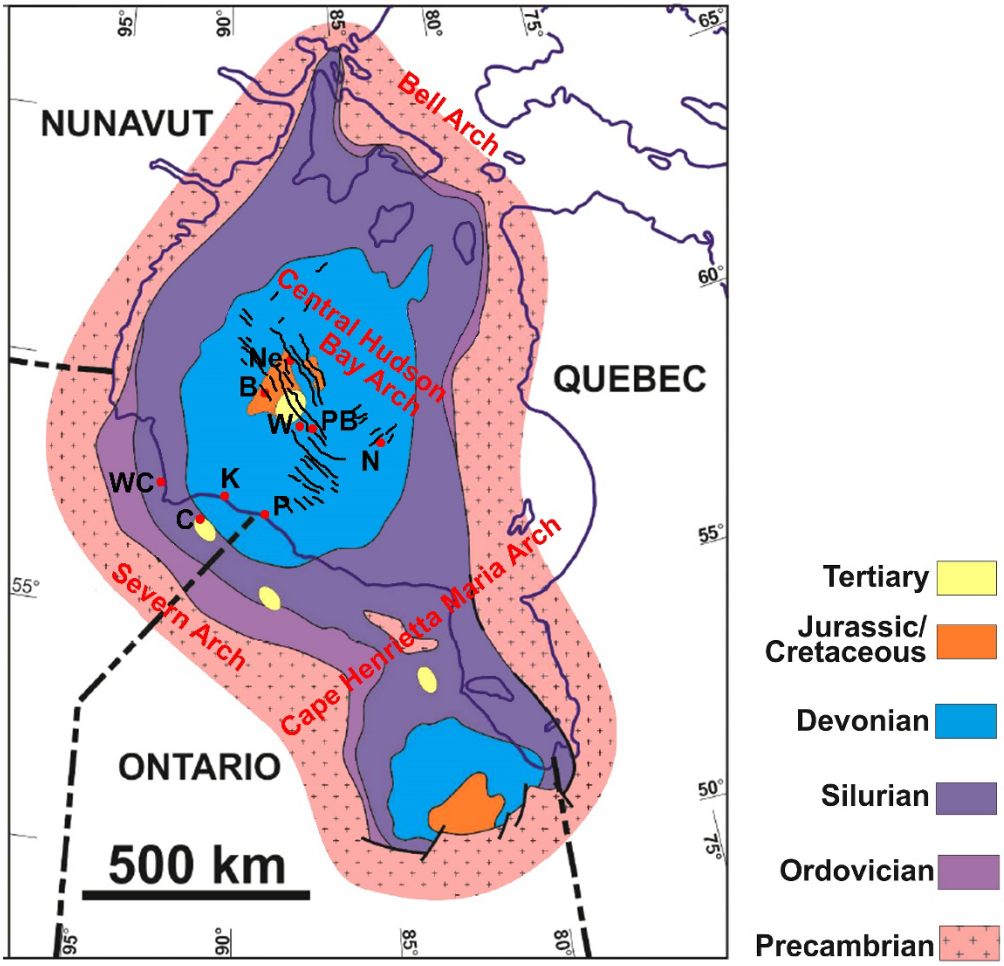

Figure 52. Simplified large-scale geology of Hudson Bay and Moose River Basins (modified from Sanford and Grant, 1990; Lavoie et al. 2013; and Armstrong et al., 2018). Labelled red circles are wells: B = Trillium et al. O-23 Beluga; C = Houston et al. No. 1 Comeault; K = Sogepet Aquitaine No. 1 Kaskattama; N = Aquitaine et al. O-58 Narwhal South; Ne = ICG et al. N-01 Netsiq; P = Aquitaine No. 1 Pen Island; PB = Aquitaine et al. C-11 Polar Bear; W = Aquitaine et al. A-71 Walrus; WC = Merland Exploration No. 1 Whitebear Creek.

Geophysical well-logs are available from three onshore wells southeast of the current study area: the Sogepet Aquitaine Kaskattama Prov. No. 1 well; Merland et al. Whitebear Creek Prov. well; and Houston Oil Limited, Comeault No. 1 well (Figure 52). The results from the Whitebear Creek and Comeault No. 1 well do not provide a good representation of the true resistivity of the surrounding formations. The results show little variability over much of the section, abrupt jumps in places, unrealistic resistivity variation between the Ordovician and Precambrian units, and strong inconsistencies between the two wells. So here we consider only the Kaskattama Prov. No. 1 well (Figure 52). Results from offshore wells (from N-01 to O-58) show considerable variation in the resistivity values for Ordovician and Silurian strata (McLeod and Ferguson, 2018; Figure 53). However, the Aquitaine No. 1 Pen Island and the Kaskattama Prov. No. 1 are more consistent. They show that the lower Ordovician formations, the Bad Cache Rapids and the Churchill River formations, are more resistive than the overlying Red Head Rapids formation. The Bad Cache Rapids and Churchill River groups have moderately high resistivity (between 100 and 1000 Ω·m). This result is consistent with the TEM results from the Nelson River area which suggested a value of 370 Ω·m. The Pen Island and the Kaskattama Prov. No. 1 results also show that the Silurian Severn River formation as well as the Attawapiskat, Ekwan River and Kenogami River units have an average resistivity of about 30 Ω·m.

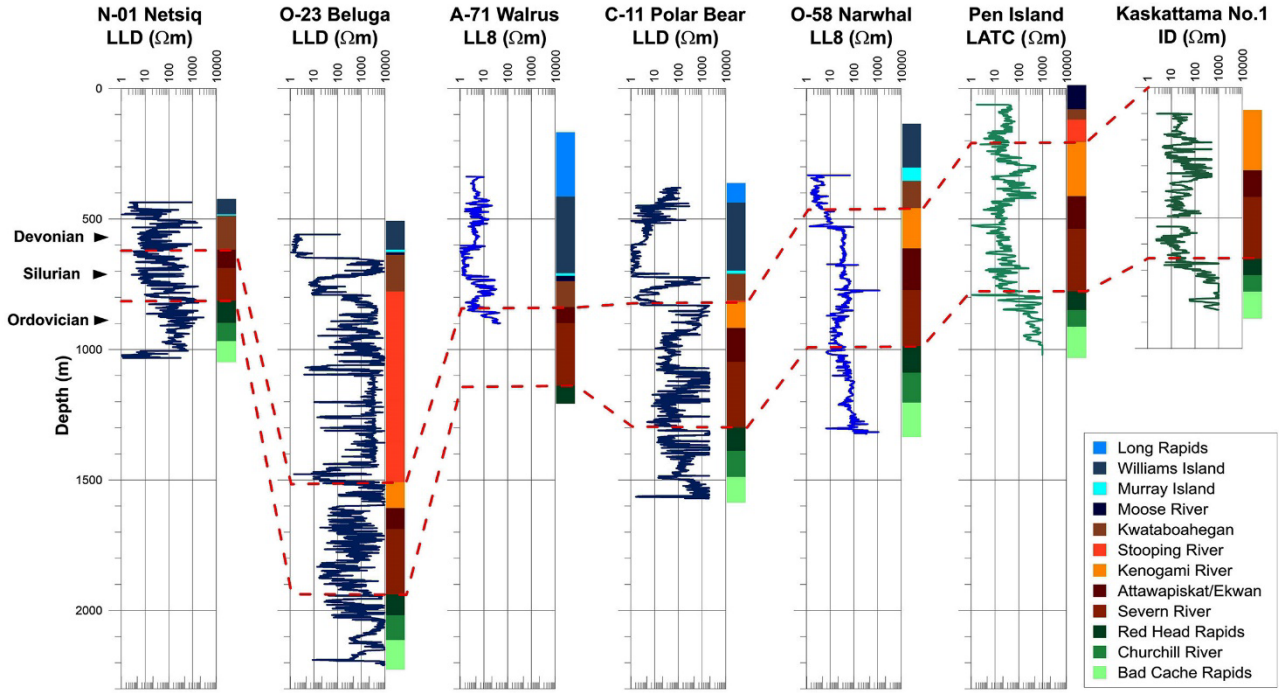

Figure 53. Resistivity logs of Hudson Bay Basin wells as derived from various deeper penetrating logging tools (Laterolog and induction log) (McLeod and Ferguson, 2018).

For surface impedances, such as for the MT method, which are based primarily on horizontal electric current flow, the response related to the longitudinal resistivity of the layers (Gowan et al., 2009; Zaporozan and Ferguson, 2017; Craven et al., 2017). The well log data were combined into single values for each geological unit by appropriate averaging of conductivity (cf. resistivity) values. Representing the well log data in each unit as a series of a sub-layers, with thickness h_i and resistivity ρ_i, the average values were calculated using a longitudinally-averaged value:

$$\rho_{\sigma}^{av} = \left[\sum_i h_i\right] \cdot \left[\sum_i \frac{h_i}{\rho_i}\right]^{-1} \qquad \text{Eq. 1}$$

This formula was also applied when combining the resistivity of multiple layers into a single composite layer. In order to provide a comparison, we also computed a transverse-averaged value

$$\rho_{\rho}^{av} = \left[\sum_i h_i \rho_i\right] \cdot \left[\sum_i h_i\right]^{-1} \qquad \text{Eq. 2}$$

The ratio of the transverse to the longitudinal resistivity defines the amount of anisotropy present in the geological unit. The coefficient of anisotropy is:

$$\lambda = \left(\frac{\rho_{\sigma}^{av}}{\rho_{\rho}^{av}}\right)^{1/2} \qquad \text{Eq. 3}$$

Equations 1 and 2 simplify for the case of equal thickness layers (i.e., equally-spaced well log values). In the case of equal thickness values, we also calculated a geometric mean value for the resistivity using:

$$\rho_{gm}^{av} = \left[\prod_{i=1}^{N} \rho_i\right]^{1/N} = \exp\left(\left[\sum_{i=1}^{N} \ln \rho_i\right] / N\right) \qquad \text{Eq. 4}$$

Tables 3 and 4 show the averaged resistivity of each of the geological units in the Kaskattama Prov. No. 1 and Aquitaine No. 1 Pen Island wells calculated using the three methods. As required by the theory, the longitudinal resistivity values are the smallest and the transverse resistivity values are the highest. The coefficients of anisotropy are mostly in the moderate range. Lower values in the Stooping River Formation and Upper Kenogami member are due in large part to the limited amount of data in these units.

Table 3. Detailed unit thickness and resistivity measurements from Kaskattama Prov. No. 1 well log data (Zaporozan and Ferguson, 2017)

Age	Unit	Thickness (m)	Resistivity Average (Ω·m)			Coeff Anisotr.
			Transverse Resistivity	*Longitudinal Resistivity*	*Geometric Mean Resist.*	
Devonian	Stooping River	24.92	22.37	19.08	20.53	1.083
Devonian	Upper Kenogami R.	3.66	31.54	29.23	30.42	1.039
Silurian	Middle Kenogami R.	185.62	50.19	17.47	26.14	1.695
Silurian	Lower Kenogami R.	13.41	117.94	83.26	99.45	1.417
Silurian	Attawapiskat	65.53	121.15	34.84	62.77	1.865
Silurian	Ekwan River	42.37	23.80	15.23	18.89	1.250
Silurian	Severn River	231.65	24.40	16.16	19.81	1.510
Ordovician	Red Head Rapids	32.0	106.14	33.93	57.88	1.769
Ordovician	Churchill River	92.05	357.49	238.74	301.12	1.497
Ordovician	Bad Cache Rapids	79.48	479.55	245.93	362.27	1.396

Table 4. Calculation of layer resistivity values for Aquitaine Sogepet Pen Island well (McLeod and Ferguson, 2018).

Age	Unit	Thickness (m)	Resistivity Average (Ω·m)			Coeff Anisotr.
			Transverse Resistivity	*Longitudinal Resistivity*	*Geometric Mean Resist.*	
Devonian	Moose River	92.00	11.50	7.35	9.19	1.25
Devonian	Kwataboahegan	38.80	34.42	30.54	32.42	1.06
Devonian	Stooping River	85.80	22.50	11.36	15.99	1.41
Silurian	Kenogami River	207.80	101.72	30.28	55.50	1.83
Silurian	Attawapiskat/Ekwan	124.60	17.26	6.69	10.75	1.61
Silurian	Severn River	239.00	32.40	19.33	25.03	1.30
Ordovician	Red Head Rapids	71.80	211.33	136.35	169.75	1.25
Ordovician	Churchill River	63.80	431.82	345.89	386.47	1.12
Ordovician	Bad Cache Rapids	94.80	691.20	492.22	583.29	1.19

The results show quite good agreement with the highest coefficients of anisotropy being observed in the Silurian units. Table 5 compares results for the longitudinal resistivity of the units relevant to the current study. A comparison of the averaged resistivity values of the two logs (Table 2) defines a range of reasonable resistivity values to be used as constraints for modeling responses of Hudson Bay Basin rocks along the Gillam-Kivalliq corridor.

Table 5. Comparison of calculated Paleozoic unit resistivity values from Pen Island and Kaskattama No. 1 wells (McLeod and Ferguson, 2018).

Pen Island	*Geometric Mean Resist.* (Ω·m)	Kask. no. 1	*Geometric Mean Resist.* (Ω·m)
Severn River	25.03	Severn River	19.81
Red Head Rapids	169.75	Red Head Rapids	57.88
Churchill River	386.47	Churchill River	301.12
Bad Cache Rapids	583.29	Bad Cache Rapids	362.27

4. Constraints on the NACP

The MT responses and resistivity models for the NACP are considered in more detail in this section because of its regional significance and expected crossing of the Gillam-Kivalliq corridor (Figure 11).

4.1 Responses of the NACP

The response of the NACP will depend on whether its Paleoproterozoic host rocks are exposed or covered by a sedimentary basin. Figure 54 and 55 shows the MT and tipper response along LITHOPROBE Line L on the exposed Precambrian shield. The NACP is located within the La Ronge domain and is observed in the tipper and the MT TE and TM mode responses. The associated strike direction is sub-parallel to the strike in adjacent geological domains, and to the large-scale geological structures, demonstrating geological control on the NACP geometry. In the 30 s induction arrow response, the NACP is associated with an asymmetric arrow reversal that is visible over a profile length of approximately 100 km. In the apparent resistivity response, the NACP is associated with decreased values over a 50 km wide zone at periods longer than 0.1 s. It includes apparent resistivity values decreasing with increasing period from ~100 Ω·m to <10 Ω·m. The response is visible to periods of >100 s, although there may also be a contribution to this long period response from an underlying conductive region in the mantle (Jones et al., 2005, Ferguson et al., 2005b). In the phase response, the NACP is visible at periods as short as 10^{-3} s as a reduction in the amplitude of a phase low. At periods >100 s it is observed as an increase in phase relative to that in surrounding regions.

Figure 56 shows the NACP apparent resistivity response along Line X. The period-range and apparent resistivity values of the NACP response are similar to as on Line L but the feature appears to be narrower and can be observed over a distance of only 20–30 km. Farther to the south, where the NACP is located below several thousand metres of conductive sedimentary rocks its response is visible in only the TE response (e.g., Jones and Savage 1986; Jones, 1993; Jones and Craven, 1990; Jones et al., 2005; Jones 2006). Figure 57 shows the phase responses for GSC Line S. The NACP is visible only as a ~5–15º phase anomaly relative to adjacent areas at periods of >30 s.

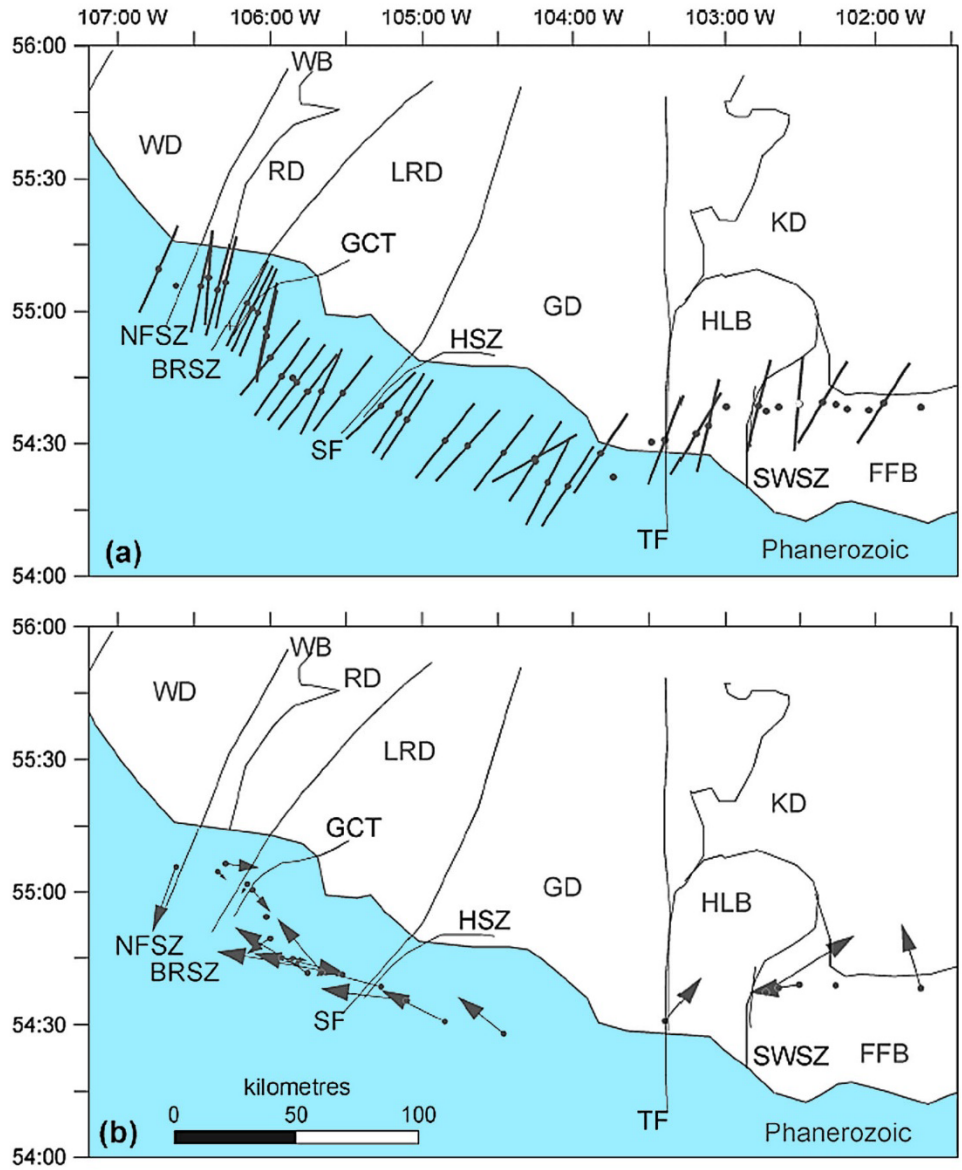

Figure 54. Geoelectric strikes determined for the study area (modified from Ferguson et al., 2005b). (a) Strike directions from single-site multi-frequency GB decompositions. The strike was determined using the period range from 10^{-4} to 10^{3} s for BBMT sites and 10^{-4} to 10^{-1} s for AMT sites. Sites at which the strike direction could not be adequately resolved are indicated by the absence of a strike direction symbol. (b) Real component of induction arrows for 30 s period. Arrows are plotted with the Parkinson (1962) convention and point toward conductive regions. Sites for which the induction arrow is not well resolved have been omitted. Induction arrow scale: a distance of 75 km on the distance scale bar corresponds to an arrow magnitude of 1.0.

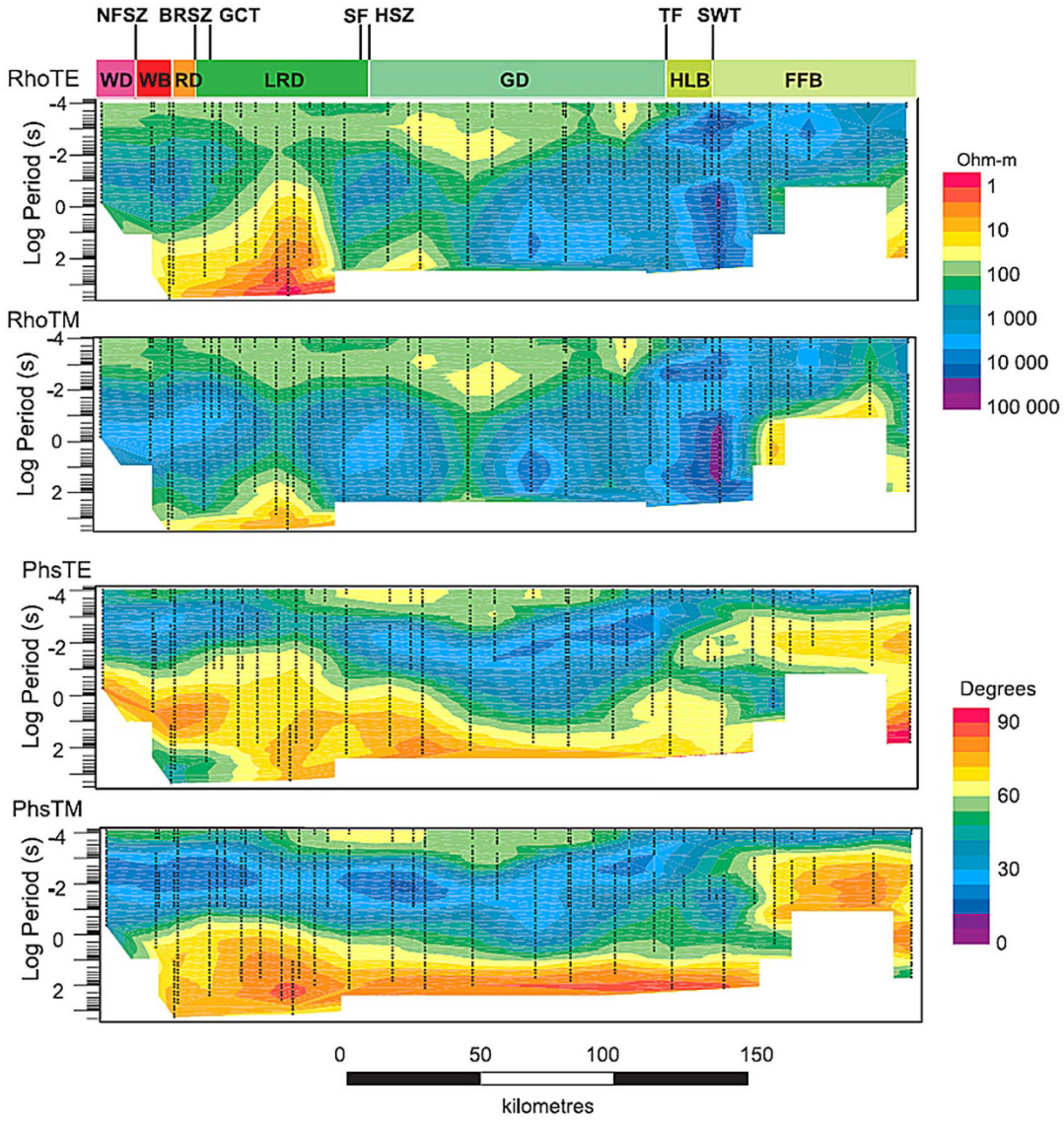

Figure 55. MT responses along LITHOPROBE line L (Ferguson et al., 2005b). The conductive feature observed in the La Ronge domain (LRD) is the NACP.

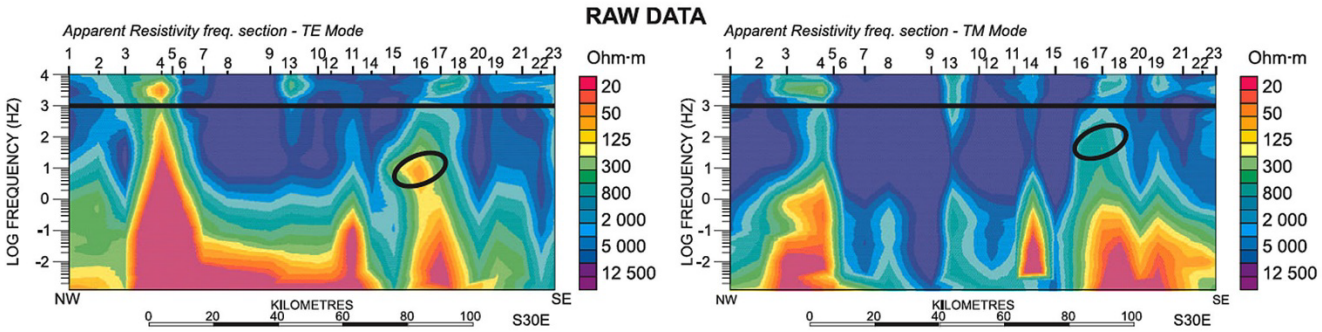

Figure 56. Apparent resistivity responses along LITHOPROBE line X (Garcia and Jones, 2005). The black ellipses mark the shorter period responses of the NACP.

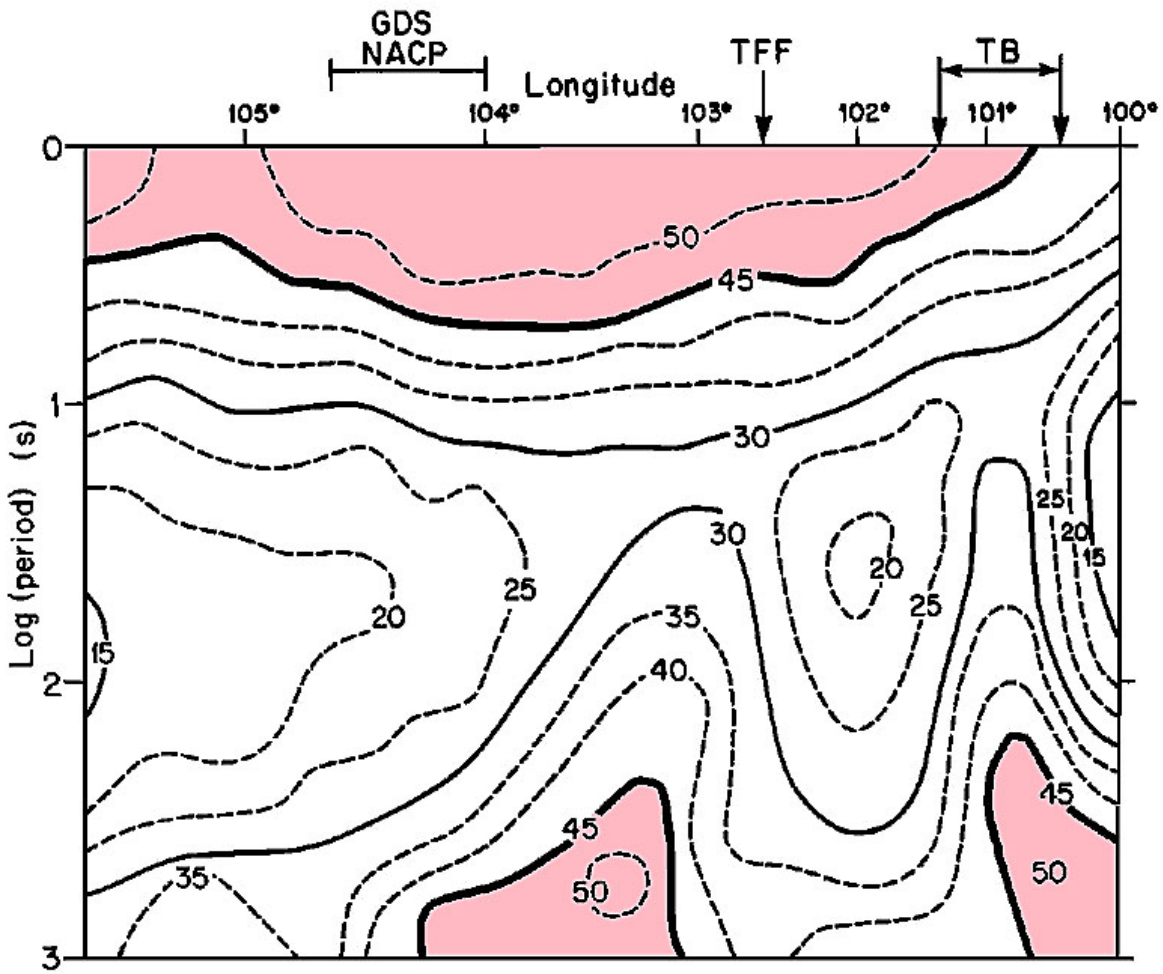

Figure 57. TE phase response on GSC Line S (modified from Jones and Savage, 1986). The NACP creates the increased phase response centred on 103.5° W.

4.2 Resistivity structure of the NACP

In resistivity models of the NACP, the feature is generally observed to be a west-dipping conductive feature or series of conductive blocks at mid-crustal depth. Jones (1993) describe the diversity of models that can be fitted to data from a southern crossing of the anomaly using different inversion methods. Figure 58 shows models for different crossings of the feature from Jones et al. (2005) with an emphasis on blocky-type models. In most cases, the data are fitted by a series of blocks with resistivity of <1 Ω·m dipping to the west at depths of between 10 and 20 km. More conventional models for LITHOPROBE Line L include a conductive feature extending to the surface (Figure 59). Figure 17 and 18 show further 2-D models for LITHOPROBE Line L and X. Finally, Figures 14, 31, and 43 show images of the conductor speculated to be the NACP on the IMS profile, the Knee Lake profile, and the Bipole III profile respectively.

Physical property measurements have been conducted on samples taken from locations corresponding to the surface projection of the NACP along LITHOPROBE Line L (Jones et al., 1997). Results from conductive surface samples show sulphides concentrated into fold hinges creating strong anisotropic conductivity responses (Fig. 60; Jones et al., 1997).

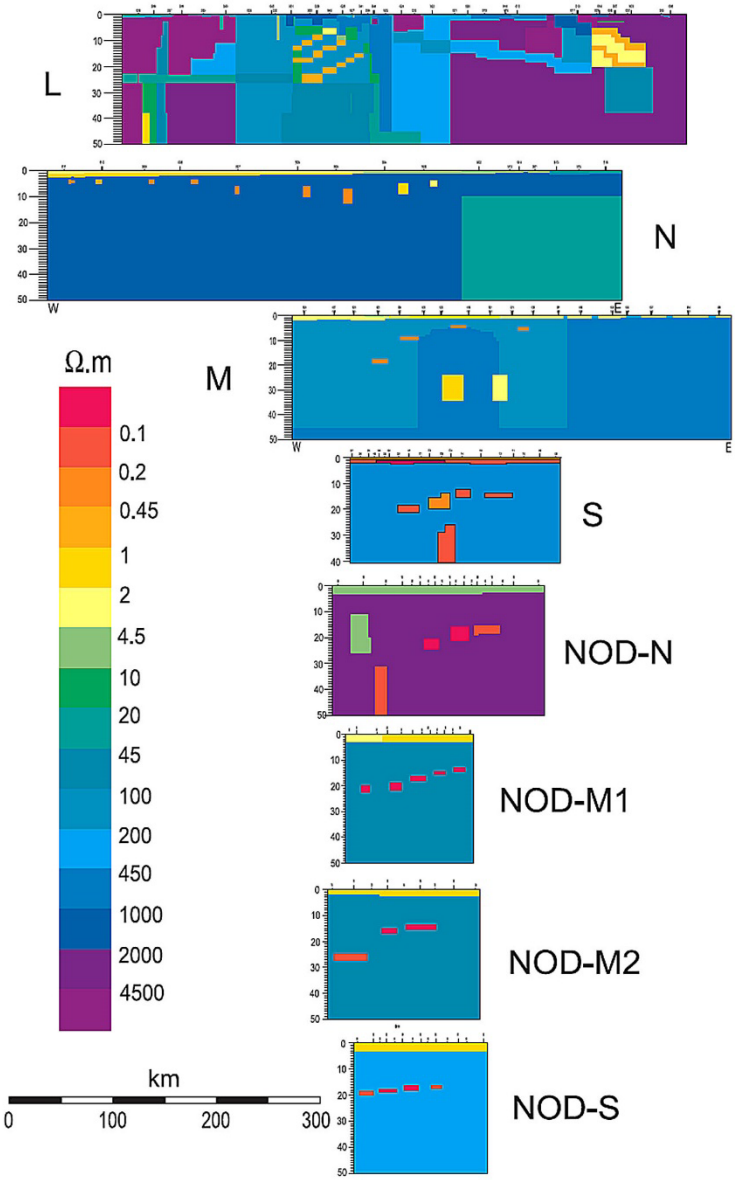

Figure 58. 2-D forward resistivity models fitting the MT data (both modes) from all profiles (Jones et al., 2005).

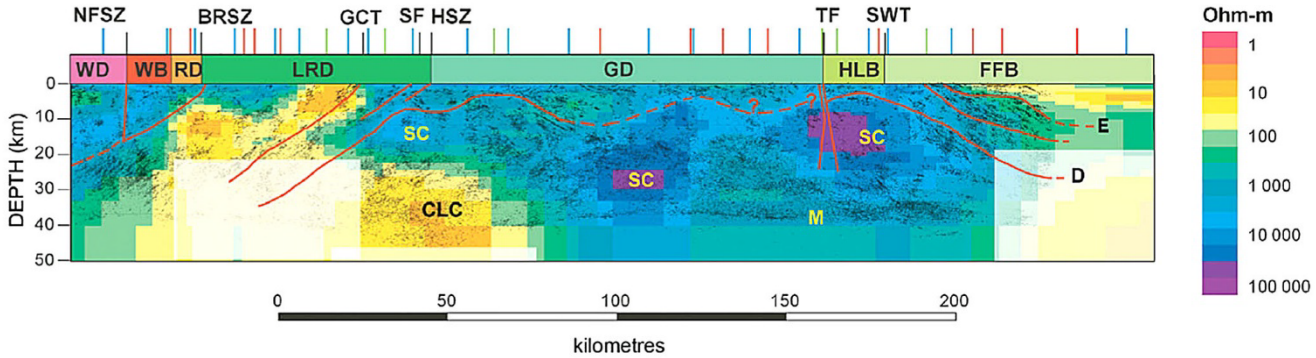

Figure 59. 2-D inversion resistivity models for LITHOPROBE Line L superimposed on seismic reflection response (Jones et al., 2005).

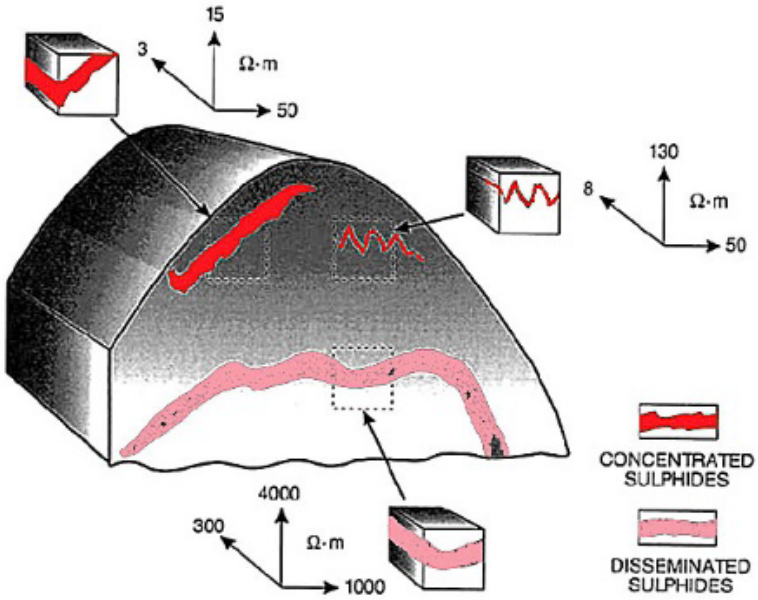

Figure 60. Schematic representation of cross-section of a rock interpreted to be responsible for the NACP conductor (modified from Jones et al. 1997). Insets show sub-samples and the results of anisotropic resistivity measurements. Each sample is a cube with a side length of 1.5 cm.

5. Definition of modelling profile and identification of data gaps

5.1 Modelling profile

Based on the path of proposed fibre-hydro link (Figure 2) it is optimal to adopt a north-south profile for the 2-D modelling of the MT data. For convenience, a 1300 km UTM-based north-south profile running from the Superior Craton to the Rae craton is used. The southern limit of the profile is UTM15E (400000 m E, 6000000 m N) and the northern limit is (400000 m E, 7300000 m N). The equivalent NAD83 geographic coordinates are: (54.13837º N, 94.53070º W) and (65.80575º N, 95.18703º W).

5.2 Geological terranes and other features along modelling profile

Figure 61 shows the position of geological terranes and their boundaries along the modelling profile. The large-scale geological divisions crossed by the profile are from south to north: Superior craton, Trans Hudson Orogen, the Hearne craton and domains on its southern margin, the Chesterfield Block, and the Rae craton. The Superior craton, Trans Hudson Orogen, and rocks on the margin of the Hearne craton are subdivided into smaller units. The region of the Hearne craton that is crossed by the corridor includes scattered mapped occurrences of the Paleoproterozoic Hurwitz group (Rainbird et al., 2010). The Hudson Bay Basin overlies the northern part of the Trans Hudson Orogen and southern part of the Hearne margin rocks.

Figure 61 also shows the position of gaps on the profile in which there are no existing MT sites. There are significant gaps in the MT data along the Gillam-Kivalliq corridor to the north and south of Churchill. The southern gap extends across an area interpreted to represent Kisseynew Gneiss Domain and the Wathaman-Chipewyan batholith and the southern margin of the Great Island Domain, a correlative of the Wollaston Fold Belt. The northern gap extends across the Great Island and Nejanilini domains, which correlate with the Wollaston Fold Belt, and much of the Hearne craton (Figure 61).

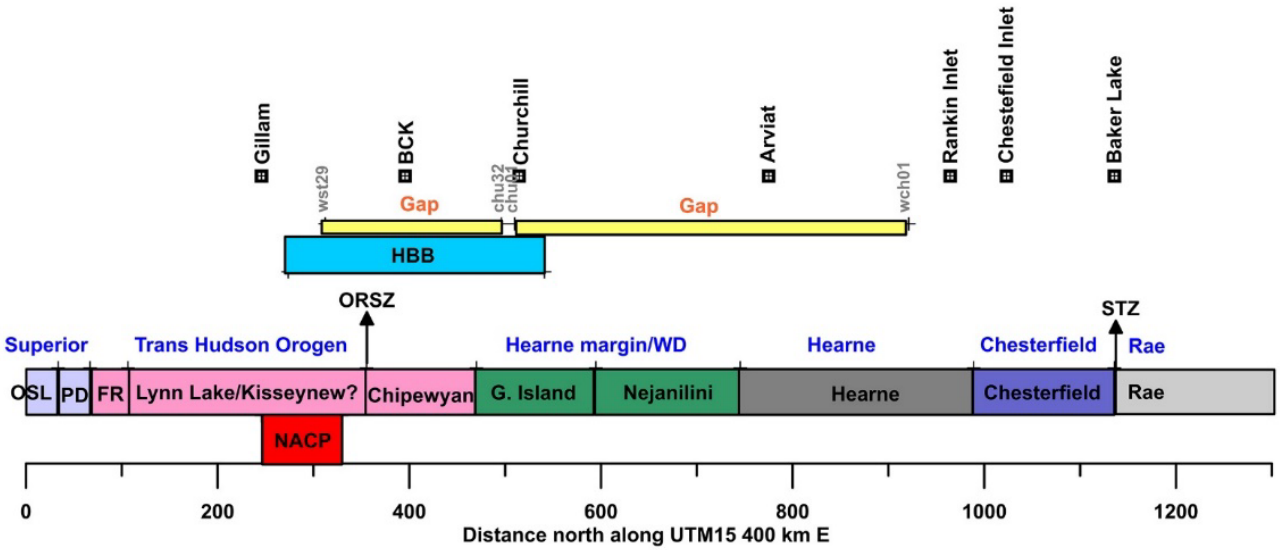

Figure 61. Geological domains and other features along the Gillam-Kivalliq corridor. Abbreviations: OSL=Oxford Stull lake domain; PD = Pikwitonei domain; FR=Fox River belt; WD=Wollaston domain; HBB=Hudson Bay Basin; ORSZ=Owl River Shear Zone; STZ=Snowbird Tectonic Zone. The position of the NACP is based on the analysis and model of Gupta et al. (1985). Large gaps in the available data are shown by yellow rectangles.

6. Synthesis of resistivity information for region

6.1 Resistivity of major Precambrian domains on Gillam-Kivalliq corridor

6.1.1 Superior craton The northeastern few hundred kilometres of the Superior craton is characterized by very resistive (>5000 Ω·m) rocks in the crust and upper mantle lithosphere. At large depth there is a transition to more conductive rocks (<300 Ω·m) occurring at around 150 km in 2-D models (Figure 17, 22) but closer to 100 km in 3-D models (Figure 23). There may also be localized areas of higher conductivity (<20 Ω·m) at more shallow depth (Figure 23, 31).

6.1.2 Rae craton and Chesterfield Block Locations more than 50–100 km north of the STZ in the Committee Block of the southern Rae craton exhibit very high crustal resistivity (>5000 Ω·m) and lithospheric mantle resistivity (>20,000 Ω·m) (Figure 26, 39). Farther to the north, more moderate mantle resistivity is observed e.g., beneath Baffin Island and the Melville Peninsula. To the south, 2-D models show an increase to more conductive rocks (<300 Ω·m at >250 km depth (Figure 39) but 3-D models suggest this transition occurs at <120 km depth. To the north of Baker Lake and the STZ, the upper Rae crust is relatively conductive (<1000 Ω·m) but the mantle lithosphere remains extremely resistive (>20,000 Ω·m). South of the STZ, the Chesterfield Block has resistive upper crust (>5000 Ω·m) and conductive lower crust (<1000 Ω·m) and the mantle lithosphere is resistive (>20,000 Ω·m).

6.1.3 Hearne craton basement rocks There is limited information on the Hearne craton from close to the Gillam-Kivalliq corridor. Sites 1 and 2 of the STZ survey suggest a heterogeneous crust with some parts having resistivity (>5000 Ω·m) and some parts being more conductive (<5000 Ω·m). The STZ results suggest the Hearne mantle lithosphere is more conductive than the Rae mantle lithosphere, although still quite resistive (>5000 Ω·m).

6.1.4 Hearne craton supracrustal cover sequences including the Wollaston Domain The small number of MT sites from near Churchill suggest the Hearne cover sequences in the Great Island domain contain both smaller (<2 km wide) moderately conductive (<100 Ω·m) zones at a few hundred metres depth and a larger (>5 km wide) very conductive (<10 Ω·m) zone at 4 km depth. There is no information available on other supracustal sequences, such as the Hurwitz Group. However, it is noted that some supracrustal sequences on Baffin Island and Melville Peninsula exhibit extremely conductive responses.

6.1.5 Trans Hudson Orogen The various regional MT studies described above define a heterogeneous resistivity structure in the crust and upper mantle of the Trans Hudson Orogen. The studies show juvenile rocks such as in the Flin Flon Belt, Kisseynew domain, and Rottenstone domain have variable crustal resistivity with some areas having resistivity of >5000 Ω·m and some areas have resistivity <100 Ω·m (Figures 17, 18, 22, 31, 43). The lithospheric mantle is more conductive (typically <1000 Ω·m) than beneath most of the older Archean cratons but it also includes more resistive zones and more conductive zones.

6.2 Resistivity of NACP on Gillam-Kivalliq corridor

In most resistivity models, the NACP conductor is characterized by a crustal conductor with a dipping upper surface. In many models, the conductor extends up to a depth of 10–20 km (Figures 14,17,18,31,43,58,59) but in some cases, e.g., on LITHOPROBE Line L there are conductive zones extending to near the surface (Figure 17,58,59). Depending on the modelled thickness of the conductive feature, its resistivity lies between 25 and <1 Ω·m. A number of crossings of the NACP also indicate that it is associated with a conductive region in the mantle (e.g., Figure 17, 18, 31, 59).

The study results from close to the Gillam-Kivalliq corridor suggest the top of the NACP is at ~15 km depth on the corridor and that it has a northward dip (Figure 14,31,44). When modelled as having 10-15 km width in the north-south direction, the resistivity of the NACP body is <10 Ω·m. When it is modelled as being wider in the north-south direction, it has a higher resistivity (e.g., 25 Ω·m for a >75 km wide body in Figure 14).

6.3 Resistivity of Hudson Bay Basin rocks on Gillam-Kivalliq corridor

Well-log results, control-source electromagnetic soundings, along with the MT soundings from the Western Superior and Kaskattama surveys collectively suggest an average resistivity for the Ordovician Bad Cache Rapids Group and Churchill River Group of the Hudson Bay Basin of ~300–500 Ω·m (Figure 51, Table 5). The overlying Red Head Rapids is more conductive, with a value of 50–150 Ω·m (Table 5). The values for the Ordovician units contrast with MT results from Churchill which resolved very low resistivity of <10 Ω·m just above the Precambrian basement. The observations suggest localized enhancement of the conductivity of the deepest part of the Ordovician sequence near Churchill, due to either hydrothermal dolomitic alteration and/or sea-water intrusion. Well-log and MT survey results suggest the Silurian Severn River Formation is more conductive than the underlying Ordovician units and has a resistivity of 20–30 Ω·m.

6.4 Resistivity of near-surface sediments on Gillam-Kivalliq corridor

The thickness and resistivity of near-surface sediments on the Gillam-Kivalliq corridor will vary considerably between different physiographic regions. TEM results from the Gillam area suggest that in the southern part of the corridor, the depth to bedrock is 40–60 m. Along with conductivity logs, the TEM results suggest an integrated conductance of near-surface sediments as high as 1–2 S.

6.5 Resistivity elsewhere of terranes in MT gaps on the Gillam-Kivalliq corridor

6.5.1 Chipewyan Batholith LITHOPROBE Line L includes one MT and one AMT site over the Wathaman-Chipewyan batholith (M30 and A39) as shown in Figure 62. Figure 17 suggests the corresponding part of 2-D models show moderate resistivity at both crustal and mantle depth.

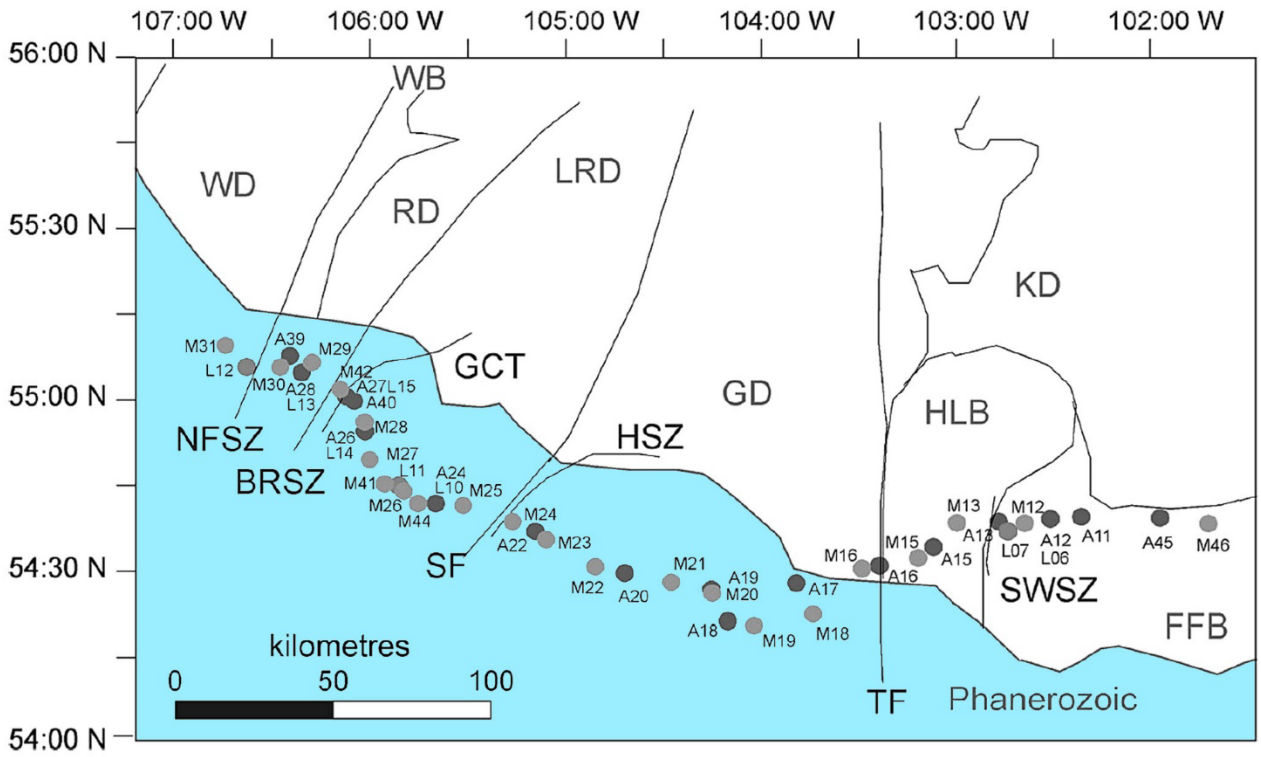

Figure 62. Central part of LITHOPROBE Line L showing two sites in the Wathaman Batholith (WB) (Ferguson et al., 2005b).

6.5.2 Wollaston domain LITHOPROBE Line L includes five sites extending over a ~60 km crossing of the Wollaston Domain (Figures 17) and Line X includes five sites extending over the southwestern 80 km of the Wollaston Domain (Figure 18) The results suggest a similar resistivity structure. Line L includes moderately resistive zones in the shallow crust (~3000 Ω·m) overlying relatively conductive middle crust and slightly more resistive lower crust. Line X includes resistive upper crust (>5000 Ω·m), relatively conductive middle crust (<100 Ω·m), and moderately conductive lower crust (~500 Ω·m). The lithospheric mantle beneath the Wollaston Domain on both lines is relatively conductive (<300 Ω·m).

6.5.3. Hearne craton The closest information to the Gillam-Kivalliq corridor on the resistivity in the Hearne domain is from LITHOPROBE Line L which includes five sites extending over the southwestern 80 km of the Hearne domain. The results indicate a relative heterogeneous structure with some zones with resistivity >5000 Ω·m and some with resistivity <30 Ω·m. The lithospheric mantle is relatively conductive (<1000 Ω·m).

MT surveys from the Melville Peninsula (Spratt et al., 2013), Southampton Island (Spratt et al., 2012), and Baffin Island (Evans et al., 2005; Craven et al., 2013) do not sample regions identified as Hearne domain (e.g., Rainbird et al., 2010; Berman et al., 2013b). The study to the west by Tschirhart et al. (in press) examining the basement of the Athabasca Basin is entirely in the southern Rae craton and other studies in the Athabasca Basin, including those above the Hearne basement, appear to be based on AMT rather than BBMT soundings. There are some results for the Hearne domain from southern and central Alberta (e.g., Nieuwenhuis et al., 2014)

although the overlying rocks of the Western Canada Sedimentary Basin limit the resolution at crustal depths (Figure 63, 64). There are also soundings extending farther to the south into the Wyoming craton (e.g., Fultz, 2017). The Alberta results suggest heterogeneous crustal resistivity and moderately resistive lithospheric mantle (Figure 64).

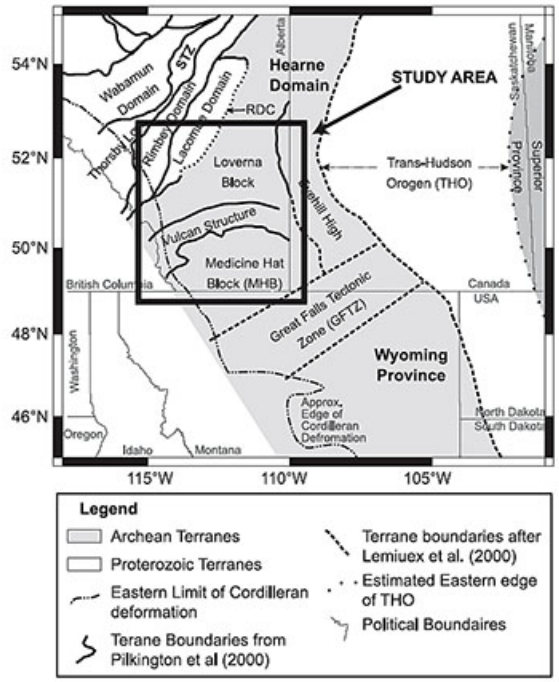

Figure 63. Location of study area in southern Alberta (Nieuwenhuis et al., 2014).

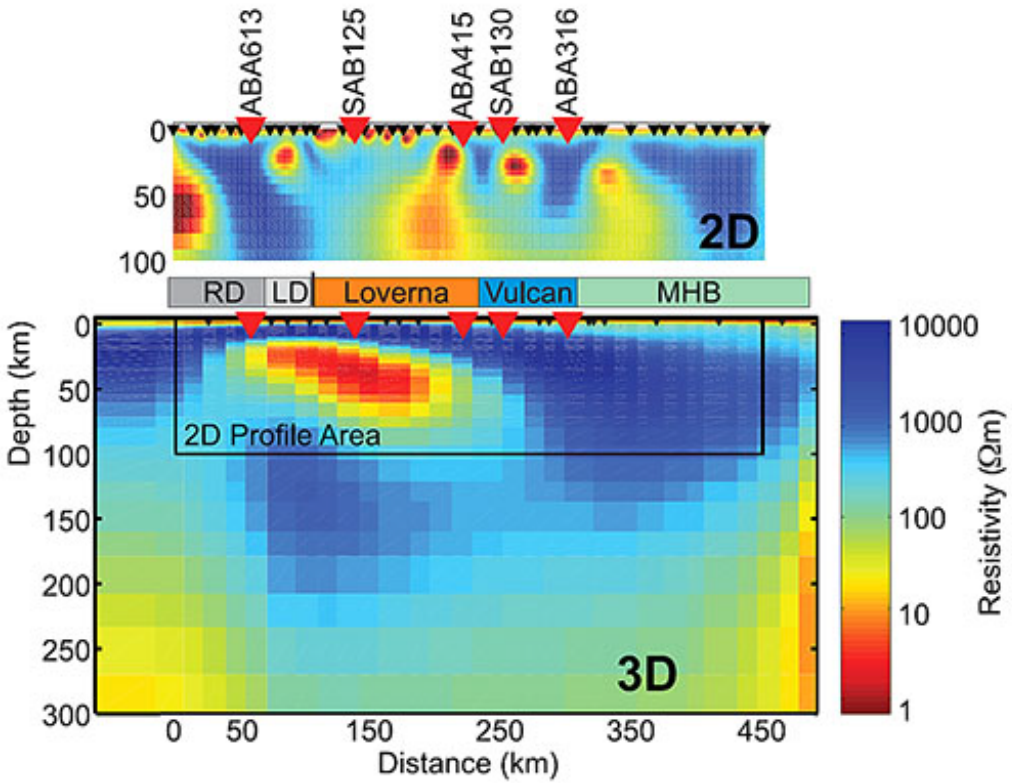

Figure 64. 2-D and 3-D models of region likely corresponding to Hearne Domain (Nieuwenhuis et al., 2014).

6.6 Deep lithospheric and asthenospheric resistivity structure

The MT surveys reviewed in Section 3.1 resolve the resistivity to typical maximum depths of between 100 km and 300 km depending on whether the surveys included LMT data acquisition and the resistivity at crustal and shallow mantle depths. BBMT surveys typically provide MT responses to maximum periods of 2000–3000 s and LMT surveys typically provide MT responses to maximum periods of 10,000–20,000 s. These maximum periods are more severely limited in the auroral zone by heterogeneous ionospheric source-fields.

For GIC modelling it is desirable to determine MT responses for periods from 1 s to 1 day (86,400 s or ~10^5 s). There is thus insufficient information in the existing MT data sets to constrain the longest period impedance responses. The optimum source for deeper responses is the very long period MT sounding conducted in Carty Lake in the southeastern Superior craton in 1992–1993 (Schultz et al., 1993). This survey provided responses to a period of >1 day and the response was extended to even longer periods using a geomagnetic depth sounding response from Virginia. Figure 65 shows the resulting data and a 1-D model fitted to the response.

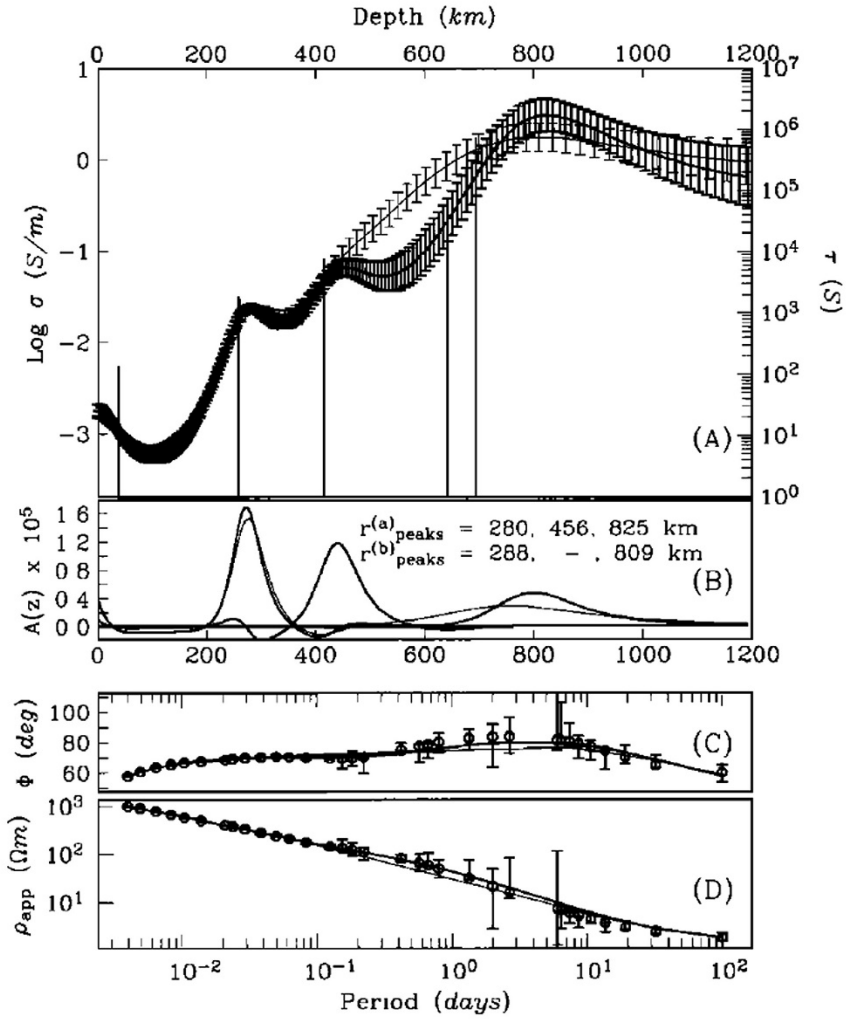

Figure 65. Ultra long period MT response and 1-D model from the southeastern Superior craton (Schultz et al., 1993). (A) Flattest conductivity model with confidence limits for different sub-data sets. Left-hand axis gives the conductivity scale and right-hand axis gives the conductance scale for D+ (delta function) model. (B) Resolving kernels for depths centred on conductive zones in flattest models. (C) and (D) Fit of flattest model for the two sub-data sets. The longest 8 periods are derived from the GDS response and the remaining 25 periods are the undistorted lake-bottom MT response.

7. Development of 2-D resistivity models

7.1 Inversion purpose and strategy

A series of 2-D resistivity models was developed for the Gillam-Kivalliq profile. The purpose of the modelling was to create models for computing 2-D impedance responses at arbitrary locations along the profile and for an arbitrary range of specified periods. The models thus provide a means of interpolating between the locations at which MT soundings already exist.

7.1.1 2-D modelling versus statistical interpolation of observed responses The 2-D modelling approach used in this study contrasts with direct spatial statistical interpolation of observed impedances in a number of ways.

1. The use of a 2-D resistivity model to produce output impedances means that the physics of electromagnetic induction is fully respected in the production of responses at new locations and periods. The 2-D resistivity model is fitted to the observed responses using an inversion algorithm based on the electromagnetic principles and the generation of new responses using forward modelling is also based on these principles. In contrast, many statistically-based interpolation methods will not adhere to these principles.
2. The 2-D resistivity model provides an excellent framework for introducing additional constraints such as information on the very deep resistivity structure (>250 km) that is not available from the MT soundings in the Gillam-Kivalliq region. As the MT response is a non-linear function of the Earth resistivity, it would be impossible to introduce this information except using an electromagnetic modelling approach.
3. The 2-D resistivity models are simplified representations of the true Earth resistivity structure and will provide reduced aliasing of small-scale features, such as small-scale 2-D and 3-D structures and 3-D galvanic distortion due to local heterogeneities, relative to the actual MT soundings. Although, the individual MT soundings capture the local variability in the resistivity structure to a greater degree than the 2-D model, the sparse distribution of available MT sites means that this information will be grossly aliased in the data. The development of a relatively smooth 2-D resistivity approach provides a way of producing a model that captures the main features of the resistivity structure.
4. Notwithstanding the previous point, there are some important large-scale 3-D structures in the Gillam-Kivalliq region that will not be properly represented in the 2-D model, and in particular the 3-D form of Hudson Bay and the Hudson Bay Basin sedimentary rocks. Additional modelling is required to assess the impact of these features on the MT responses.

7.1.2 2-D modelling for GIC computations versus geological interpretation The objectives of the GIC-based modelling in this study (representing and interpolating MT impedance responses) is in contrast to Earth structure studies in which the objective is to provide accurate information on subsurface resistivity structure. This difference requires differences in approach. For example, in most 2-D Earth structure studies, the TE mode apparent resistivity response is down-weighted relative the TM mode response in data inversions because it is more susceptible to distortion by 3-D structures (Jones 1983; Wannamaker 1999; Ledo et al. 2002; Ledo 2005). In contrast, for the GIC-based study it is important to give balanced weight to both TE and TM modes in order to provide a superior representation of the full impedance response responses. In GIC-based modelling there is also reduced importance in assessing the reliability of the model in representing the true Earth structure e.g., less need for resolution testing of various features of the resistivity model.

In both Earth-structure modelling and GIC-based modelling, increased emphasis is placed in fitting the phase response than the apparent resistivity response. In the current study this weighting is used to reduce the effects of local galvanic distortion in the MT data set by local heterogeneities that degrade its representation of larger-scale regional structures. Although, there are tensor decomposition methods available for reducing

galvanic distortion (e.g., Groom and Bailey, 1989; McNeice and Jones, 2001; Caldwell et al., 2004; Becken and Burkhardt 2004; Jones, 2012; Booker, 2014), they have not been employed in this study.

7.1.3 Inversion strategy Inversion and forward modelling used the 2-D non-linear conjugate gradient (NLCG) code of Rodi and Mackie (2001, 2012) in Geosystem's WinGLink software.
The 2-D inversions were done to create four models.

a) A model A based on the available MT data along the modelling profile.
b) A model B based on the available MT data that incorporates deep layers determined in the Carty Lake study in the southeastern Superior craton in 1992–1993 (Schultz et al., 1993). Inclusion of these layers at the base of the previous 2-D model will provide responses to periods exceeding 24 hours (86,400 s, $8.6x10^4$ s)
c) A model C in which the gaps in the MT profile are padded with MT data from the corresponding geological terranes from LITHOPROBE Line L (see Section 6.5).
d) A model D with the padded data and the deeper layers from the Carty Lake study.

Table 6 lists the thickness and resistivity of layers providing a representation of the continuous conductivity profile of Schultz et al. (1993). Because the MT data likely has some resolution at depths >180 km in more resistive regions and the resistivity is potentially more variable in this depth range the layers at >260 km depth were used as constraints in models B and D above. The same model grid was used for models A and B and for models C and D, but in the model with deep layers the resistivity at depths >260 km was constrained to the values listed in Table 6. An extremely large damping constant was specified to ensure the resistivity values remained close to the specified values during the inversion, and a horizontal tear (break in smoothing) was added at 250–60 km depth, in order to allow the resistivity just above to the constrained layers to not be affected by these layers.

Table 6. Deep resistivity model for central Canada from Schultz et al. (1993)

Depth range (km)	Conductivity (S/m)	Resistivity (Ω·m)	Comments
180–260	0.004	250	Value will be poorly representative of the actual resistivity structure in the shallower part of this depth range.
260–420	0.02	50	
420–640	0.08	12.5	
640745	0.5	2	
>745	3.0	0.33	

7.2 Data preparation for inversion models

The 2-D resistivity model was derived for the north-south profile based on an east-west geoelectric strike. The transverse electric (TE) response corresponds to east-west electric current flow and the transverse magnetic (TM) response to north-south current flow.

7.2.1 Models based on available MT sites Models A and B were created using MT sites available from within 200 km of the actual Gillam-Kivalliq corridor. The responses from all sites were rotated to a 90º azimuth so that the east-west impedance component (unrotated *yx*-mode) corresponded to the 2-D TE mode and the north-south impedance component (unrotated *xy*-component) corresponded to the 2-D TM mode. The location of each site was projected in an east-west direction to the modeling profile.

In the initial phases of inversion, all available sites were included in the model, but this approach resulted in very close projection of some sites on the profile. The selection of sites to be included in the model

was therefore carefully adjusted to ensure they had a better distribution after projection. Where possible the included sites were also chosen so that their original locations crossed the local geological strike rather than them sampling a limited cross-strike range. Table 7 lists the 37 sites included in the final phases of the inversion and Figure 66 shows their location. The sites that are included are from the LITHOPROBE Trans Hudson Orogen Survey and LITHOPROBE Western Superior, and the GSC Knee Lake, Churchill, STZ and Central Rae craton surveys (Table 1). Some further editing of these sites and of data form particular period ranges from other sites was done during the various inversion phases.

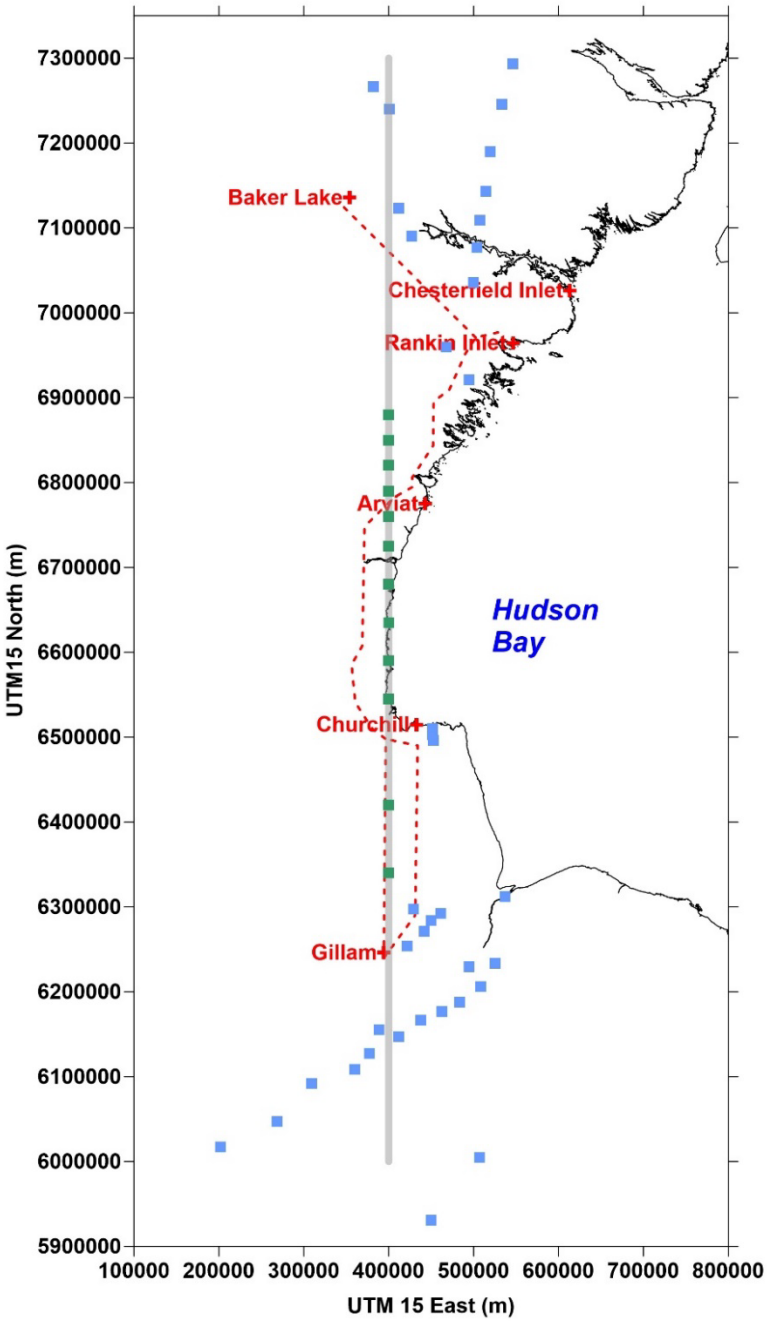

Figure 66. Location of modelling profile and MT sites. The grey line is the model profile; blue squares show location of available MT sites used in the inversion; green squares show the location of MT sites imported from the corresponding geological terrane from LITHOPROBE Line L; and red dashed line show planned route and alternative route for the Kivalliq Hydro-Fibre corridor.

Table 7. MT sites used in inversions for Gillam-Kivalliq corridor

Site	Survey	Latitude (deg)	Longitude (deg)	UTM15 East (m)	UTM15 North (m)	Profile (km)
wst28	LITHOPROBE West Superior	53.52253	-93.7555	449916	5930666	-69.3
wst27	LITHOPROBE West Superior	54.19423	-92.8924	507019	6005137	5.1
tho-m55s	LITHOPROBE THO	54.21528	-97.5714	201996	6017127	17.1
wst34	LITHOPROBE West Superior	54.51827	-96.5742	268680	6047066	47.1
wst33	LITHOPROBE West Superior	54.93483	-95.976	309350	6091594	91.6
knl-002	GSC Knee Lake	55.10583	-95.1917	360178	6108762	108.8
wst32	LITHOPROBE West Superior	55.27617	-94.9294	377437	6127220	127.2
knl-005	GSC Knee Lake	55.46305	-94.3895	412144	6147199	147.2
knl-004	GSC Knee Lake	55.53222	-94.7618	388803	6155429	155.4
wst31	LITHOPROBE West Superior	55.63898	-93.9853	437978	6166340	166.3
knl-010	GSC Knee Lake	55.73583	-93.5945	462669	6176839	176.8
knl-012	GSC Knee Lake	55.83695	-93.2598	483727	6187963	188.0
knl-xt2	GSC Knee Lake	55.99945	-92.8678	508243	6206026	206.0
wst30	LITHOPROBE West Superior	56.21022	-93.0827	494872	6229480	229.4
knl-013	GSC Knee Lake	56.24806	-92.5893	525453	6233764	233.8
mh03n	Manitoba Hydro Bipole III	56.42365	-94.2672	421834	6253953	254.0
mh06n	Manitoba Hydro Bipole III	56.58202	-93.9426	442099	6271257	271.2
mhrmn-hf	Manitoba Hydro Bipole III	56.69398	-93.8128	450223	6283617	283.6
mh10n	Manitoba Hydro Bipole III	56.7752	-93.6366	461095	6292543	292.5
mh11n	Manitoba Hydro Bipole III	56.81577	-94.1586	429274	6297477	297.5
wst29	LITH West Superior	56.95289	-92.3963	536719	6312304	312.3
chu32	GEM Churchill Project	58.60445	-93.8166	452551	6496297	496.3
chu21	GEM Churchill Project	58.66325	-93.8363	451485	6502858	502.9
chu01	GEM Churchill Project	58.72553	-93.8377	451491	6509793	509.8
wch001	GSC STZ	62.42166	-93.0969	494993	6921159	921.2
wch002	GSC STZ	62.76666	-93.6314	467764	6959750	959.8
dmn-204a	GEM Central Rae	63.44978	-92.9979	500107	7035704	1035.7
dmn-205	GEM Central Rae	63.82155	-92.9183	504024	7077132	1077.1
wch004	GSC STZ	63.92805	-94.4881	427034	7089848	1089.8
dmn-206	GEM Central Rae	64.10511	-92.8492	507346	7108736	1108.7
wch005	GSC STZ	64.22167	-94.8106	412153	7122966	1123.0
dmn-007	GEM Central Rae	64.41214	-92.6935	514769	7142977	1143.0
dmn-008	GEM Central Rae	64.83303	-92.5884	519532	7189910	1189.9
wch007	GSC STZ	65.26778	-95.128	400669	7239974	1240.0
dmn-009	GEM Central Rae	65.33209	-92.2808	533491	7245657	1245.7
wch008	GSC STZ	65.49806	-95.5544	381814	7266362	1266.4
dmn-017b	GEM Central Rae	65.75928	-91.9900	546270	7293451	1293.5

7.2.2 Padding of profile gaps with data from remote MT sites Models C and D were created using MT sites available from within 200 km of the actual Gillam-Kivalliq corridor and MT data imported from the corresponding geological terranes from LITHOPROBE Line L (see Section 6.5). The importing of sites from the

same geological terranes is intended to provide responses with the same general statistical character as the true responses it is not expected to reproduce the true responses.

To pad the southern gap crossing the Wathaman-Chipewyan batholith, the one available LITHOPROBE Line L site, tho-m30, was imported to two new locations spanning the gap (Table 8). In order to complete this process, the edi file for tho-m30 was edited to change the REFLAT and REFLONG to the specified new location and the site name DATAID was changed. The two new sites were renamed xxx-m30 (southern site) and yyy-m30 (northern). In contrast to the area along the Gillam-Kivalliq corridor, the geological strike along LITHOPROBE Line L is close to north-south (Figure 62) so for the Line L sites the 2-D TE mode corresponds to the north-south impedance component (unrotated *xy*-component) and the 2-D TM mode to east-west impedance component (unrotated *yx*-mode). In order to best match the Gillam-Kivalliq corridor data and the imported data, the imported data were maintained at 0º rotation in contrast to the 90º rotation used for the local sites. This process ensures that for all sites, the TE mode corresponds to the direction parallel to the geoelectric strike.

Table 8. Padding of MT sites used in inversions for Gillam-Kivalliq corridor

Original site name	Terrane	New site name	UTM15 Easting (m)	UTM15 Northing (m)	NAD83 Latitude (deg:min:sec)	NAD83 Longitude (deg:min:sec)	Profile location (km)
South Gap							
tho-m30	Wath-Chip	xxx-m30s	400000	6340069	57:11:32.1	-094:39:17.2	340.1
tho-m30	Wath-Chip	yyy-m30s	400000	6420068	57:54:38.0	-094:41:15.7	420.1
North Gap							
tho-m31	Wollaston	xxx-m31s	400000	6544961	59:01:57.8	-94:44:32.5	545.0
tho-m32	Wollaston	xxx-m32s	400000	6590130	59:26:11.9	-94:45:47.1	590.1
tho-m43	Wollaston	xxx-m43s	400000	6635007	59:50:26.0	-94:47:03.8	635.0
tho-m33	Wollaston	xxx-m33s	400000	6679979	60:14:39.9	-94:48:22.8	680.0
tho-m34	Wollaston	xxx-m34s	400000	6724977	60:38:53.7	-94:49:44.0	725.0
tho-m35	Hearne	xxx-m35s	400000	6760035	60:57:44.4	-94:50:48.8	760.0
tho-m36	Hearne	xxx-m36s	400000	6790056	61:13:53.5	-94:51:45.6	790.1
tho-m37	Hearne	xxx-m37s	400000	6820129	61:30:02.5	-94:52:43.5	820.1
tho-m38	Hearne	xxx-m38s	400000	6849963	61:46:11.5	-94:53:42.5	850.0
tho-m39	Hearne	xxx-m39s	400000	6879983	62:02:20.4	-94:54:42.7	880.0

To pad the northern gap, the part in the Hearne margin terranes (Great Island and Nejanilini terranes) was padded with LITHOPROBE Line L sites from the Wollaston domain. The part in the Hearne craton was padded with LITHOPROBE Line L sites from the Hearne craton (Table 8; Figure 66). A total of 10 sites from LITHOPROBE Line L were imported, with sites ordered from east-to-west on LITHOPROBE Line L imported to a south-to-north order on the Gillam-Kivalliq corridor to maintain their correct Superior-to-Rae sequencing (Table 8). The method used for importing the sites was the same as for the Wathaman-Chipewyan importing. In order to best match the two data sets, the imported data were again maintained at 0º rotation in contrast to the 90º rotation used for the local sites. The padded data set included a total of 49 sites (Figure 66).

7.3 MT pseudosections for unpadded and padded data sets

Pseudosections of the available MT data set were prepared using a relatively small amount of smoothing (Figure 67). The results for the available MT data show the two large gaps in the MT coverage along the Gillam-Kivalliq profile. At the scale of the profile, the TE and TM responses are fairly similar but there are

subtle differences between the modes such as for the response of the NACP and within the Rae craton. The results reflect observations from individual surveys described in Sections 3 and 6.

- High apparent resistivity responses in the Superior and Rae cratons indicate the resistive nature of the crust and uppermost mantle lithosphere. Higher phases observed at 10^2–10^3 s beneath the Superior craton and 10^3–10^4 s beneath the Rae craton indicate the presence of more conductive underlying rocks.
- The Chesterfield Block exhibits more conductive responses than the Rae craton.
- There are only two sites available in the northern Hearne craton. They exhibit variable apparent resistivity that may be affected by static shift but both show increased phase at long periods suggesting an increase in conductivity at large depth.
- The Trans Hudson Orogen exhibits a relatively heterogeneous conductive response.
- The NACP response is clearly visible from periods as short as 0.1 s in the TE and TM phase response and 1 s in the TE and TM apparent resistivity response.
- The Hudson Bay Basin (not shown in Figure 67) extends form the middle of the NACP to the middle of the Great Island terrane. The low phase response at 0.1 s at the sites near Churchill is related to the increase in the resistivity at the base of the Hudson Bay Basin.

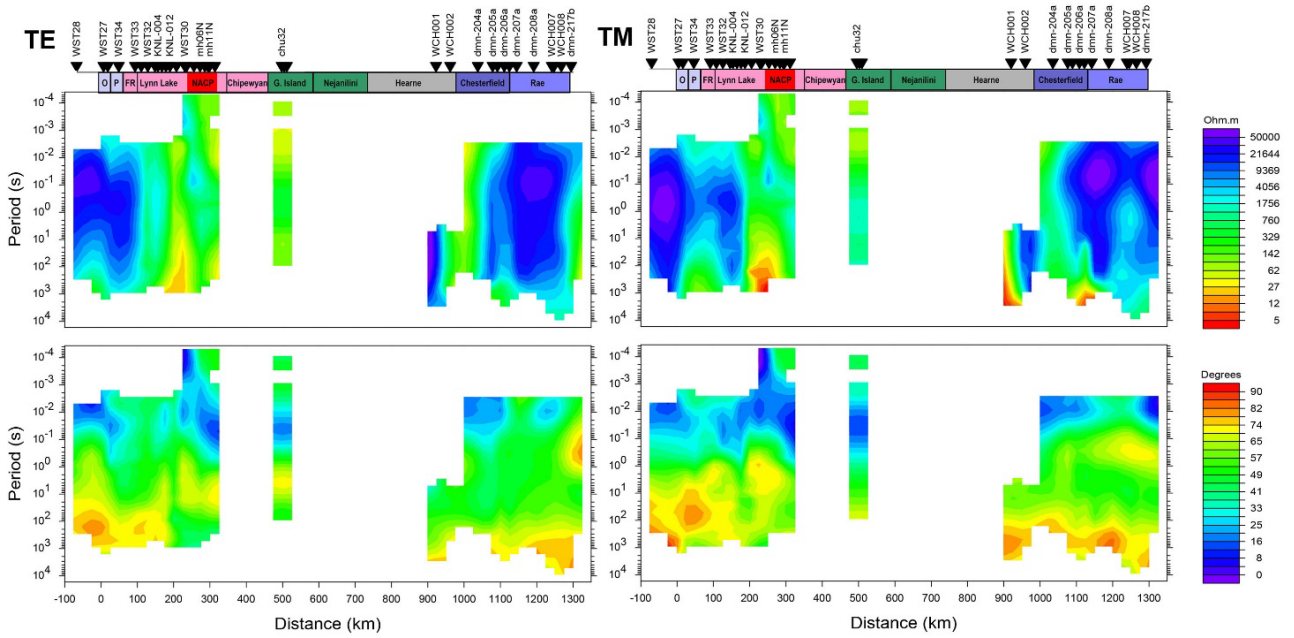

Figure 67. Apparent resistivity pseudosections (upper panels) and phase pseudosections (lower panels) of available data along the Gillam-Kivalliq corridor. The TE mode corresponds to east-west currents and the TM mode to north-south currents. Grid cell width is 25 km and grid cell height is 4 cells/decade. The interpolation radius is 1, spine weight is 1, and smoothing factor is 3.

Pseudosections of the padded MT data set were prepared using the same approach as for the available MT sites (Figure 68). The padded data introduce more complexity into the short periods MT response. For example, the imported Hearne sites include a conductive apparent resistivity response at periods of less than 0.1 s in both components. The imported phase responses are more consistent between the imported and adjacent sites. However, there are some discontinuities in the band of low phase responses at periods shorter than 0.1 s that may be associated with the absence of surface Hudson Bay Basin rocks in the imported data. These shorter period effects are not expected to have a major impact on the 1–10^5 s period range of greatest concern in GIC modelling. However, the imported sites do include some local structures at long periods. For example, at period

exceeding 10 s the imported Wathaman-Chipewyan TE responses are more conductive than surrounding sites and the TM responses are more resistive.

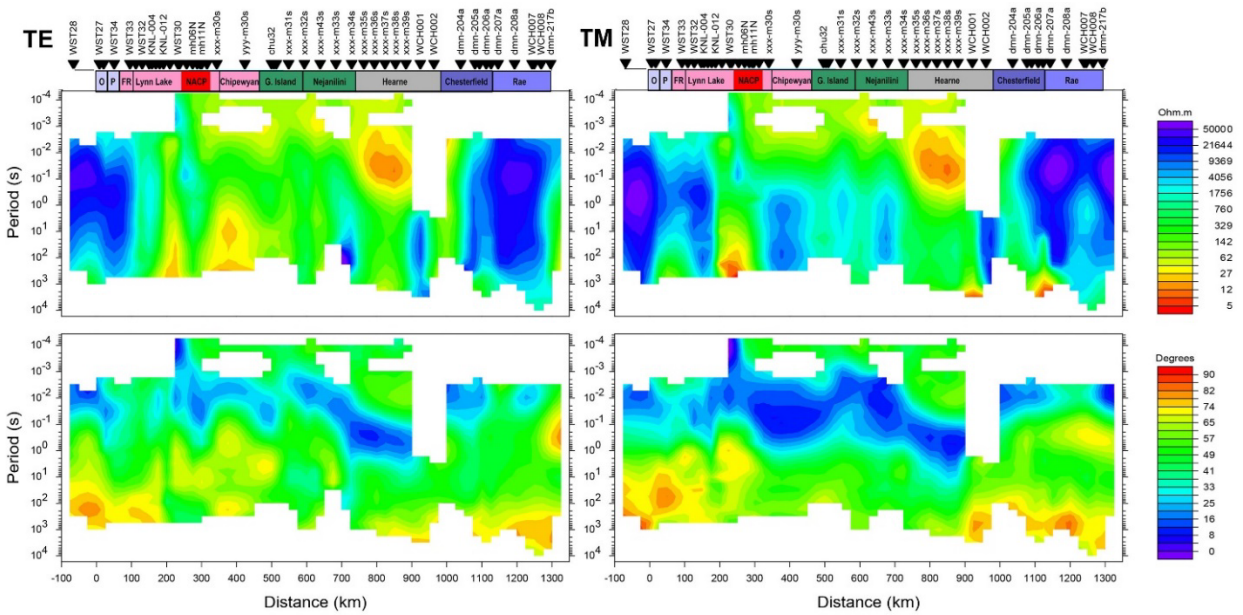

Figure 68. Apparent resistivity pseudosections (upper panels) and phase pseudosections (lower panels) of padded data along the Gillam-Kivalliq corridor. The TE mode corresponds to east-west currents and the TM mode to north-south currents. Grid cell width is 25 km and grid cell height is 4 cells/decade. The interpolation radius is 1, spine weight is 1, and smoothing factor is 3.

7.4 Inversion parameters

Inversion parameters were established during a series of trial inversions and then used consistently in a final inversion run for each of the final four models. The inversion parameters are shown in Table 7.

Table 9. 2-D inversion parameters

Parameter	Value(s)	Comments
Inverted data	TE+TM ρ_a,ϕ 10^{-3}–10^{3} s	Tipper response was not included in the analysis. Full period range was not available at all sites. Station data inverted.
Errors	TE+TM ϕ: 5% TE+TM ρ_a: 20%	Both errors and error floors were set to these values and no estimated error values were used.
Static shift	Not inverted	Static values were reset to 1 prior to inversion
Model extent	Horizontal: 900–1900 km Depth: 0–1000 km	Padded >600 km beyond sites
Grid-size	82x91 unpadded model 96x94 padded model	Unpadded model included 37 sites and padded model included 49 sites
Starting model	1000 Ω·m half-space	With constrained deep layers at >260 km depth in Models B and D.
Regularization	Smoothest model	
Regularization parameters	Uniform grid Laplacian; Minimize the integral of Laplacian^2	
Weighting	α=3.0, β=3.0, Min block 1x1 km	
Range	0.3–50,000 Ω·m	30 range levels
No. iterations	50	

8. 2-D inversion resistivity models

Table 10 lists the normalized RMS misfits for the four models based on the error floors defined in Table 9. The inversion models provide a good overall representation of the observed responses. However, larger misfits do occur at some sites and can be attributed to both galvanic distortion and local 3-D effects. The misfit levels could be reduced to slightly lower levels by fitting distortion-corrected data and/or by fitting some of the static shift in the MT responses. However, considering the relatively larger number of total sites included in the models, the complexity of the geological structures, and the distance of projection of sites to the model profile (Figure 66) the RMS misfit attained is considered quite satisfactory and the inversions models are considered to provide a good representation of the large scale resistivity structure.

Table 10. RMS misfit for the inversion models

Model	RMS misfit
A	2.825
B	2.769
C	3.024
D	2.900

8.1 Unpadded MT model with no deep constraints

Figure 69 shows the model fitted to the available MT data with no constraints on the resistivity of the layers deeper than 260 km. As required by the smoothing constraints used in the inversion the model exhibits strong lateral smoothness. Figure 70 compares the model response with the observed data. The model reproduces the large-scale features of the response although small-scale aspect of the geometry of some of features in the model response is not identical to the observed data, e.g., the internal structure within the resistive zone beneath the Rae craton.

The inversion model includes very resistive crust and uppermost mantle beneath the Superior craton and the Rae craton as noted in other studies based on the same data. The resistor beneath the Superior craton extends to depths of ~75 km whereas beneath the Rae craton it extends to 130 km. The model includes some more conductive zones within the resistive crust of the two cratons but the geometry of these features is not well resolved by the data set. In the other inversions the conductive zones exhibit different geometry. The Hearne craton and Chesterfield Block exhibit relatively resistive crust, but these units have less resistive upper mantle than the Rae craton. The upper crust of the Trans Hudson Orogen and Hearne margin rocks is relative resistive but the lower crust and upper mantle is conductive. The model shows the NACP clearly as a break in the resistive upper crust, with the most conductive part of the NACP located at ~10 km depth. The exact depth of the feature is not tightly resolved by the data and in some other inversions the most conductive part of the NACP occurs at depths ranging from 5 km to 20 km.

At depths of >250 to 300 km the resistivity in model A approaches 1000 Ω·m, the resistivity of the starting model. This result suggests the longest period MT data provides some resolution to depths exceeding 200 km, especially beneath the resistive Superior and Rae cratons. However, the MT data provide no resolution at depths exceeding 300 km.

The fit of Model A to the data can be decreased slightly by running additional iterations. However, that approach leads to models that appear to be less geologically reasonable. Those models contain pervasively resistive crust and mantle (>50,000 Ω·m) with isolated conductive zones.

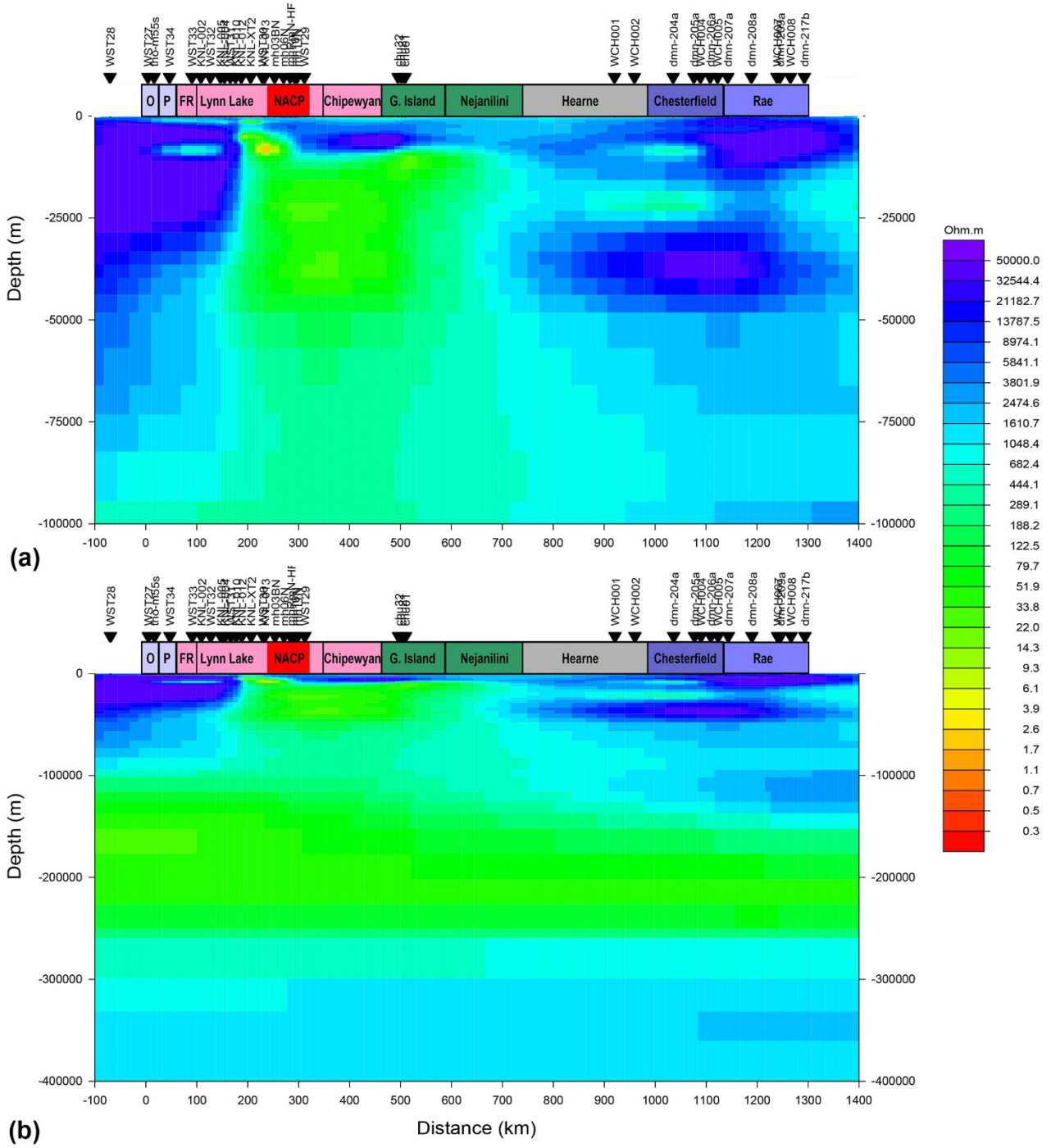

Figure 69. Model A (available MT data and no deep layer constraints). (a) Shallow part of model shown at vertical exaggeration of 8. (b) Deep part shown at a vertical exaggeration of 2.

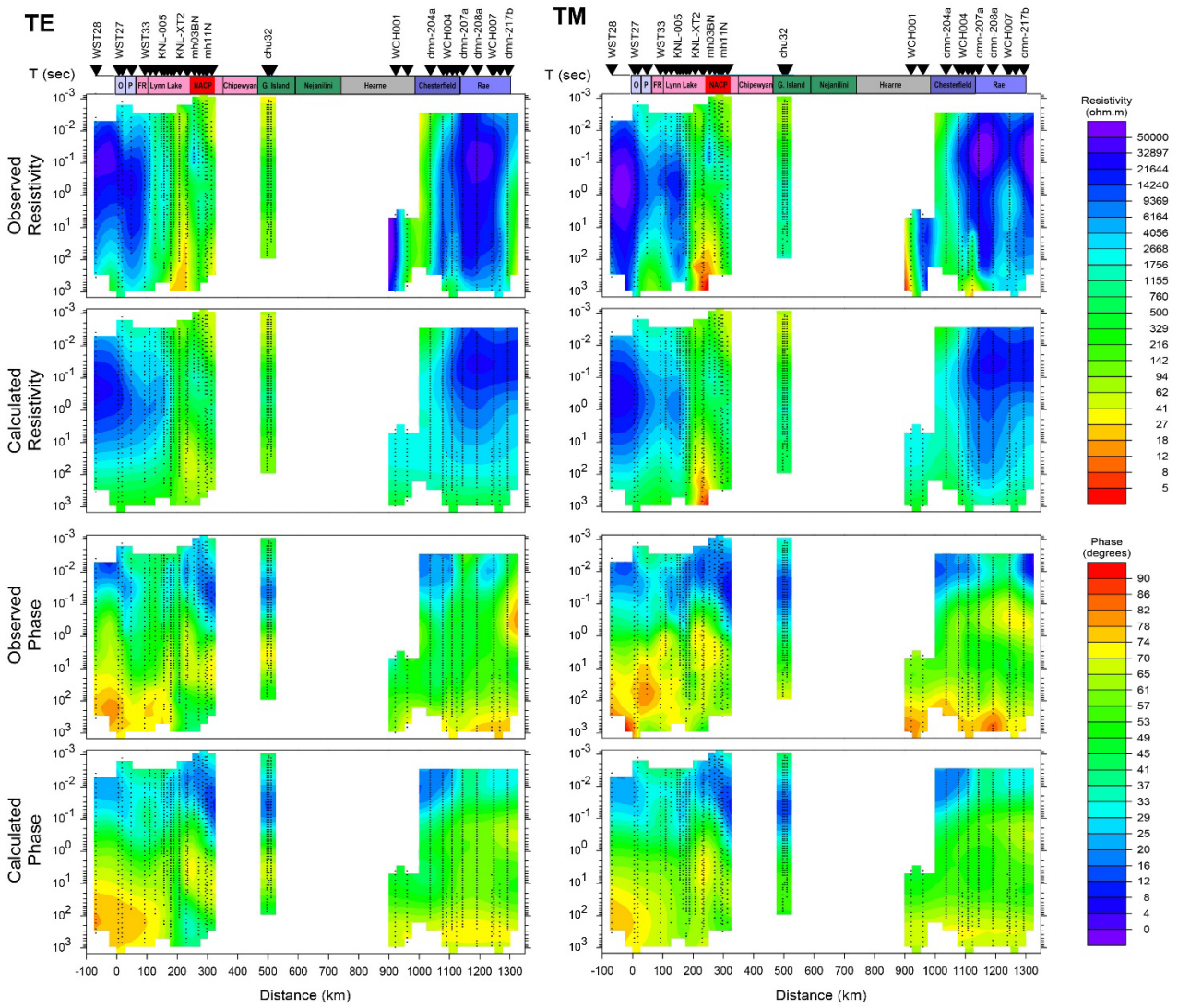

Figure 70. Pseudosection comparison of observed data and model response for the available data model with no deep layer constraints. The TE mode corresponds to east-west currents and the TM mode to north-south currents. Gridding parameters are the same as those for Figure 67.

8.2 Data-based MT model with deep constraints

Figure 71 shows the model fitted to the available MT data with constraints on the resistivity of the layers deeper than 260 km. The top layers with constrained resistivity can be seen in the lower part of the deeper section. Over the period range of the MT data, the response of the constrained model is very similar to that for the unconstrained model (Figure 70) so it has not been illustrated here.

The shallow part of the constrained model is very similar to the unconstrained model (compare Figures 69 and 70). There are only subtle differences such as a slightly deeper extent of the resistive mantle beneath the Rae craton in the constrained model.

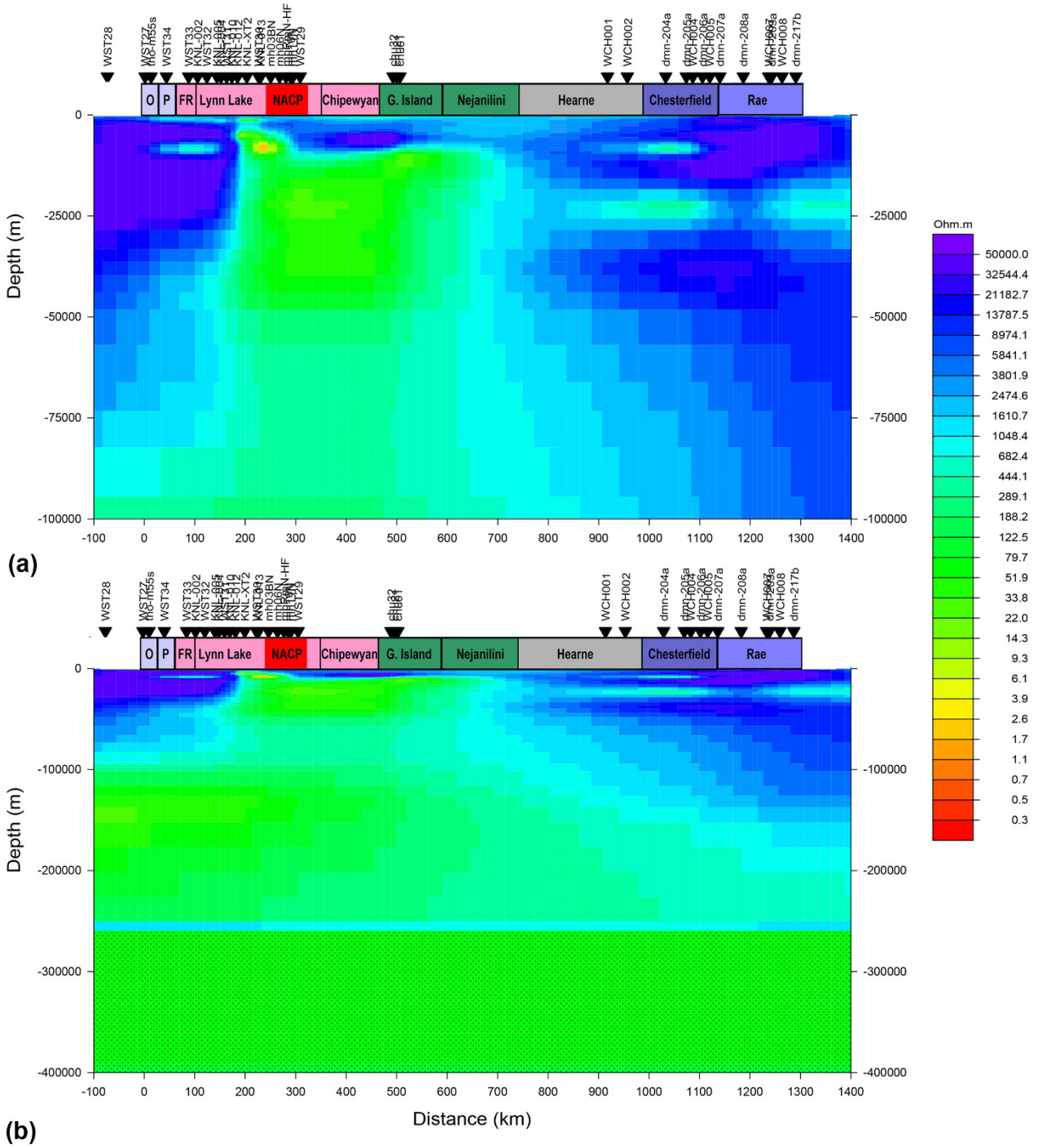

Figure 71. Model B (available MT data and deep layer constraints). (a) Shallow part of model shown at vertical exaggeration of 8. (b) Deep part shown at a vertical exaggeration of 2. Stippling indicates layers with constrained resistivity.

8.3 Geologically-padded MT model with no deep constraints

Figure 72 shows the model fitted to the padded MT data with no constraints on the resistivity of the layers deeper than 260 km. Figure 73 compares the model response with the observed data. The model again reproduces the large-scale features of the response, in the parts of the profile corresponding to both the original MT data and the padded data.

Model C contains additional conductive zones in the upper crust associated with the imported data, including a zone beneath the Wathaman Chipewyan Batholith and a zone at the margin of the Great Island and Nejanilini terranes. The models are best interpreted as showing these geological terranes can contain conductive zones in the upper crust rather than there necessarily being a conductor in these exact locations on the Gillam-Kivalliq corridor. Away from the padded sites, the resistivity models for the unpadded and padded models are very similar. The deeper (>100 km) parts of the resistivity model are very similar for the two inversions.

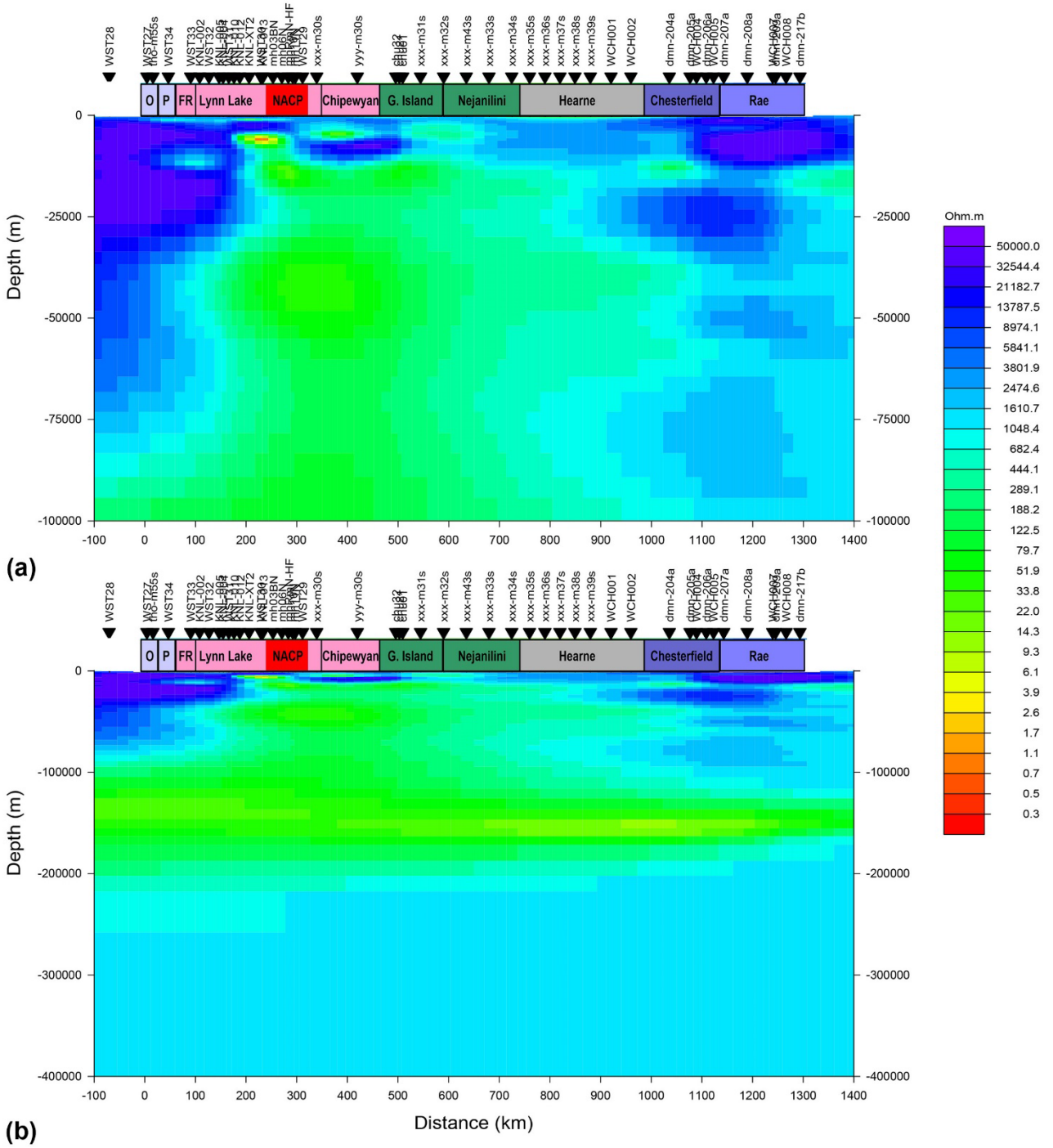

Figure 72. Model C (padded MT data and no deep layer constraints). (a) Shallow part of model shown at vertical exaggeration of 8. (b) Deep part shown at a vertical exaggeration of 2.

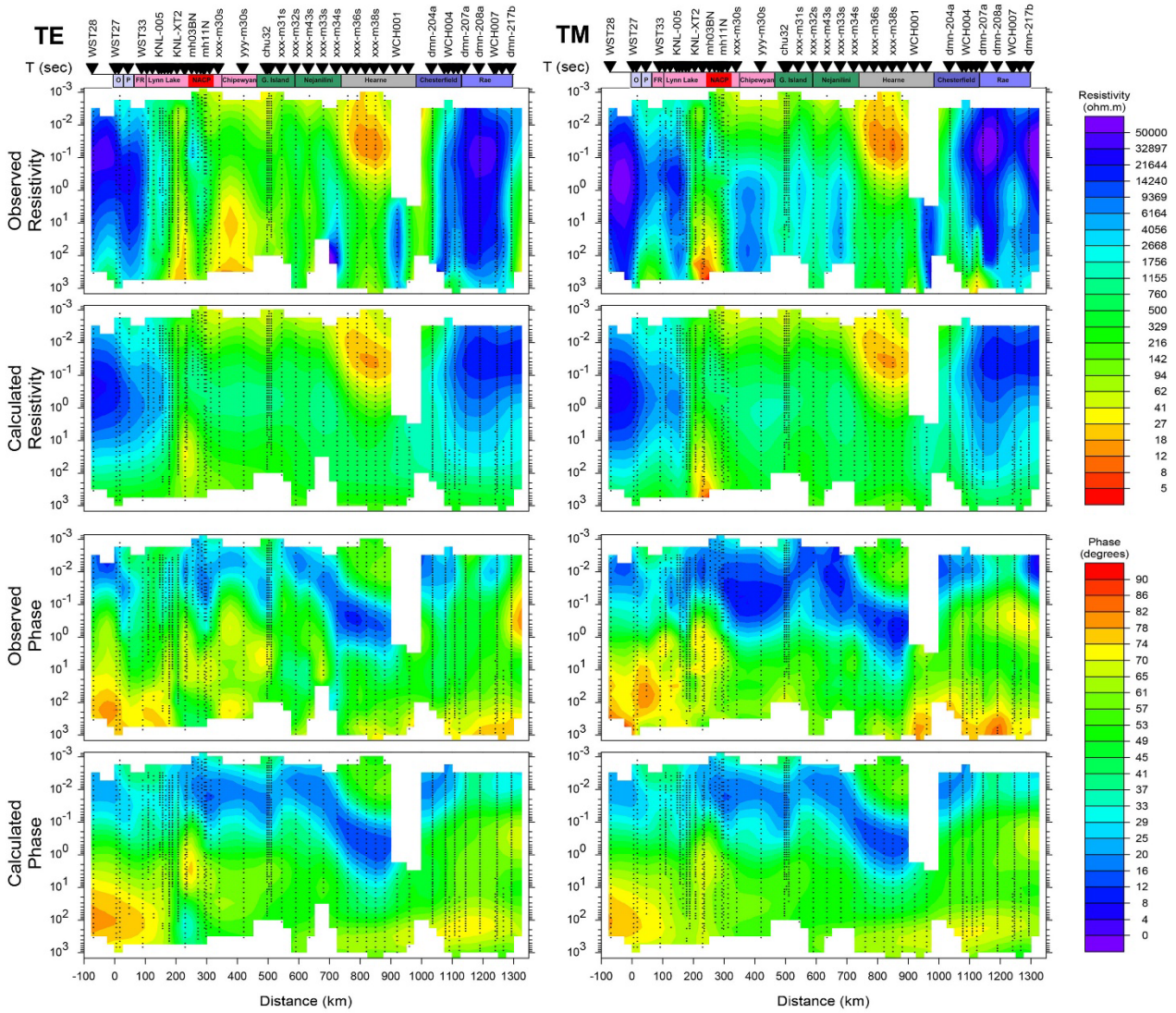

Figure 73. Pseudosection comparison of observed data and model response for the padded data model with no deep layer constraints. The TE mode corresponds to east-west currents and the TM mode to north-south currents. Gridding parameters are the same as those for Figure 68.

8.4 Geologically-padded MT model with deep constraints

Figure 74 shows the model fitted to the padded MT data with constraints on the resistivity of the layers deeper than 260 km. Over the period range of the MT data, the response of the constrained model is again very similar to that for the unconstrained model (Figure 70) so it has not been illustrated here. For the padded data, the shallow part of the constrained model is very similar to the unconstrained model (compare Figures 72 and 74).

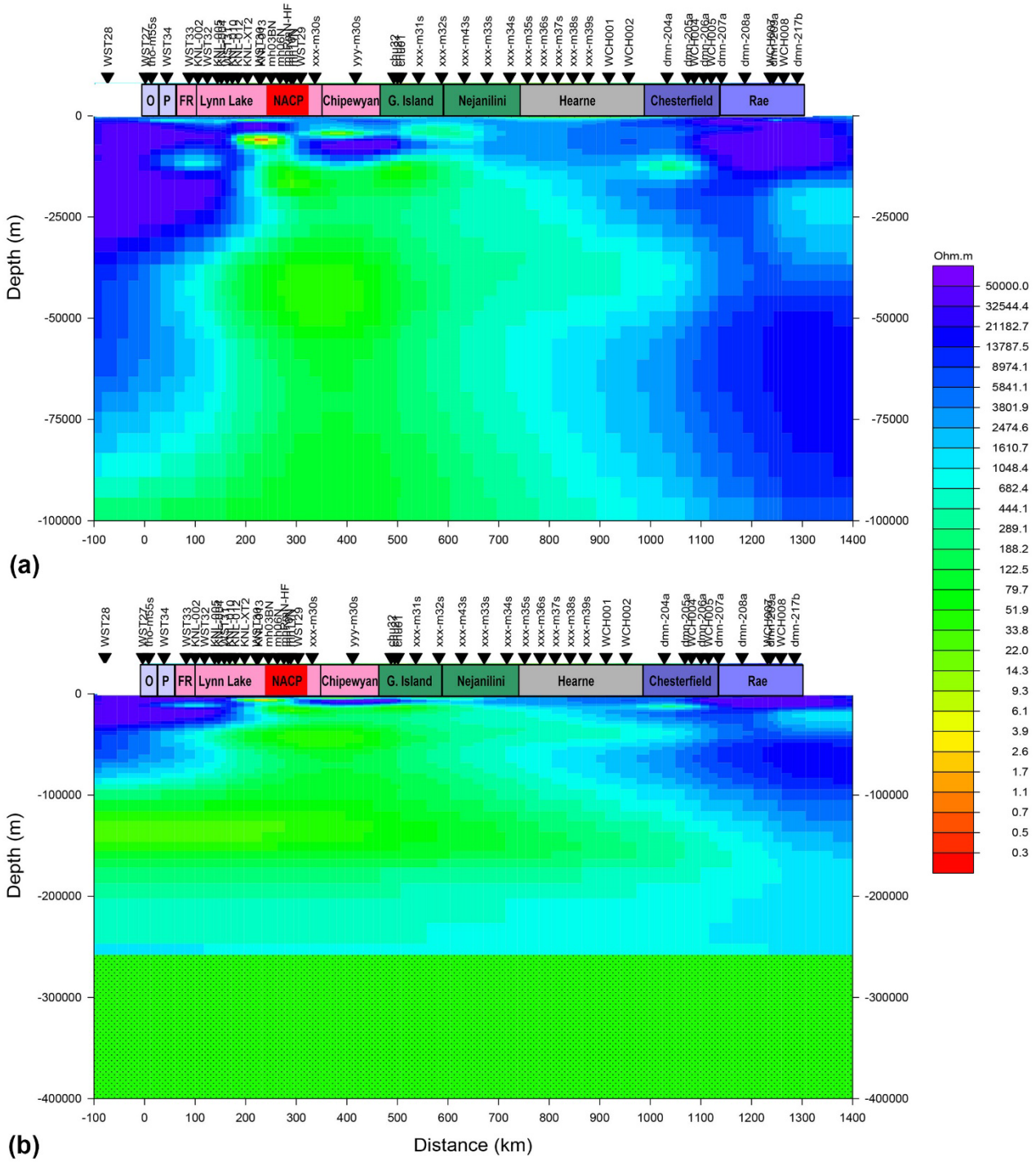

Figure 74. Model D (padded MT data and deep layer constraints). (a) Shallow part of model shown at vertical exaggeration of 8. (b) Deep part shown at a vertical exaggeration of 2. Stippling indicates layers with constrained resistivity.

9. MT impedance for 2-D resistivity models

9.1 MT data export from 2-D models

A key objective of extracting synthetic data from the 2-D resistivity models was to avoid the need for spatial interpolation of the resulting data sets. In this way, the regulation used in the inversion of the 2-D model provides the only smoothing of the MT data and the exported data are fully compatible with the 2-D electromagnetic theory. The available MT site locations and the padded MT site locations would provide data with an average spacing of 27 km along the profile. While this data spacing would be adequate for some applications, the actual spacing in some areas would exceed 40 km. It was desirable to derive results for more densely-spaced output data.

Higher density data, with a spacing of 10 km, was obtained for Models A–D using WinGLink and the following procedure.

1. A file of the 131 site locations with dummy sites names and UTM15 site coordinates was prepared
2. Using Golden Software SURFER for the coordinate transform a new file containing dummy site names and NAD83 longitude and latitude was created.
3. The WinGLink data base containing the MT data and Models A–D was duplicated.
4. The site location file was imported into the Gillam-Kivalliq project in the duplicate data base.
5. Using WinGLink map mode, the original MT site on the modelling profile were removed and replaced with the imported sites.
6. Using WinGLink 2D modelling mode, the model corresponding to Model A, B, C or D was opened.
7. The WinGLink option to correct the model for the new sites was accepted.
8. A 2-D forward model was created for a specified frequency range of 10^{-5}–10^{2} Hz and 5 frequencies/decade using the option under the Tools menu. It was necessary to turn off the default option to add random noise to the output data.
9. The MT data were then saved as Station Data to the synthetic sites using the option in the Tools menu.
10. Finally, each of the 131 sites was opened and edited in the WinGLink Soundings menu and the output 2-D data copied to an external spreadsheet. An electronic file containing the exported MT responses is available as part of this report (Appendix 1).

Figures 75 and 76 show the unconstrained unpadded and padded models model after the automated adjustment in WinGLink for the higher site density (Step 7 in the data export process). The adjustment results in minimal change to the models.

9.2 Pseudosections and profiles of exported MT data

Figures 77 and 78 shows the apparent resistivity and phase pseudosections for Models A and B after the transition to 131 synthetic MT sites, and for the extended seven-decade period range of 10^{-2} to 10^{5} s at 5 periods/decade density. The results can be compared with the pseudosections of the original data pseudosections in Figures 67 and 70. However, the exported data pseudosections do not include the shortest two period two-decades of data present in the original data set and they include an additional two decades of responses at long periods.

The exported data pseudosections show the resistive apparent resistivity responses associated with the Superior and Rae craton crust and uppermost mantle, and the higher phases at long periods associated with the transition to be more conductive rocks. The lower resistivity of the other crustal blocks is observed at periods of <10 s. The signature of the NACP can be seen in the phase response at 1–10 s period and in the apparent resistivity response at 10^{2}–10^{3} s. A surprising result in the exported data is the presence of a conductive response beneath the data gap across the Wathaman-Chipewyan Batholith. This feature is only weakly constrained by the data from MT sites adjacent to this area and it is likely extremely poorly resolved.

The responses for Model A at periods >10^3–10^4 s are not constrained by the MT data so depend heavily on the starting model used in the inversion. The responses are not properly resolved. In contrast, the results for Model B are based on a reasonable deep resistivity structure and can be considered much more reliable. The long period phase responses and the long period TE apparent resistivity for Model B are spatially smooth responses. In contrast, the TM apparent resistivity response contains strong lateral changes. These changes can be attributed to charge build-up occurring on margins of shallow features such as the NACP and are a characteristic of 2-D TM mode responses (e.g., Jones, 1983).

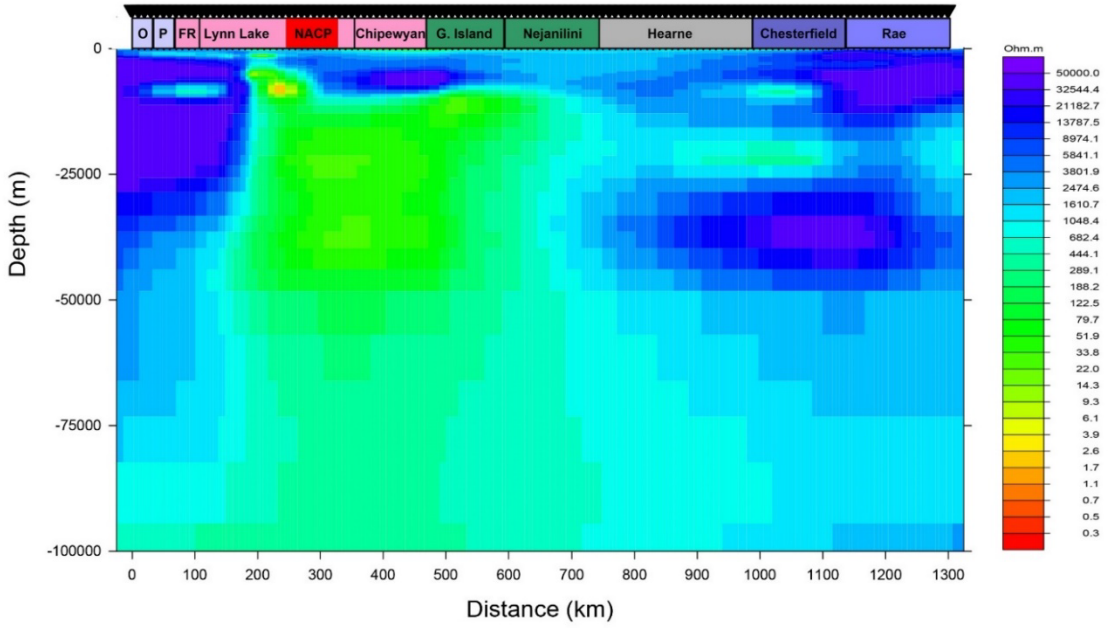

Figure 75. Model A after readjustment to 131 10 km-spaced MT sites. Compare with the initial version of the model shown in Figure 69a.

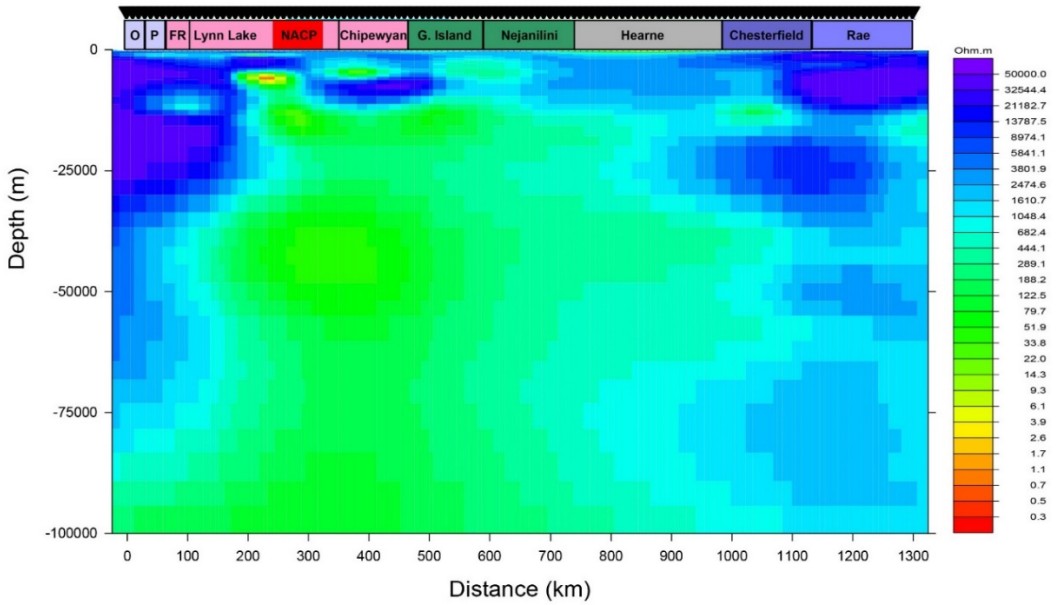

Figure 76. Model C after readjustment to 131 10 km-spaced MT sites. Compare with the initial version of the model shown in Figure 72a.

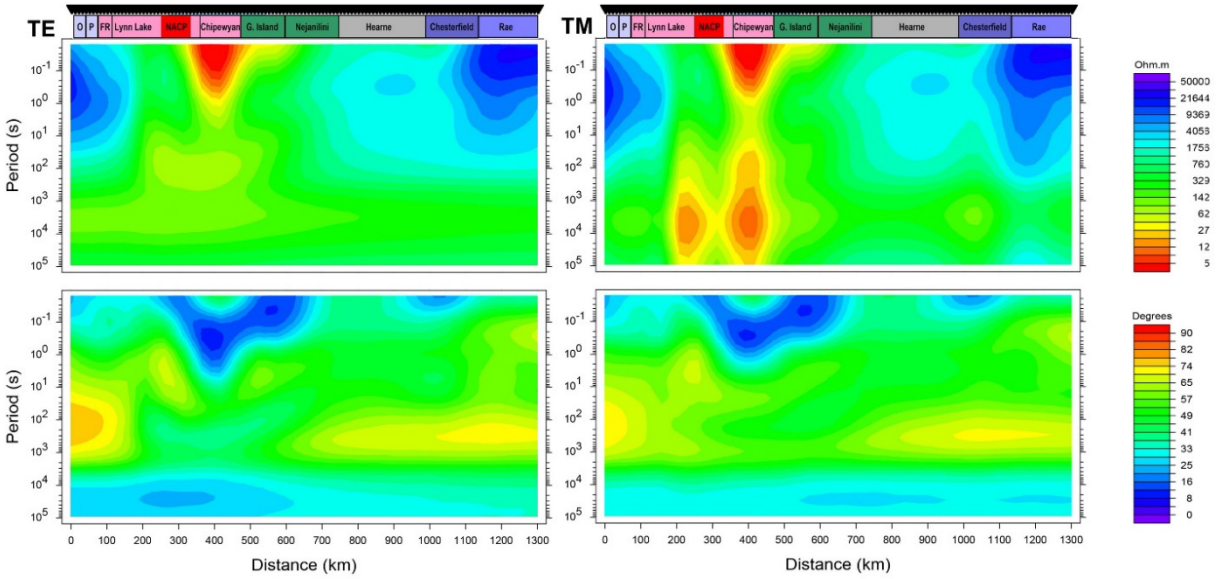

Figure 77. Data for Model A (available sites and no constrained deep layers) at 131 sites and period range 10^{-2}-10^{5} s. The TE mode corresponds to east-west currents and the TM mode to north-south currents. Gridding parameters are the same as for previous pseudosections.

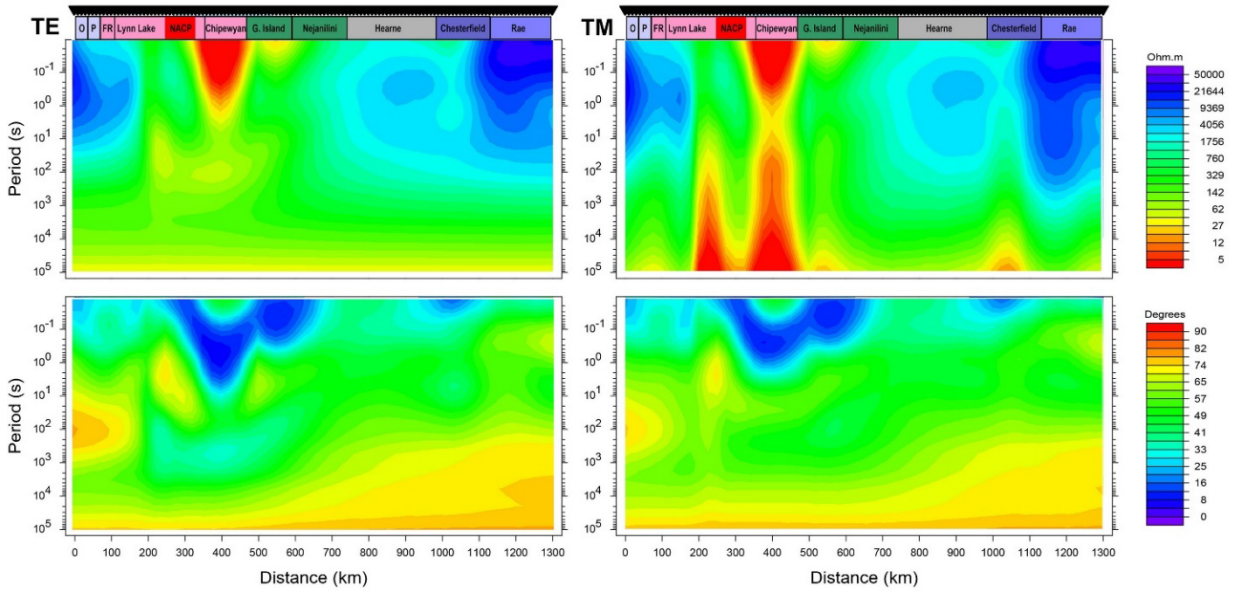

Figure 78. Data for Model B (available sites and constrained deep layers) at 131 sites and period range 10^{-2}-10^{5} s. The TE mode corresponds to east-west currents and the TM mode to north-south currents. Gridding parameters are the same as for previous pseudosections.

Figures 79 and 80 shows the apparent resistivity and phase pseudosections for Models C and D after the transition to 131 synthetic MT sites, and for the extended seven-decade period range. The results can be compared with the pseudosections of the original data pseudosections in Figures 68 and 73.

Most of the larger scale features in the exported data for the padded profiles are similar to the results for the unpadded profile. However, the are some differences. The padded data do not contain the conductive anomaly in the Wathaman-Chipewyan Batholith. The imported data provide much stronger constraints on the resistivity structure in the southern gap. In contrast, the padded data cause an additional anomaly in the Hearne craton in the northern gap. The deep layer constraints have a similar effect in the padded and unpadded data.

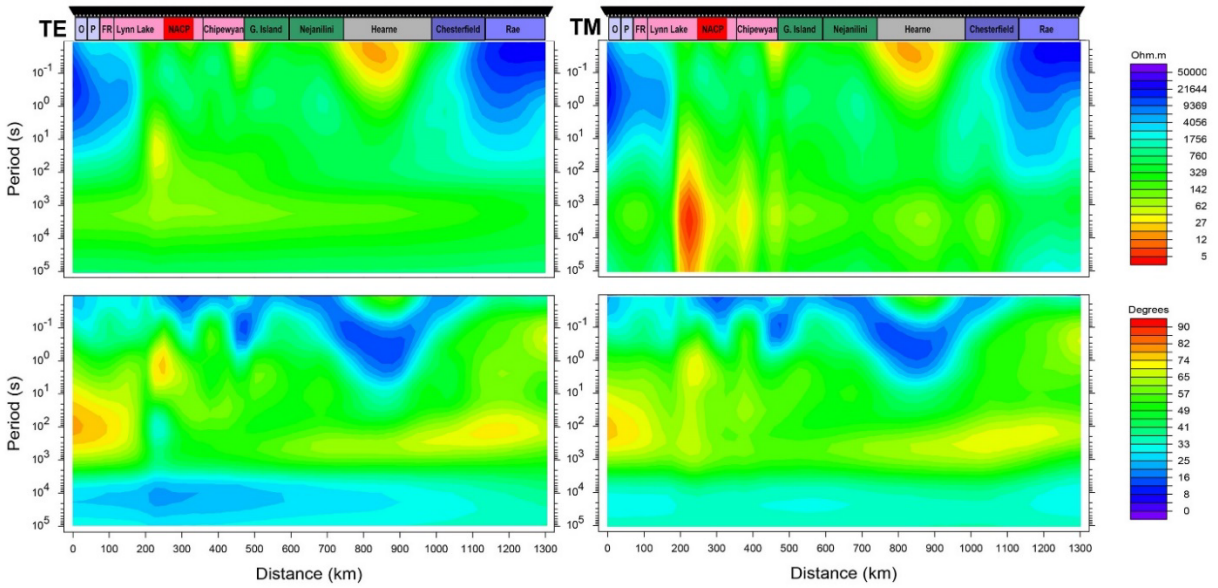

Figure 79. Data for Model C (available plus padded sites and no constrained deep layers) at 131 sites and period range 10^{-2}-10^{5} s. The TE mode corresponds to east-west currents and the TM mode to north-south currents. Gridding parameters are the same as for previous pseudosections.

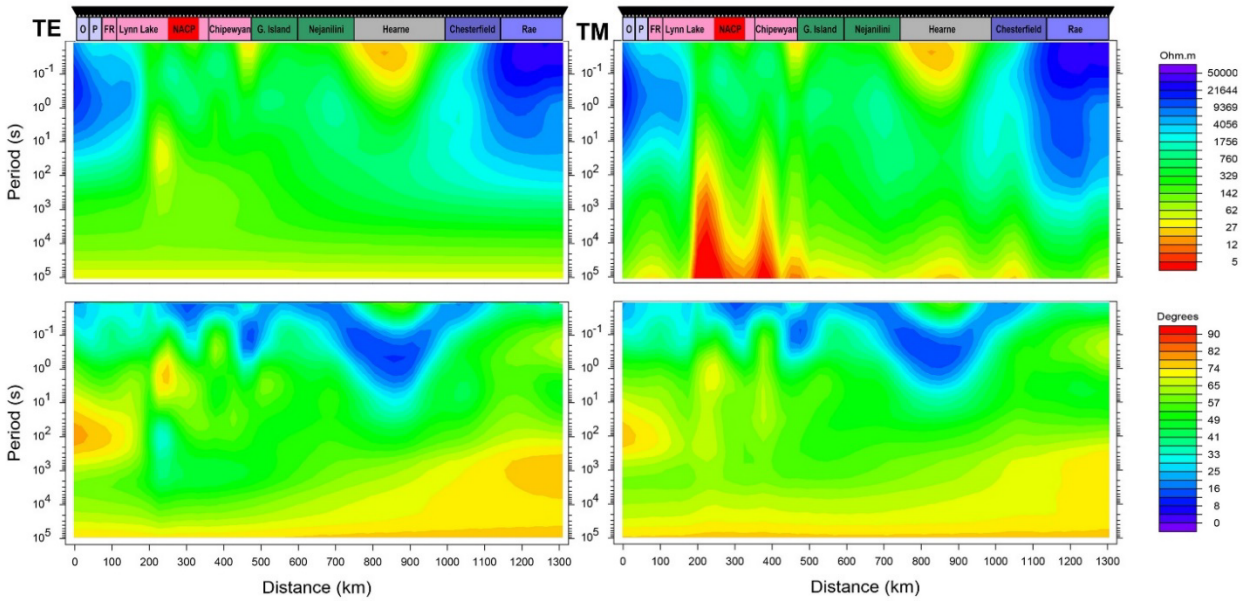

Figure 80. Data for Model D (available plus padded MT sites and constrained deep layers) at 131 sites and period range 10^{-2}-10^{5} s. The TE mode corresponds to east-west currents and the TM mode to north-south currents. Gridding parameters are the same as for previous pseudosections.

Figure 81 compares responses at representative periods for the four model in profile form. The results show that the deeper layers affect the responses mainly at periods longer than 10^4 s. This is as expected since the available MT data are mostly for periods shorter than 1,000 s. The padding of the gaps with additional MT sites has greatest effect at periods shorter than 10 s. As seen in the pseudosections, in all models the TM or north-south apparent response shows significant lateral changes extending to the longest periods. This is a consequence of the north-south profile being the TM mode for the 2-D model and exhibiting "static-effects".

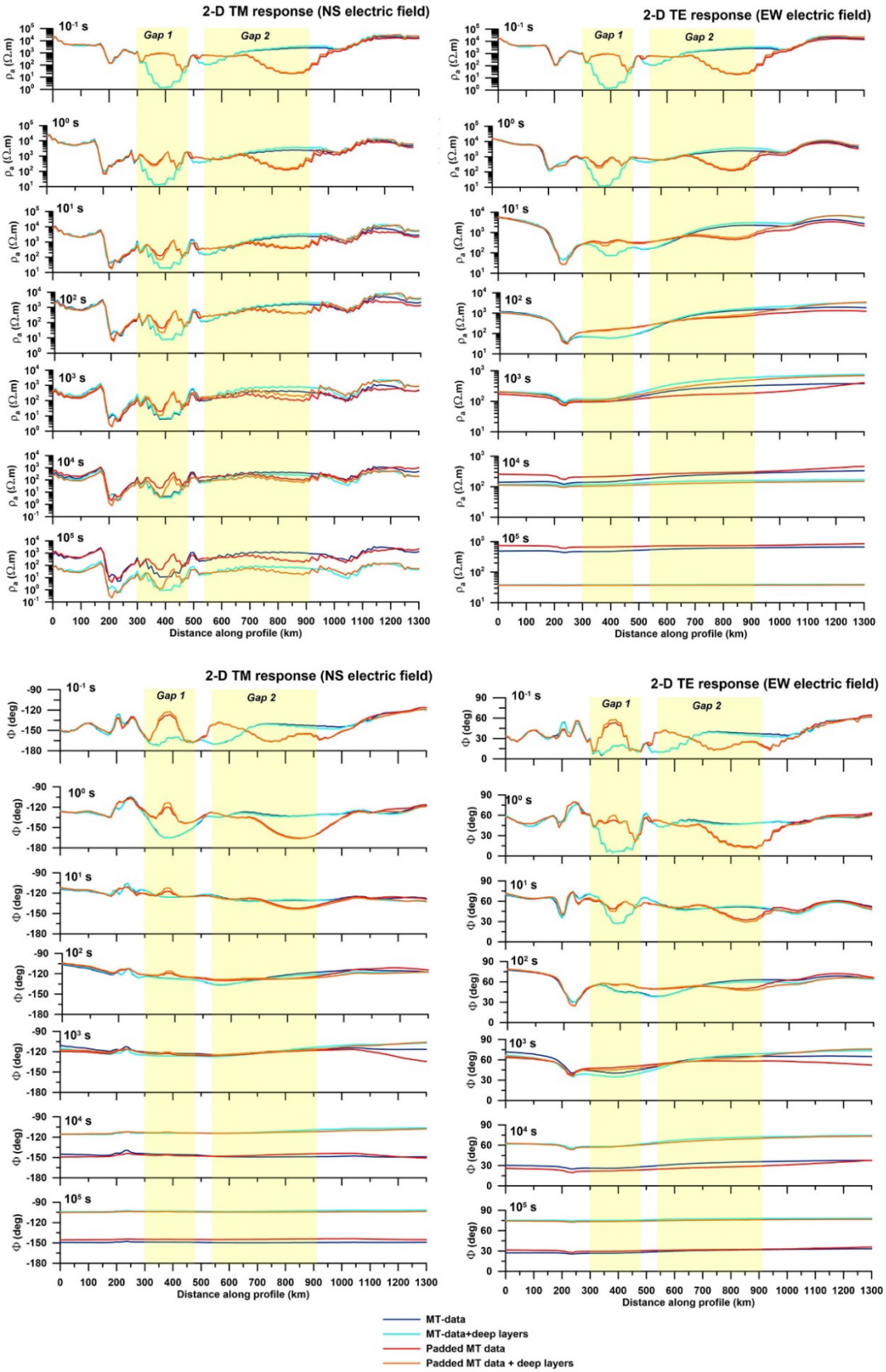

Figure 81. Comparison of the exported data from the four resistivity models. Yellow shaded areas show the location of gaps in available MT sites.

Each of the exported responses exhibits an extremely large variation along the profile and over the extended period range. The apparent resistivity values for Models B and D range from smallest values of between 0.2 and 11 Ω·m up to largest values of 33,000–38,000 Ω·m i.e., over four orders of magnitude. The phase ranges from smallest values of 4–11º up to largest values of 76–82º.

10. Examination of impedance responses

10.1 Calculation of impedance responses

The impedance magnitude is calculated from the apparent resistivity using:

$$|Z(\omega)| = [\rho_a(\omega)\omega\mu]^{1/2} \qquad \text{Eq. 5}$$

and in this form the impedance is defined in terms of the ratio of the electric field E and magnetic field strength H and has units of Ω. For period T in seconds, the equations can be written:

$$|Z(\omega)| = 2.810 \cdot 10^{-3}\left[\frac{\rho_a(\omega)}{T}\right]^{1/2} \qquad \text{Eq. 6}$$

Values in practical units of $\mu V.m^{-1}.nT^{-1}$ (defined as the ratio of the electric field and magnetic flux density) can be derived by multiplying the value in Ω by an appropriate constant. The MT phase response corresponds to the impedance phase. For the purpose of examining the impedance results, both the TE and TM phase will be displayed in the first quadrant.

In order to examine the rate of change of the impedance along the corridor the numerical first derivative between adjacent points was calculated using:

$$\frac{\Delta|Z(\omega)|}{\Delta x} = \frac{|Z_i(\omega) - Z_{i+1}(\omega)|}{10\ \text{km}} \qquad \text{Eq. 7}$$

The result is given in units of $\Omega.km^{-1}$ and it is positive for decreasing resistivity (increasing conductivity) with increasing distance to the north. The gradient could alternatively be calculated more rigorously using the magnitude of the difference of the complex impedance response. An electronic file containing the impedance responses at 10 km intervals is available as part of this report (Appendix 1).

10.2 Examination of impedance results

Figures 82–85 compares the impedance responses for Models B and D with the location of the geological terranes along the Gillam-Kivalliq corridor. Results are presented in terms of log|*Z*|, |*Z*|, impedance phase, and $\Delta|Z|/\Delta x$. When plotted in terms of the logarithm of impedance magnitude (Figure 82) the shape of the responses resemble those for the logarithm of apparent resistivity in Figure 81. The largest differences between Models B and D occur in the available data gaps. When examined in terms of the linear impedance magnitude (Figure 83) it becomes evident that the changes between models, and especially those in the south gap, are small when compared with the impedance variation along the profile. The changes between models are relatively large proportional changes, but because they occur in lower magnitude responses, they represent relatively small absolute changes. The linear response also shows that the impedance magnitude is significantly larger in the Superior and Rae craton than in other parts of the profile. For both the logarithmic and linear presentations, the lateral impedance magnitude changes at longer periods are much larger for the TM mode than for the TE mode. The largest difference between the phase response of the two models (Figure 84) again occur in the data gaps and therefore corresponds to relatively low magnitude responses.

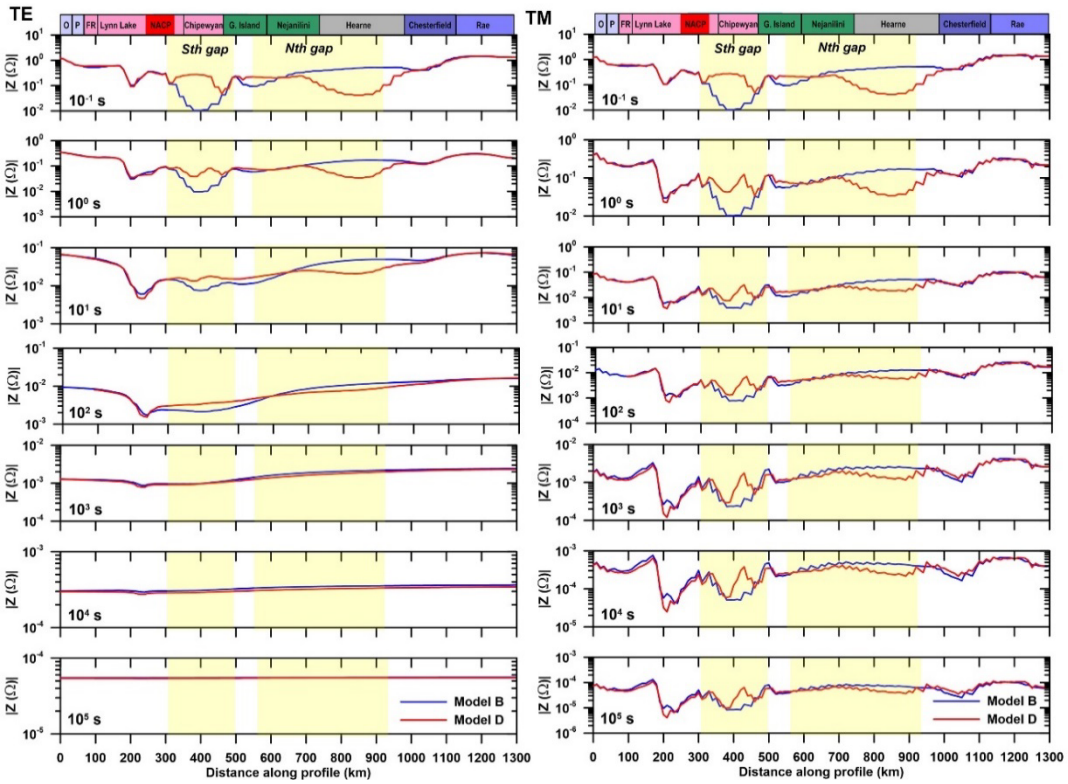

Figure 82. Impedance magnitude for Models B and D (available and padded MT data with deep layer constraints). Results are plotted in terms of the logarithm of the impedance magnitude.

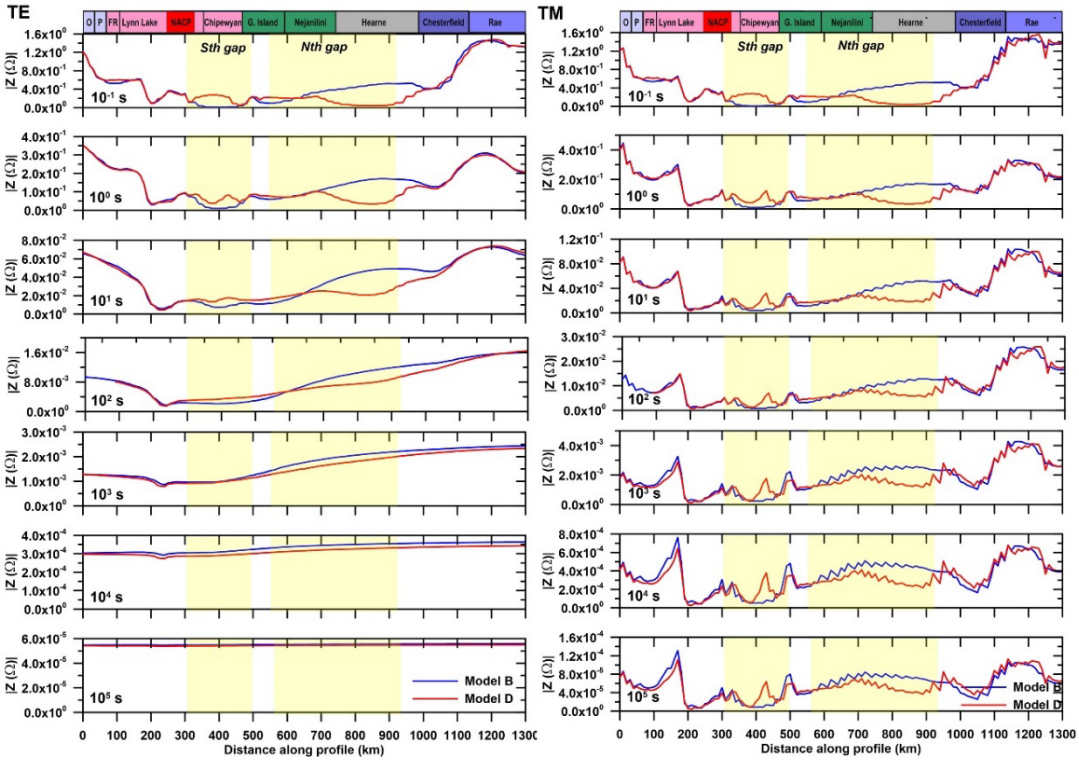

Figure 83. Impedance magnitude for Models B and D (available and padded MT data with deep layer constraints). Results are plotted in terms of the linear impedance magnitude.

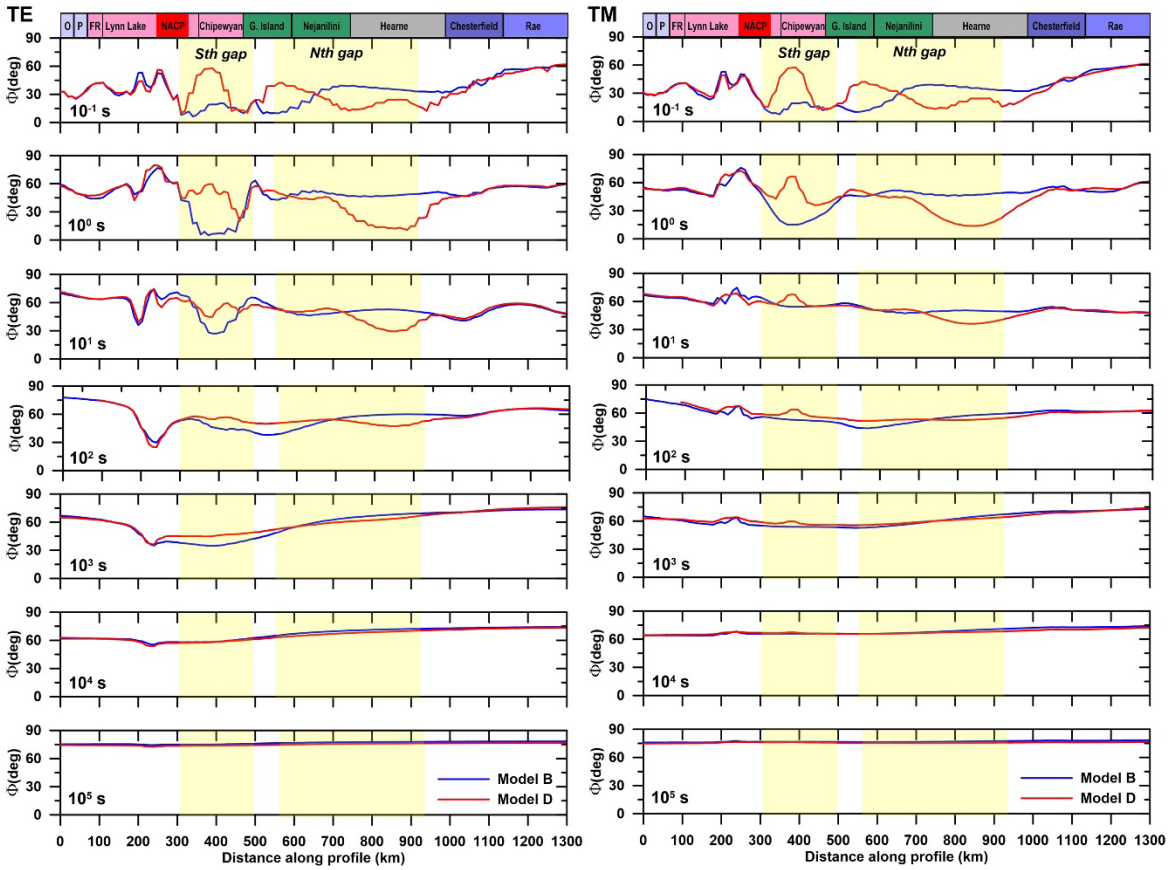

Figure 84. Impedance phase for Models B and D (available and padded MT data with deep layer constraints).

The strongest impedance magnitude gradients (Figure 85) in the TE mode response occur between 175 and 275 km along the profile in the vicinity of Gillam (which is located at 246 km). The responses are associated with the NACP and conductive uppermost crust in the Lynn Lake domain (e.g., Figures 72 and 74). The strongest gradients in the TM response occur between 175 and 200 km and this peak is visible at all periods. The TM response also includes a number of other peaks throughout the profile reflecting the greater variability in this response.

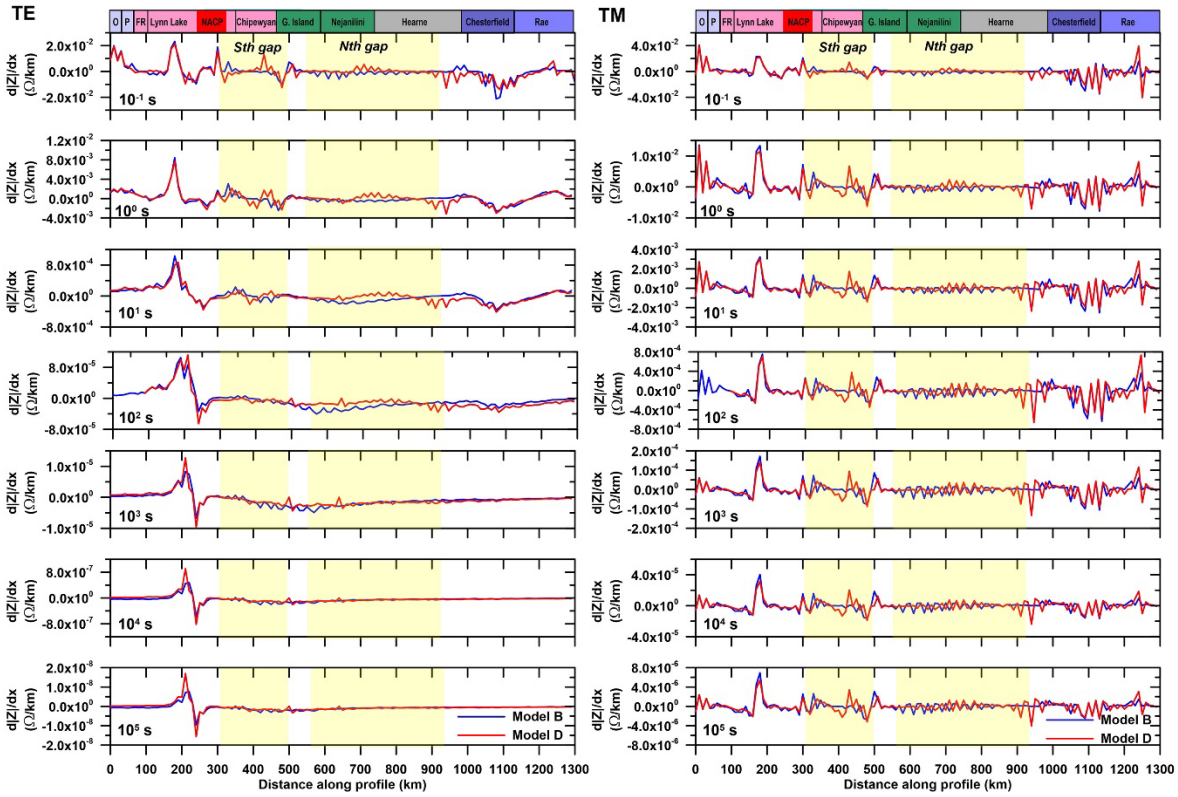

Figure 85. Impedance magnitude gradient for Models B and D (available and padded MT data with deep layer constraints).

10.3 Spatial averaging of impedance results

For the purpose of GIC modelling, it is necessary to combine the impedance data into constant values for 50 km segments along the profile. Apart from the observation of high impedance magnitude in the Superior and Rae cratons, the spatial variations in impedance and impedance gradient do not provide strong correlation with mapped geological boundaries. The results suggest that it is a reasonable approach to extract results in exact 50 km segments.

Since the purpose of the impedance results is the calculation of electric field responses, the most appropriate method for extracting the information is linear averaging of the complex impedance responses for the 50 km profile segments. The output from this process would correspond to an approximation of the integrated electric field across the segment produced by a unit orthogonal magnetic field variation of 1 $A.m^{-1}$. A drawback of this approach is that the resulting impedance may not represent a valid 1-D MT response estimate, e.g., with its phase constrained to 0–90º and its amplitude and phase obeying the normal dispersion relationships (e.g., Weidelt and Chave, 2012). The approach also contrasts with determination of representative sub-surface resistivity values, which would typically be based on geometrical averaging in order to respect the log-normal distribution of resistivity.

The averaging was done using the even 50 km segments along the profile, with the responses at each 50 km point included in the average for the segments on either side of that point. There are thus 6 evenly spaced 10 km impedance estimate used for each segment. The real and imaginary parts of the impedance were calculated using the standard equations:

$$\mathrm{Re}[Z] = |Z|\cos[\Phi(Z)] \qquad \text{Eq. 8}$$

and

$$\mathrm{Im}[Z] = |Z| \sin[\Phi(Z)] \qquad \text{Eq. 9}$$

The complex values of Z=Re[Z]+iIm[Z] were then averaged in sets of 6 points. Finally, the averaged results were converted back into magnitude and phase form.

The resulting 50 km–averaged impedance magnitude and phase values are compared with the 10 km values in Figures 86 and 87. The averaged values match the 10 km sampled data correctly and the averaging process did not produce any phase values lying outside the normal 1-D range. The averaged values capture most of the variability in the higher density data but there are some features that are not represented exactly, such as the peak in the TM impedance magnitude at 175–200 km along the profile (Figure 86) or the peaks in the shorter period TE phase response at 200–300 km along the profile (Figure 87). In this sense, the averaged responses represent a conservative estimate of the spatial variability in the impedance data.

An electronic file containing the averaged impedance data and corresponding coordinates in UTM15 and NAD83 latitude and longitude format is available as part of this report (Appendix 1).

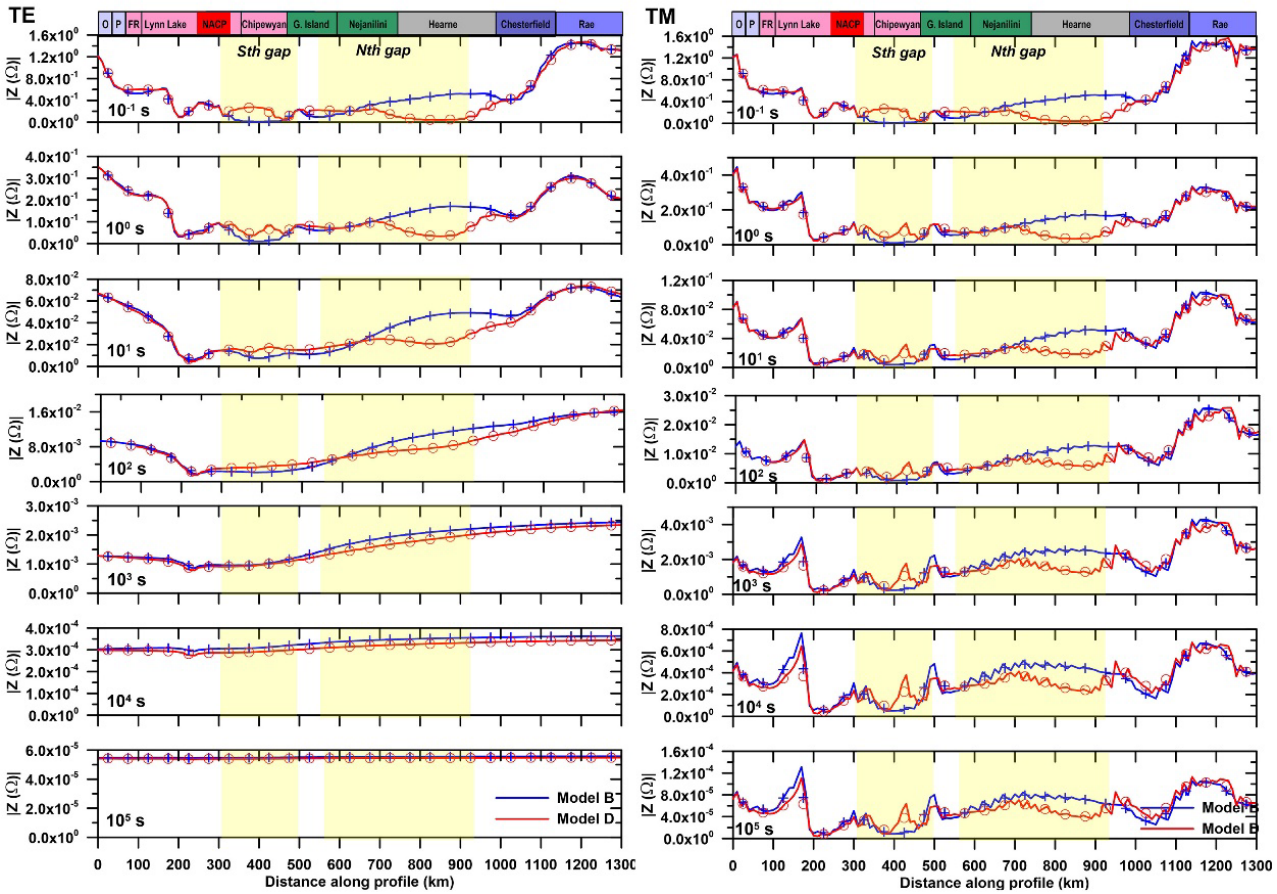

Figure 86. Comparison of higher density and averaged impedance magnitude for Models B and D (available and padded MT data with deep layer constraints). Results are plotted in terms of the linear impedance magnitude. The cross and circle symbols denote the averaged Model B and Model D responses respectively.

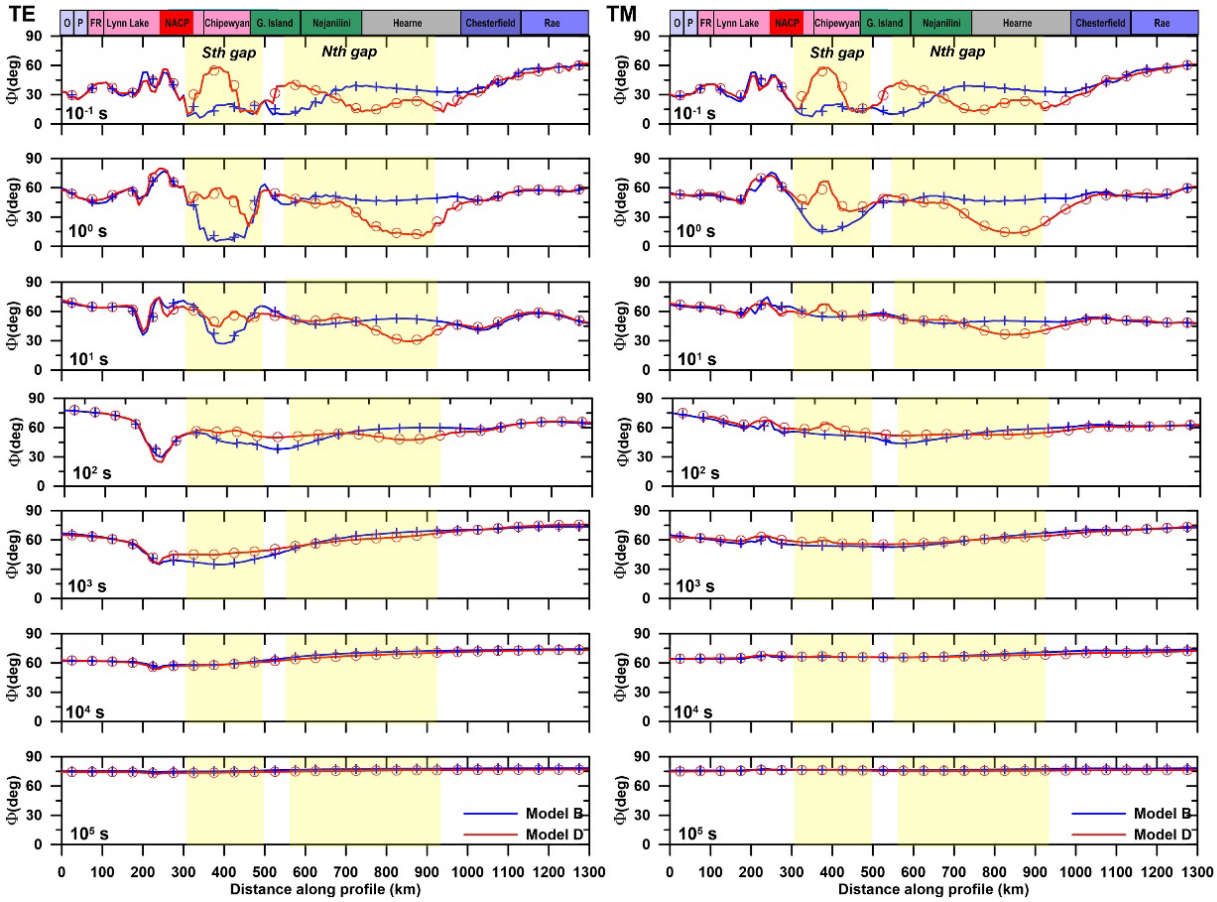

Figure 87. Comparison of higher density and averaged phase for Models B and D (available and padded MT data with deep layer constraints). The cross and circle symbols denote the averaged Model B and Model D responses respectively.

11. Conclusions and recommendations

This report was completed as part of NRCan GEM-GeoNorth project and specifically as part of the Churchill-Kivalliq corridor sub-priority (Figure 1). The ultimate aim of the work was to compute synthetic MT impedance responses along the path of the planned Kivalliq Hydro-Fibre link from Gillam, Manitoba to Kivalliq, Nunavut (Figure 2). These impedance responses will subsequent be used to predict the levels of geomagnetic induced currents on the hydro link.

This work included a review of legacy MT and geomagnetic depth soundings conducted near the Gillam-Kivalliq corridor as well as relevant soundings completed in the same geological terranes crossed by the corridor. The planned hydro-fibre corridor crosses the North American Central Plains conductor to the north of Gillam so other MT soundings of the NACP were also reviewed. More than 15 individual studies were considered in this review. The main features of the responses revealed by these studies included very high crustal resistivity in the southern Rae craton near the north end of the hydro-fibre corridor and in the Superior craton south of south end of the hydro-fibre corridor. The Chesterfield Block exhibits decreasing resistivity at crustal levels with distance to the south. MT studies in the Trans Hudson Orogen and Hearne margin rocks of the Wollaston domain exhibit more conductive and more heterogeneous crust and mantle. The top of the NACP in many studies is at a depth of 10–20 km but in some cases, e.g., on LITHOPROBE Line L, there are conductive zones extending to near the surface. Depending on the modelled thickness of the conductive feature, its resistivity lies between 25 and <1 Ω·m. A number of crossings of the NACP also indicate that it is associated with a conductive region in the mantle.

The information provided by the legacy surveys primarily relates to the Precambrian bedrock but several surveys also provide results on the resistivity of Hudson Bay Basin rocks. Additional information on these rocks from well-logs was also examined. Finally, information on the resistivity of surficial sediments in the region was examined. The modelling results indicate the Hudson Bay Basin rocks and surficial sediments have limited effect on the impedance responses at periods relevant for GIC studies but the information on the resistivity of these units is retained in the report in case it is needed for other purposes such as smaller-scale studies.

A north-south profile was established for 2-D inversion and modelling of the legacy data set based on the observation of pervasively east-west strikes for the large-scale geological features. The 2-D TE component corresponds to east-west electric current flow and the TM component to north-south electric current flow. The profile extended from the Superior craton to the Rae craton over a distance of 1300 km. Gillam is located about 250 km north of the southern end of the profile. The southern limit of the profile is UTM15E (400000 m E, 6000000 m N) and the northern limit is (400000 m E, 7300000 m N). The equivalent NAD83 geographic coordinates are: (54.13837º N, 94.53070º W) and (65.80575º N, 95.18703º W). Projection of the legacy MT data onto this profile (from distances of up to 200 km away from the profile) leaves two large gaps in the data coverage, with the south gap located mainly above the Wathaman-Chipewyan Batholith and the north gap crossing the Great Island and Nejanilini (Hearne margin) terranes and well as the southern and central parts of the Hearne craton.

For the purposes of GIC modelling, it is desirable to consider MT impedance responses for the period range of 1 s to 1 day (~10^5 s) and at 50 km spatial scale. The longest period response available in most of the legacy data sets is between 10^2 and 10^4 s so the MT data alone is unable to constrain the longest period impedance responses needed for GIC modelling. To overcome this issue, inversions models were examined in which the resistivity of layers at depths of 260–800 km was constrained by a very deep penetrating MT and geomagnetic depth sounding study in the southern Superior craton (Schultz et al. 1993). To overcome the problems of the gaps in the profile, the MT responses from 12 sites in corresponding geological terranes crossed by LITHOPROBE Line L to the southwest were imported to form a padded MT data set. The rotation of these data was set to account for the different large-scale geological strikes in the two regions.

Four MT inversion models were produced. Model A is based on the available MT data along the modelling profile. Model B is based on the available MT data but incorporates deep layers determined in the Carty Lake study (Schultz et al., 1993). In Model C gaps in the MT profile are padded with MT data from the corresponding geological terranes from LITHOPROBE Line L. Model D is based on the padded data and the deeper layers from the Carty Lake study. The two models incorporating deep layer resistivity constraints (Models B and D) are considered to provide the more reliable MT impedance responses at periods exceeding 10^4 s. After careful selection of MT sites to ensure a reasonable spacing of the projected data along the profile, Models A and B included 37 MT sites and Models C and D included 49 sites. While the corresponding unpadded model (Model B) uses only data from the study area, the gaps in the data coverage are susceptible to possible inversion artifacts resulting from the regularized inversion approach e.g., the inclusion of structures in regions weakly constrained by the MT data. In contrast, the importation of data from elsewhere (Model D) is intended to provide responses with the same statistical character as those in the terranes crossed, but not to necessarily provide the true structure.

The four inversion models are quite similar, but as expected, display some differences at large depth and in the padded sections. The models fit the edited observed data reasonably well, with normalized RMS misfit values of ~3.0 for error floors of 5% for the phase and 20% for apparent resistivity for both modes. The 2-D inversion model reproduce the large-scale resistivity structures observed in earlier studies of the legacy data, including very resistive crust and upper mantle in the Rae and Superior cratons underlain at 75 to 150 km depth by more conductive rocks. More conductive crust and mantle is present in the Chesterfield Block, Hearne

craton, and Trans Hudson Orogen. In the inversion models, the most conductive part of the NACP is at ~10 km depth but this geometry is not tightly constrained by the modelling. The models include relatively conductive crust at shallow depths adjacent to the NACP.

MT apparent resistivity and phase responses for both the TE and TM were exported from the four MT models at 10 km spacing using a series of synthetic sites created in the WinGLink software. The period range for these responses was 10^{-2} to 10^{5} s. This process means that the high spatial density data are produced directly as part of the 2-D modelling rather than requiring any additional spatial interpolation. The least-squares fitting process and regularization used in the MT inversion also creates some smoothing and reduction of aliasing of smaller scale resistivity heterogeneity inherent in the observed data set.

The TE and TM apparent resistivity and phase responses were converted into equivalent impedance values (in units of Ω). The impedance responses define significantly higher impedance magnitude in the Rae and Superior cratons at periods less than 10^{3} s. There are low impedance magnitudes and high spatial gradients in the southern 300 km of the profile, including in the region around Gillam. The largest relative differences between the available MT data models (A and B) and the padded models (C and D) occur at moderate to low impedance magnitudes so represent smaller absolute differences. The results show that the TM impedance magnitude exhibits stronger spatial gradients than the TM impedance phase or the TE responses. These effects extend to the longest periods and can be attributed to static effects associated with the TM mode electromagnetic induction process.

Finally, the TE and TM impedance responses were spatially averaged into 50 km segments using arithmetic averaging of complex impedance responses over segments of these lengths. Examination of the results in terms of the corresponding impedance magnitude and phase show that the 50 km averaged values capture most of the spatial variability observed in the 10 km responses, but they do not accurately represent some smaller wavelength features.

The study results indicate the need for future research in several areas to support more the development of more reliable and more accurate MT impedance responses in the study region. These areas include:

1. Collection of new MT data along the Gillam-Kivalliq corridor would allow production of significantly more reliable impedance estimates. In particular, the acquisition of such a data set would remove the need to project MT legacy data the large distances (up to 200 km) onto the profile and would remove the need to import data from outside the study area to fill gaps in the data coverage.
2. 3-D forward modelling should be conducted to evaluate the effects of large-scale 3-D features including Hudson Bay and the Hudson Bay Basin on the MT responses. It may also be useful to examine the effects of the large-scale 3-D geometry of the NACP.
3. It would be of value to conduct some smaller-scale modelling studies to closely examine the effects of the surficial geology and Hudson Bay Basin rocks on the shortest period MT responses considered in GIC modelling.
4. More detailed studies of the effects of the NACP on the MT impedances could be conducted to examine the role of the exact geometry of this feature. What are the effects of the depth to the top of the main conductor? What are the effects of associated conductive crust extending to shallow depth? What are the effects of an associated region of conductive mantle?

Finally, it would be useful to examine the effects of small scale resistivity heterogeneity on the responses? How does the averaging of such heterogeneity compare in statistically based spatial interpolation versus in MT inversion and modelling? What is the exact effect of heterogeneity and galvanic distortion on GIC models?

Acknowledgements

MT datasets examined in this report were provided by NRCan except for the BIPOLE III data which were collected by Manitoba Hydro. The MT examination, presentation, inversion and modelling described in

this report was done using WinGLink software from Geosystem. V. Tschirhart provide a valuable review of this document.

References

Adetunji, A. and Ferguson, I.J., 2012. Manitoba Hydro Bipole III HVDC Converter Project, Site Selection and Design of Bipole III DC Land Electrodes: Earth Electrical Resistivity at Bipole III North Candidate Electrode Site. Report prepared for Teshmont Consultants LP, Winnipeg, Manitoba, submitted to Manitoba Hydro. 83 p. and appendices.

Ansdell, K.M. 2005. Tectonic evolution of the Manitoba-Saskatchewan segment of the Paleoproterozoic Trans-Hudson Orogen, Canada; Canadian Journal of Earth Sciences, v. 42, p. 741–754.

Armstrong, D.K., Nicolas, M.P.B., Hahn, K.E., and Lavoie, D., 2018. Stratigraphic synthesis of the Hudson Platform in Manitoba, Ontario, and Nunavut: Ordovician–Silurian; Geological Survey of Canada, Open File 8378, 48 p.

Bancroft, B., Craven, J.A., Enkin, R.J., Nicolas, M.P.B., and Roberts, B., 2014. Results from a Magnetotelluric and Rock Property Study near Churchill, Manitoba; Geological Survey of Canada, Open File 7549, 21 p.

Barager, W.R.A. and Scoates, R.F.J., 1981. The Circum-Superior belt: a Proterozoic plate margin? *In* Precambrian Plate Tectonics, (ed.) Kröner, A. Elsevier, Amsterdam, p. 297–330.

Becken, M. and Burkhardt, H., 2004. An ellipticity criterion in magnetotelluric tensor analysis; Geophysical Journal International, v. 159, p. 69–82.

Bedrosian, P.A. and Finn, C.A., 2021. When Wyoming became Superior: Oblique convergence along the southern Trans-Hudson Orogen; Geophysical Research Letters, v. 48, p. e2021GL092970.

Bedrosian, P.A., and Love, J.J., 2015. Mapping geoelectric fields during magnetic storms: Synthetic analysis of empirical United States impedances; Geophysical Research Letters, v. 42, p. 10,160–10,170.

Beggan, C.D., 2015. Sensitivity of geomagnetically induced currents to varying auroral electrojet and conductivity models; Earth, Planets and Space, v. **67,** p. 1–12.

Berman, R.G., Davis, W.J., and Pehrsson, S., 2007. Collisional Snowbird tectonic zone resurrected: Growth of Laurentia during the 1.9 Ga accretionary phase of the Hudsonian orogeny; Geology, v. 35, p. 911–914.

Berman, R.G., Sanborn-Barrie, M., Rayner, N. and Whalen, J., 2013a. The tectonometamorphic evolution of Southampton Island, Nunavut: Insight from petrologic modeling and in situ SHRIMP geochronology of multiple episodes of monazite growth; Precambrian Research, v. 232, p. 140–166.

Berman, R.G., Pehrsson, S., Davis, W.J., Ryan, J.J., Qui, H., and Ashton, K.E., 2013b. The Arrowsmith orogeny: Geochronological and thermobarometric constraints on its extent and tectonic setting in the Rae craton, with implications for pre-Nuna supercontinent reconstruction; Precambrian Research, v. **232,** p. 44–69.

Böhm, C.O., Heaman, L.M., Creaser, R.A., and Corkery, M.T., 2000. Discovery of pre-3.5 Ga exotic crust at the northwestern Superior Province margin, Manitoba; Geology, v. 28, p. 75-78.

Booker, J.R., 2014. The magnetotelluric phase tensor: a critical review; *Surveys in Geophysics,* v. **35,** p. 7–40.

Boteler, D. H. 2001. Space weather effects on power systems; *in* Space Weather (ed.) Song, P., Singer, H.J., and Siscoe, G.L., Geophysical Monograph Series, v. 125, Washington, DC: American Geophysical Union, p. 347–352.

Boteler, D.H., 2019. A 21st century view of the March 1989 magnetic storm; Space Weather, v. **17**, p. 1427–1441.

Boteler, D.H., Boutilier, S., Swatek, D., Bui-Van, Q., Leonard, R., Hughes B, Hajagos, L., Ferguson, I.J., and Odwar, H.D., 1998. Geomagnetically induced currents: Geomagnetic Hazard Assessment Phase II, Final Report; Geological Survey of Canada and Canadian Electrical Association, 121 p.

Caldwell, T.G., Bibby, H.M., and Brown, C., 2004. The magnetotelluric phase tensor; Geophysical Journal International, v. 158, p. 457‑469.

Chave, A.D. and Jones, A.G. (ed.), 2012. The Magnetotelluric Method: Theory and Practice, Cambridge Univ. Press, 552 pp.

Corrigan, D., Galley, A.G., and Pehrsson, S., 2007, Tectonic evolution and metallogeny of the southwestern Trans-Hudson Orogen, *in* Mineral Deposits of Canada: A Synthesis of Major Deposit-Types, District Metallogeny, the Evolution of Geological Provinces, and Exploration Methods, ed. Goodfellow, W.D., Geological Association of Canada, Mineral Deposits Division, Special Publication No. 5, p. 881–902.

Cowan, W.R.,1993. Hudson platform – Geology (Quaternary). Sedimentary Cover of the Craton in Canada, (ed.) Stott D.F. and Aitken, J.D., Geological Survey of Canada, Geology of Canada, No. 5; Chapter 8 653–700.

Craven, J.A., Ferguson, I.J., Nicolas, M.P.B., Zaprozan, T., Hodder, T., Roberts, B.R., and Clark, N., 2017. Report of activities for the ground geophysical survey across the Kaskattama highlands, Manitoba: GEM-2 HudsonUngava Project; Geological Survey of Canada, Open File 8321, 30 p.

Craven, J.A., Ferguson, I.J. and Roberts, B.J., 2018. Ground geophysics in the Hudson Bay area, Nunavut: GEM-2 Kaskattama highlands and Southampton Island Project, report of activities 2018; Open File 8487, 10 p.

Craven, J.A., Kurtz, R.D., Boerner, D.E., Skulski, T., Spratt, J., Ferguson, I.J., Wu, X., and Bailey, R.C., 2001. Conductivity of western Superior Province upper mantle in northwestern Ontario; Geological Survey of Canada, Current Research 2001-E6, 10 p.

Craven, J.A., Sanborn-Barrie, M., Roberts, B.J., Stefanescu, M. and Young, M., 2013. Preliminary insights into the architecture of southern Cumberland Peninsula from magnetotelluric data. Geological Survey of Canada, Current Research (Online), no. 2013-3, 15 p.

Davis, W.J., Hanmer, S., Tella, S., Sandeman, H.A., and Ryan, J.J., 2006. U-Pb geochronology of the MacQuoid supracrustal belt and Cross Bay plutonic complex: key components of the northwestern Hearne subdomain, western Churchill Province, Nunavut, Canada; Precambrian Research, v. 145, p. 53–80.

Eaton, D.W. and Darbyshire, F. 2010. Lithospheric architecture and tectonic evolution of the Hudson Bay region; Tectonophysics, v. 480, p. 1–22.

Epp, D., 2014. Constrained re-examination of the resistivity structure of the Fox River Belt, using an integrated audiomagnetotelluric, magnetic, and geological approach. B.Sc. (Honours) Thesis, University of Manitoba, Winnipeg, Canada.

Evans, S., Jones, A.G., Spratt, J., and Katsube, J., 2005. Central Baffin electromagnetic experiment (CBEX): Mapping the North American Central Plains (NACP) conductivity anomaly in the Canadian arctic; *Physics of the Earth and Planetary Interiors*, v. **150,** p. 107–122.

Ferguson, I.J., Craven, J.A, Kurtz, R.D., Boerner, D.E. Bailey, R.C., Wu, X., Orellana, M.R., Spratt, J., Wennberg, G. and Norton, M. 2005a. Geoelectric responses of Archean lithosphere in the western Superior Province, central Canada; Physics of the Earth and Planetary Interiors, v. 150, p. 123–143.

Ferguson, I.J., Epp, D., Saturnino, T., Orellana, M., Craven, J., and Jones, A.G., 2015. Interpretation of resistivity and magnetic anomalies from the Fox River Sill, Trans Hudson Orogen, Canada. Australian Society of Exploration Geophysicists Conference, Perth, February, 2015.

Ferguson, I.J., Jones, A.G., Yu Sheng, Wu, X., and Shiozaki, I., 1999. Geoelectric response and crustal electrical-conductivity structure of the Flin Flon Belt, Trans-Hudson Orogen, Canada; Canadian Journal of Earth Sciences, v. 36, p. 1917–1938.

Ferguson, I.J., Stevens, K. and Jones, A.G., 2005b. Electrical-resistivity imaging of the central Trans-Hudson Orogen; Canadian Journal of Earth Sciences, *v.* **42, p.** 495–515.

Fultz, T.L., 2017. A Geophysical Analysis of the Great Falls Tectonic Zone and the Surrounding Area, Montana USA. M.Sc. Thesis, Missouri State University.

Garcia, X. and Jones, A.G., 2005. Electromagnetic image of the Trans-Hudson orogen THO94 transect; Canadian Journal of Earth Sciences, v. 42, p. 479–493.

GEM GeoNorth, 2021. GEM GeoNorth DRAFT Priority Regions – Jan 19, 2021. Natural Resources Canada.

Gowan, E.J., Ferguson, I.J., Jones, A.G. and Craven, J.A., 2009. Geoelectric structure of the northeastern Williston basin and underlying Precambrian lithosphere; Canadian Journal of Earth Sciences, v. 46, p. 441–464.

Groom, R.W. and Bailey, R.C., 1989. Decomposition of magnetotelluric impedance tensors in the presence of local three-dimensional galvanic distortion; *Journal of Geophysical Research (Solid Earth)*, v. **94,** p. 1913–1925.

Gupta, J.C., Kurtz, R.D., Camfield, P.A., and Niblett, E.R., 1985. A geomagnetic induction anomaly from IMS data near Hudson Bay, and its relation to crustal electrical conductivity in central North America; Geophysical Journal International, v. 81, p. 33–46.

Hayden, A.M., Wilmes, S.B., Gomez, N., Green, J.A.M., Pan, L., Han, H., and Golledge, N.R., 2020. Multi-century impacts of ice sheet retreat on sea level and ocean tides in Hudson Bay; Journal of Geophysical Research: Oceans, v. 125, p. e2019JC015104.

Hayward, T., 2014. Sensitivities of electromagnetic geophysical responses in anisotropic media and applications to a magnetotelluric survey near Churchill, Manitoba. B.Sc. (Honours) Thesis, University of Manitoba, Winnipeg, Canada.

Herath, N., Xu, X., Jayasekara, N., Jacobson, D., and Filizadeh, S., 2019. Interconnection of northern Canadian communities to the Manitoba Hydro Power System: Evaluation of AC and DC alternatives; *in* 2019 IEEE Electrical Power and Energy Conference, Institute of Electrical and Electronics Engineers, p. 1–6.

Jones, A.G., 1983. The problem of current channelling: a critical review; Surveys in Geophysics, v. 6, p. 79–122.

Jones, A.G., 1986. Parkinson's pointers' potential perfidy! Geophysical Journal International, v. 87, p. 1215–1224.

Jones, A.G., 1993. The COPROD2 dataset: Tectonic setting, recorded MT data, and comparison of models; Journal of geomagnetism and geoelectricity, v. 45, p. 933–955.

Jones, A.G., 2006. Electromagnetic interrogation of the anisotropic Earth: Looking into the Earth with polarized spectacles; Physics of the Earth and Planetary Interiors, v. 158, p. 281–291.

Jones, A.G., 2012. Distortion of magnetotelluric data: its identification and removal; in: The Magnetotelluric Method: Theory and Practice (ed.) Chave, A.D. and Jones, A.G., Cambridge University Press, Cambridge, p. 219–302.

Jones, A.G. and Craven, J.A, 1990. The North American Central Plains conductivity anomaly and its correlation with gravity, magnetics, seismic and heat flow data in the Province of Saskatchewan; Physics of the Earth and Planetary Interiors, v. 60, p. 169–194.

Jones, A.G. and Savage, P.J., 1986. North American Central Plains conductivity anomaly goes east; Geophysical Research Letters, v. 13, p. 685–688.

Jones, A.G., Craven, J.A., McNeice, G.W., Ferguson, I.J., Boyce, T.T., Farquharson C., and Ellis, R, 1993. North American Central Plains conductivity anomaly within the Trans Hudson orogen in northern Saskatchewan, Canada; Geology, v. 21, p. 1027–1030.

Jones, A.G., Katsube, T.J., and Schwann, P., 1997. The longest conductivity anomaly in the world explained: sulphides in fold hinges causing very high electrical anisotropy; Journal of Geomagnetism and Geoelectricity, v. 49, p 1619-1629.

Jones, A.G., Ledo, J., and Ferguson, I.J., 2005. Electromagnetic images of the Trans-Hudson orogen: The North American Central Plains (NACP) anomaly revealed; Canadian Journal of Earth Sciences, v. 42, p. 457–478.

Jones, A.G., Ledo, J., Ferguson, I.J., Craven, J.A., Unsworth, M.J., and Chouteau, M., 2014. The electrical resistivity of Canada's lithosphere: Contributions from Lithoprobe and other programmes; Canadian Journal of Earth Sciences, v. 51, p. 573–617.

Jones, A.G., Snyder, D., Hanmer, S., Asudeh, I., White, D., Eaton, D. and Clarke, G., 2002. Magnetotelluric and teleseismic study across the Snowbird Tectonic Zone, Canadian Shield: A Neoarchean mantle suture? Geophysical Research Letters, v. 29, p. 10-1.

Josenhans, H., Balzer, S., Henserson, P., Nielson, E., Thorliefson, H., and Zevenhuizen, J., 1988. Preliminary seismostratigraphic and geomorphic interpretations of the Quaternary sediments of Hudson Bay; *in* Current research, Part B, Eastern and Atlantic Canada. Geological Survey of Canada, Paper 88-1B, p. 271–286.

Kelbert, A., Bedrosian, P.A., and Murphy, B.S., 2019. The first 3D conductivity model of the contiguous United States: Reflections on geologic structure and application to induction hazards; *in* Geomagnetically Induced Currents from the Sun to the Power Grid; ed. Gannon, J.L., Swidinsky, A., and Xu, Z., Geophysical Monograph 244, American Geophysical Union, p. 127–151.

Kivalliq Hydro-Fibre Link, 2021. Kivalliq Hydro-Fibre Link. https://www.kivalliqlink.ca/ Accessed July 2021.

Kivalliq Inuit Association and ANBARIC Development Partners, 2020. Kivalliq Hydro-Fibre Link: Pre-Budget Submission in Advance of the 2020 Federal Budget. Submission to House of Commons Standing Committee on Finance, 5 p.

Lavoie, D., Pinet, N., Dietrich, J., Zhang, S., Hu, K., Asselin, E., Chen, Z., Bertrand, R., Galloway, J., Decker, V., Budkewitsch, P., Armstrong, D., Nicolas, M., Reyes, J., Kohn, B.P., Duchesne, M.J., Brake, F., Keating, P., Craven, J., and Roberts, B. 2013. Geological framework, basin evolution, hydrocarbon system data and conceptual hydrocarbon plays for the Hudson Bay and Foxe basins, Canadian Arctic; Geological Survey of Canada, Open File 7363, 200 p.

Ledo, J., 2005. 2-D versus 3-D magnetotelluric data interpretation; Surveys in Geophysics, v. 26, p. 511–543.

Ledo, J., Queralt, P., Martí, A., and Jones, A.G., 2002. Two-dimensional interpretation of three-dimensional magnetotelluric data: an example of limitations and resolution; Geophysical Journal International, v. 150, p. 127–139.

Love, J.J., Lucas, G.M., Kelbert, A., and Bedrosian, P.A., 2018. Geoelectric hazard maps for the Pacific Northwest; Space Weather, v. 16, p. 1114–1127.

Love, J.J., Pulkkinen, A., Bedrosian, P.A., Jonas, S., Kelbert, A., Rigler, E.J., Finn, C.A., Balch, C.C., Rutledge, R., Waggel, R.M., and Sabata, A.T., 2016. Geoelectric hazard maps for the continental United States; Geophysical Research Letters, v. 43, p. 9415–9424.

McLeod J., 2013. Assessment of electrical conductivity structure of the northwest Superior craton and adjacent Trans Hudson Orogen using the magnetotelluric method. B.Sc. (Honours) Thesis, University of Manitoba, Winnipeg, Canada.

McLeod, J. and Ferguson, I.J., 2018. Analysis of 2017 Kaskattama Highlands magnetotelluric dataset. Report submitted to the Geological Survey of Canada, GEM2 Hudson Ungava project, 44 p.

McNeice, G.W., Jones, A.G., 2001. Multisite, multifrequency tensor decomposition of magnetotelluric data; *Geophysics*, v. **66,** p. 158–173.

Mann, I.R., Milling, D.K., Rae, I.J., Ozeke, L.G., Kale, A., Kale, Z.C., Murphy, K.R., Parent, A., Usanova, M., Pahud, D.M., and Lee, E.A., 2008. The upgraded CARISMA magnetometer array in the THEMIS era; Space Science Reviews, v. 141, p. 413-451.

Marks, J., 2019. Delineation of a hydrothermal dolomite occurrence on Cape Donovan, Southampton Island using magnetotellurics. B.Sc. (Honours) Thesis, University of Manitoba, Winnipeg, Canada.

Martí, A., Queralt, P., and Roca, E., 2004. Geoelectric dimensionality in complex geological areas: application to the Spanish Betic Chain; Geophysics Journal International, v. 157, p. 961–974.

Matile, G.L.D. and Keller, G.R. 2007. Surficial Geology of Manitoba; Manitoba Science, Technology, Energy and Mines, Manitoba Geological Survey, Surficial Geology Compilation Map Series, SG-MB, scale 1: 1 000 000.

Minifie, J.M., Kerr, A.C., Ernst, R.E, Hasite, A.R., Ciborowski, T.J.R., Desharnais, G., and Millar, I.L. 2013. The northern and southern sections of the western ca. 1880 Ma Circum-Superior Large Igneous Province, North America: The Pickle Crow dyke connection? Lithos, v. 174, p. 217–235.

Molinski, T.S., 2002. Why utilities respect geomagnetically induced currents; Journal of Atmospheric and Solar-terrestrial Physics, v. 64, p. 1765–1778.

Nicolas, M.P.B., 2011. Stratigraphy of the three exploratory oil-well cores in the Hudson Bay Lowland, northeastern Manitoba (parts of NTS 54B10, F8, G1); *in* Report of Activities 2011, Manitoba Innovation, Energy and Mines, *Manitoba Geological Survey,* p. 165-170.

Nicolas, M.P.B. and Armstrong, D.K. 2017. Update on Paleozoic stratigraphic correlations in the Hudson Bay Lowland, northeastern Manitoba and northern Ontario; *in* Report of Activities 2017, Manitoba Growth, Enterprise and Trade, Manitoba Geological Survey, p. 133–147.

Nicolas, M.P.B. and Clayton, B.W. 2015: Lineament mapping of the Hudson Bay Lowland using remote-sensing methods, northeastern Manitoba (parts of NTS 53N, O, 54); *in* Report of Activities 2015, Manitoba Mineral Resources, Manitoba Geological Survey, p. 89–96.

Nicolas, M.P.B. and Lavoie, D. 2012. Oil shale reservoir rocks of the Hudson Bay Lowland, northeastern Manitoba (part of NTS 54); *in* Report of Activities 2012, Manitoba Innovation, Energy and Mines, *Manitoba Geological Survey,* p. 124–133.

Nieuwenhuis, G., Unsworth, M.J., Pana, D., Craven, J. and Bertrand, E., 2014. Three-dimensional resistivity structure of Southern Alberta, Canada: implications for Precambrian tectonics; Geophysical Journal International, 197, p. 838–859.

Norris, A.W., 1993a. Hudson platform – Introduction *in* Sedimentary Cover of the Craton in Canada, (ed.) Stott D.F. and Aitken, J.D., Geological Survey of Canada, Geology of Canada, No. 5; Chapter 7, p. 643–651.

Norris, A.W., 1993b. Hudson platform – Geology; *in* Sedimentary Cover of the Craton in Canada, (ed.) Stott D.F. and Aitken, J.D., Geological Survey of Canada, Geology of Canada, No. 5; Chapter 8, p. 653–700.

Orellana, M.R. 2006. An evaluation of the conductivity structure of the northwestern Superior Province, Canadian Shield through the use of magnetotelluric and audiomagnetotellurics methods. M.Sc. Thesis, University of Manitoba, Winnipeg, Canada.

Parkinson, W.D. 1962. The influence of continents and oceans on geomagnetic variations; Geophysical Journal of the Royal Astronomical Society, v. 6, p. 441–449.

Pehrsson, S.J., Berman, R.G., Eglington, B., and Rainbird, R., 2013. Two Neoarchean supercontinents revisited: The case for a Rae family of cratons; Precambrian Research, v. 232, p. 27–43.

Pelletier, B.R., 1986. Seafloor morphology and sediments; *in* Canadian Inland Seas, (ed.) Martini, I.P., Elsevier Oceanography Series, 44, Elsevier, Chapter 8, 143–162.

Percival, J.A., Sanborn-Barrie, M., Skulski, T., Stott, G.M., Helmstaedt, H., and White, D.J., 2006. Tectonic evolution of the western Superior Province from NATMAP and Lithoprobe studies; Canadian Journal of Earth Sciences, v. 43, p. 1085–1117.

Peterson, T.D., Jefferson, C.W., and Anand, A., 2015. Geological setting and geochemistry of the ca. 2.6 Ga Snow Island Suite in the central Rae Domain of the Western Churchill Province, Nunavut; Geological Survey of Canada, Open File 7841, 1 .zip file.

Prinsenberg, S.J., 1986. Salinity and temperature distributions of Hudson Bay and James Bay; *in* Canadian Inland Seas, (ed.) Martini, I.P., Elsevier Oceanography Series, 44, Elsevier, Chapter 9, p. 163–186.

Pulkkinen, A., Bernabeu, E., Eichner, J., Viljanen, A., and Ngwira, C., 2015. Regional-scale high-latitude extreme geoelectric fields pertaining to geomagnetically induced currents; Earth, Planets and Space, v. 67, p. 1–8.

Rainbird, R.H., Davis, W.J., Pehrsson, S.J., Wodicka, N., Rayner, N., and Skulski, T., 2010. Early Paleoproterozoic supracrustal assemblages of the Rae domain, Nunavut, Canada: Intracratonic basin development during supercontinent break-up and assembly; Precambrian Research, v. 181, p. 167–186.

Roberts, B. and Craven, J., 2012. Results of a Magnetotelluric Survey in Churchill, Manitoba: GEM Energy, Hudson Bay; Geological Survey of Canada, Open File 7151, 21 p.

Rodi, W., and Mackie, R.L., 2001. Nonlinear conjugate gradients algorithm for 2-D magnetotelluric inversions; Geophysics, v. 66, p. 174–187.

Rodi, W., Mackie, R.L., 2012. The inverse problem, *in* The Magnetotelluric Method: Theory and Practice; (ed.) Chave, A.D. and Jones, A.G., Cambridge University Press, Cambridge, p. 347–420.

Roots. E. and Craven, J.A., 2017. 3-D modelling of magnetotelluric data from the western Superior Province, Ontario; Geological Survey of Canada, Open File 8237 (revised), 1 .zip file.

Sanford, B.V., and Grant, A.C., 1990: New findings relating to the stratigraphy and structure of the Hudson Platform. Geological Survey of Canada, Paper 90-1D, p. 17–30.

Schultz, A., Kurtz, R.D., Chave, A.D. and Jones, A.G., 1993. Conductivity discontinuities in the upper mantle beneath a stable craton; Geophysical Research Letters, v. 20, p. 2941–2944.

Scoates, R.F.J., 1990. The Fox River Sill, Northeastern Manitoba – a major stratiform intrusion. Geological Report GR82-3, Manitoba Energy and Mines, Geological Services.

Shilts, W.W., 1986. Glaciation of the Hudson Bay region; *in* Canadian Inland Seas (ed.) Martini, I.P., Elsevier Oceanography Series, 44, Elsevier, Chapter 4, p. 55–78.

Simpson, F. and Bahr, K., 2005. *Practical magnetotellurics*. Cambridge University Press, 254 p.

Skulski, T., Corkery, M.T., Stone, D., Whalen, J., and Stern, R.A., 2000. Geological and geochronological investigations in the Stull Lake–Edmund Lake Greenstone Belt and graintoid rocks of the northwestern Superior Province. Manitoba, Industry, Trade and Mines Geological Survey, Report of Activities 2000, p. 117–128.

Snyder, D.B., Craven, J.A., Pilkington, M., and Hillier, M.J., 2015. The 3-dimensional construction of the Rae craton, central Canada. Geochemistry, Geophysics, Geosystems, v. 16, p 3555-3574.

Spratt, J.E., Craven, J.A., and Sanborn-Barrie, M., 2012. Southampton Island magnetotelluric survey: data acquisition and preliminary analysis; Geological Survey of Canada, Open File 6988, 39 p.

Spratt, J.E., Jones, A.G., Corrigan, D., and Hogg, C., 2013. Lithospheric geometry beneath Melville Peninsula, Nunavut, revealed by deep probing magnetotelluric surveying, Current Research, 2013-12, 18 pp.

Spratt, J.E., Skulski, T., Craven, J.A., Jones, A.G., Snyder, D.B., and Kiyan, D., 2014. Magnetotelluric investigations of the lithosphere beneath the central Rae craton, mainland Nunavut, Canada; Journal of Geophysical Research: Solid Earth, v. 119, p. 2415–2439.

Torta, J.M., Marsal, S., and Quintana, M., 2014. Assessing the hazard from geomagnetically induced currents to the entire high-voltage power network in Spain; Earth, Planets and Space, v. 66, p. 1–17.

Tournerie, B. and Coulson, S., 2010. Geophysical Survey Report: BIPOLE III DC electrodes, Resistivity Survey Keewatinoow Candidate Electrode Sites on Behalf of Manitoba Hydro (Manitoba, Canada). Quantec Geoscience Ltd., Toronto, Ontario, Canada. 245 pp.

Trichtchenko, L., Fernberg, P.A., and Boteler, D.H., 2019a. One-dimensional layered earth models of Canada for GIC applications Part 1. General description; Geological Survey of Canada, Open File 8594, 66 p.

Trichtchenko, L., Fernberg, P.A., and Boteler, D.H., 2019b. One-dimensional layered earth models of Canada for GIC applications Part 2. Detailed description; Geological Survey of Canada, Open File 8595, 586 p.

Tschirhart, V., Potter, E.G., Powell, J.W., Roots, E.A. and Craven, J.A., in press. Deep geological controls on formation of the highest-grade uranium deposits in the world: magnetotelluric imaging of unconformity-related systems from the Athabasca Basin, Canada, Geophysical Research Letters.

Vozoff, K. 1991. The magnetotelluric method; *in* Electromagnetic Methods in Applied Geophysics, v. 2, Applications, ed. Nabighian, M.N., Society of Exploration Geophysicists, Tulsa, p. 641–711.

Wannamaker, P.E., 1999. Affordable magnetotellurics: interpretation in natural environments, *in* Three-Dimensional Electromagnetics, (ed.) Oristaglio, M. and Spies, B., Geophysical Development Series v. 7, Society of Exploration Geophysicists, p. 349–379,

Weber, W., 1990. The Churchill–Superior Boundary Zone, southeast margin of the Trans-Hudson orogen; a review *in* The Early Proterozoic Trans-Hudson Orogen of North America, (ed.) Lewry, J.F. and Stauffer, M.R., Geological Association of Canada Special Paper, 37, 41–55.

Weidelt, P. and Chave, A.D., 2012. The magnetotelluric response function, *in* The Magnetotelluric Method: Theory and Practice; (ed.) Chave, A.D. and Jones, A.G., Cambridge University Press, Cambridge, p. 219–302.

White, D., Boerner, D., Wu, J., Lucas, S., Berrer, E., Hannila, J. and Somerville, R., 2000. Mineral exploration in the Thompson nickel belt, Manitoba, Canada, using seismic and controlled-source EM methods; *Geophysics*, v. **65,** v. 1871–1881.

White, D.J., Jones, A.G., Lucas, S.B. and Hajnal, Z., 1999. Tectonic evolution of the Superior Boundary Zone from coincident seismic reflection and magnetotelluric profiles; *Tectonics*, v. **18**, p. 430–451.

Williams, H.R., Stott, G.M., Thurston, P.C., Sutcliffe, R.H., Bennett, G., Easton, R.M., and Armstrong, D.K., 1992. Tectonic Evolution of Ontario: Summary and Synthesis, *in* Geology of Ontario, (ed.) Thurston, P.C., Williams, H.R., Sutcliffe, R.H., Stott, G.M., Ontario Geological Survey, Special volume 4, p. 1255–1332.

Wu, N. 1994. High-resolution electromagnetic images of conductivity structure in the mid-lower crust and upper mantle — a magnetotelluric experiment conducted primarily in North Dakota. Ph.D. thesis, Department of Earth and Space Sciences, University of Washington, Seattle, Washington.

Wu, N., Booker, J.R., and Smith, J.T. 1993. Rapid two-dimensional inversion of COPROD2 data; Journal of Geomagnetism and Geoelectricity, v. 9, p. 1073–1087.

Zaporozan, T. and Ferguson, I., 2017. Synthesis of magnetotelluric results from the Hudson Bay Basin and examination of magnetotelluric resolution. Report submitted to the Geological Survey of Canada, GEM2 Hudson Ungava project, 57 pp.

Appendix 1. Impedance responses

This document is accompanied by electronic file of_8907_Appendix_1_impedance_responses.xlxs containing impedance responses at 50-km and at 10-km spatial sampling for two of the 2-D resistivity models defined in the document, and apparent resistivity and impedance phase responses for the four 2-D resistivity models defined in the document. The responses are arranged in three worksheets of a Microsoft Excel® workbook (.xlxs) file.

Common information

Results are for 2-D resistivity models along a 1300 km-long north-south profile with the southern limit of UTM15E 400000 m E, 6000000 m N, and the northern limit of (400000 m E, 7300000 m N). The equivalent NAD83 geographic coordinates are: (54.13837º N, 94.53070º W) and (65.80575º N, 95.18703º W). The models are derived using an east-west geoelectric strike so that the 2-D transverse electric (TE) mode corresponds to east-west oriented electric fields (Z_{yx}-mode in data collected in a normal geographic coordinate system) and the 2-D transverse magnetic (TM) mode corresponds to north-south oriented electric fields (Z_{xy}-mode in data collected in a normal geographic coordinate system). Responses are provided for the period range of 0.0158–10^5 s sampled at five points per decade. Impedance values are given in units of ohms and phase values are given in units of degrees with both the TE and TM phase values specified for the quadrant 0º–90º.

The four models for which MT responses are provided are:

- Model A. Based on available MT sites from within 200 km of the Gillam-Kivalliq modelling profile.
- Model B. Based on same data as Model A but incorporates deep layers determined in the southern Superior craton study of Schultz et al. (1993)
- Model C. Based on available MT sites from within 200 km of the Gillam-Kivalliq modelling profile with large gaps padded with MT sites from the corresponding geological terranes from LITHOPROBE Line L.
- Model D. Based on same data as Model C but incorporates deep layers determined in the southern Superior craton study of Schultz et al. (1993)

Importation of data from LITHOPROBE Line L (Models C and D) is intended to provide responses with the same statistical character as those in the terranes crossed, but not to necessarily provide the true structure. The two models incorporating deep layer resistivity constraints (Models B and D) are considered to provide the more reliable MT impedance responses at periods exceeding 10^4 s.

50-km impedance responses

These data are 50 km sampled data for Models B and D. They are sorted by descending period first, and for points from south-to-north along the profile second. There are a total of 910 lines of data (35 periods and 26 location segments). Responses are given in terms of real and imaginary components of Z (in Ω) and corresponding impedance magnitude (in Ω) and impedance phase (in degrees with both TE and TM responses specified for the quadrant 0º–90º). Each point represents an arithmetically-averaged value (based on averaging the complex impedance) over a 50 km UTM north-south segment. The first column contains the centre of the segment in terms of the profile position (in km). The file also lists the UTM15 coordinates and NAD83 geographic latitude/longitude coordinates of the centre of the profile, and of the south (segment start) and north (segment end) end-points.

10-km impedance responses

These data are 10 km sampled data for Models B and D. They are sorted by descending period first, and for points from south-to-north along the profile second. There are a total of 4585 lines of data (35 periods and 131 location segments). Responses are given in terms of the TE and TM apparent resistivity (in Ω·m), impedance phase (in degrees with both TE and TM responses specified for the quadrant 0º–90º), impedance

magnitude (in Ω), and impedance magnitude gradient (in Ω/km) (defined as positive for decreasing impedance (decreasing resistivity or increasing conductivity) with increasing distance to the north as specified in equation 7). Each point represents an exported synthetic MT response from the corresponding 2-D resistivity model and the derived impedance response for points spaced at 10 km intervals along the model. The first column contains the position of the profile (in km) with distance increasing to the north.

10-km MT responses

These data are 10 km MT responses for Models A-D. They are sorted by descending period first, and for points from south-to-north along the profile second. There are a total of 4585 lines of data (35 periods and 131 location segments). Responses are given in terms of the TE and TM apparent resistivity (in Ω·m), and impedance phase (in degrees with the TE response specified for the 0º–90º quadrant and the TM response specified for the 2-D quadrant -180º– -90º quadrant). Each point represents an exported synthetic MT response from the corresponding 2-D resistivity model for points spaced at 10 km intervals along the model. The first column contains the position of the profile (in km) with distance increasing to the north.